

**KWAME NKRUMAH UNIVERSITY OF SCIENCE AND TECHNOLOGY  
COLLEGE OF SCIENCES DEPARTMENT OF PHYSICS**

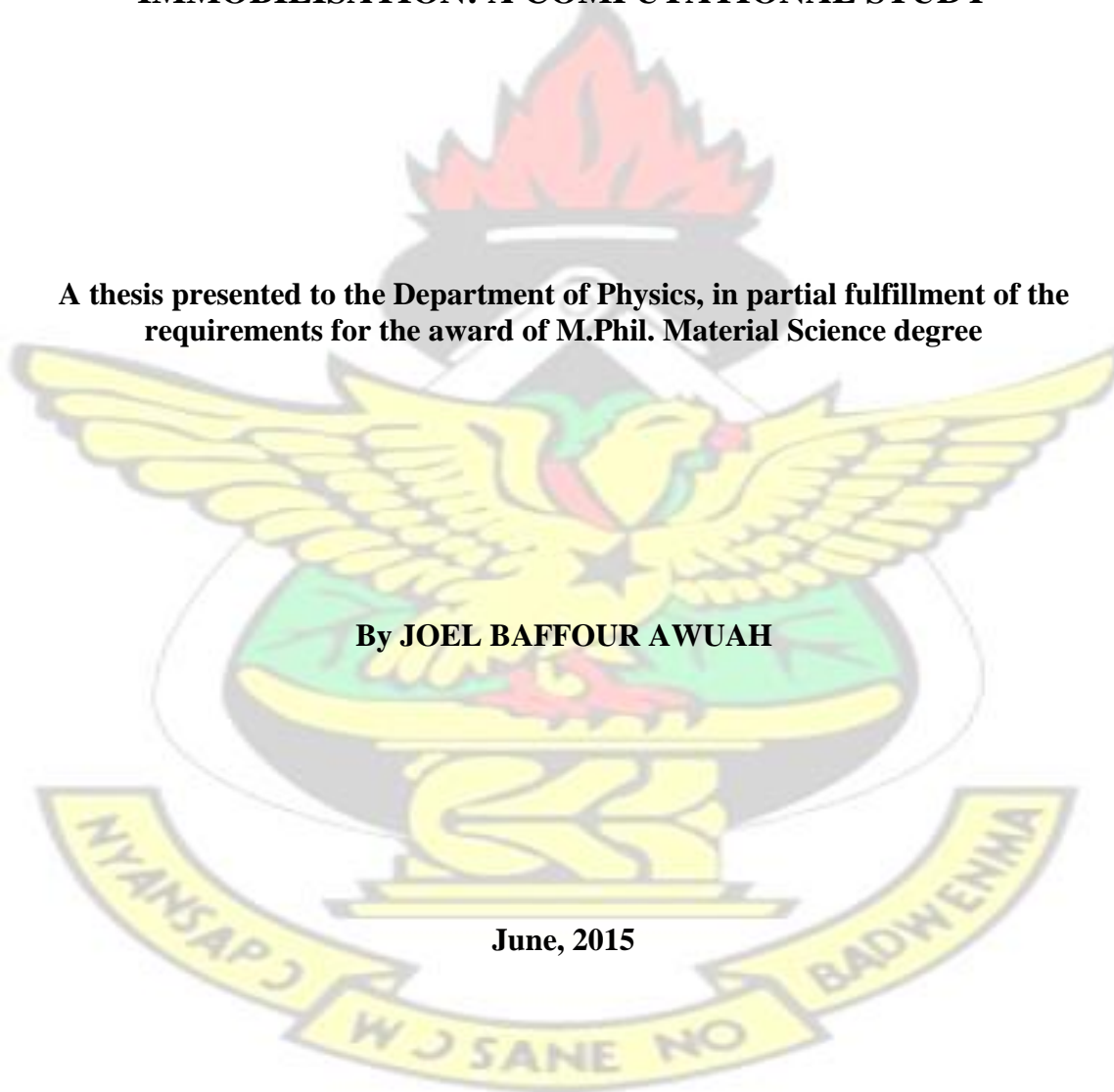
**KNUST**

**THE POTENTIAL OF ZEOLITE CLINOPTILOLITE FOR ARSENIC  
IMMOBILISATION: A COMPUTATIONAL STUDY**

**A thesis presented to the Department of Physics, in partial fulfillment of the  
requirements for the award of M.Phil. Material Science degree**

**By JOEL BAFFOUR AWUAH**

**June, 2015**



## Declaration

I, AWUAH, Joel Baffour hereby declare that this thesis is a results of my own work towards M. Phil. degree in Materials Science and that to the best of my knowledge, it contains neither material previously published by any other person nor one which has been accepted for the award of any other degree in any university, except where due reference has been made in the text of this thesis.

AWUAH, Joel Baffour .....  
(Student) Signature Date

Certified by

Dr. Bright Kwakye-Awuah .....  
(Supervisor) Signature Date

Dr. Evans Adei .....  
(Supervisor) Signature Date

Dr. Richard Tia .....  
(Supervisor) Signature Date

Prof. S. K Danuor .....  
(Head of Department) Signature Date  
Physics

## Acknowledgement

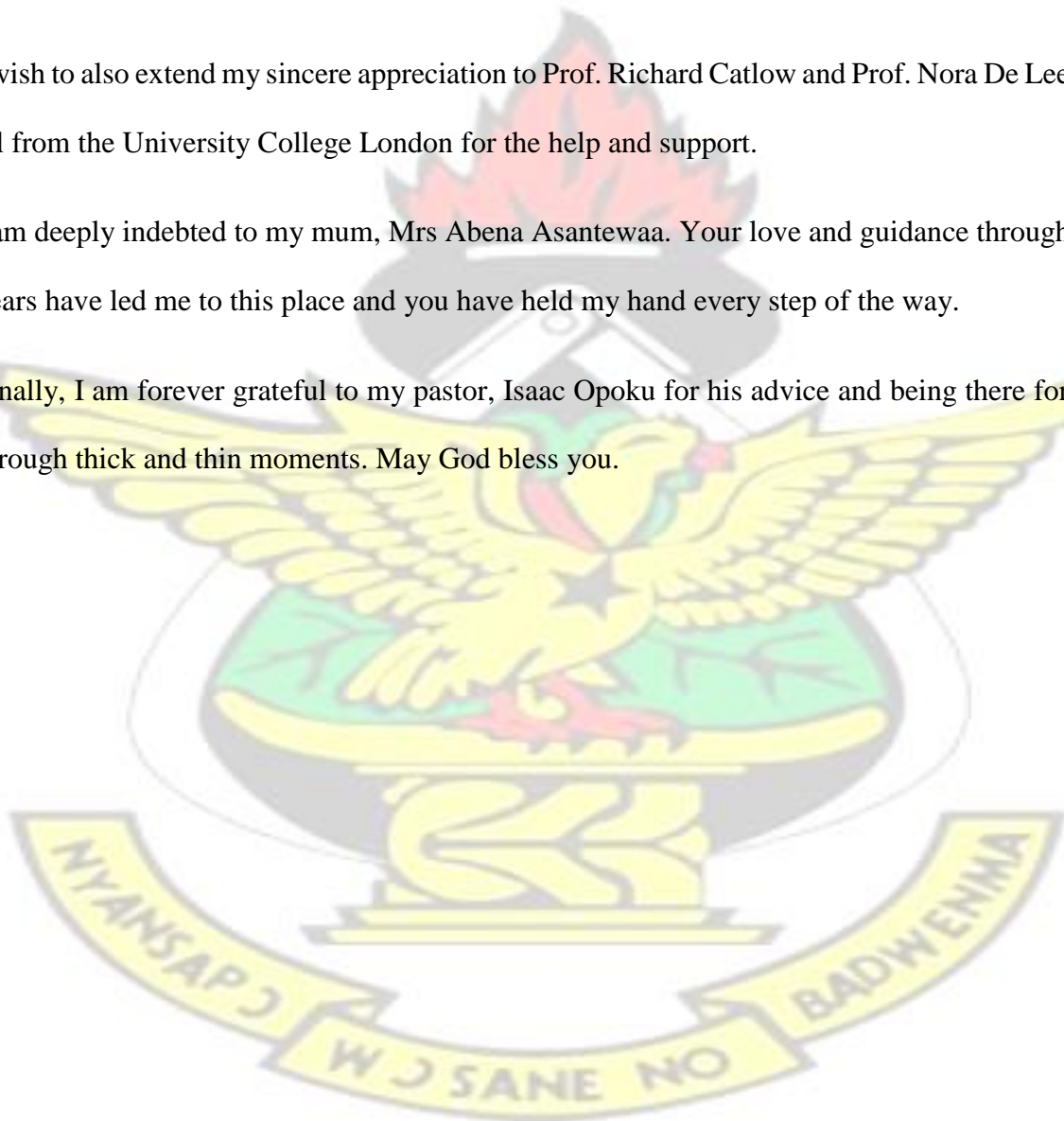
I give you thanks, O Lord, with my heart; I will sing to you all the praises, without you i would not have made it this far.

First, I am deeply grateful to all my supervisors, Dr. Bright Kwakye-Awuah, Dr. Evans Adei and Dr. Richard Tia for consistently urging me on and also giving me all the necessary help and suggestion with my work.

I wish to also extend my sincere appreciation to Prof. Richard Catlow and Prof. Nora De Leeuw, all from the University College London for the help and support.

I am deeply indebted to my mum, Mrs Abena Asantewaa. Your love and guidance through the years have led me to this place and you have held my hand every step of the way.

Finally, I am forever grateful to my pastor, Isaac Opoku for his advice and being there for me through thick and thin moments. May God bless you.



## Dedication

This work is dedicated to the Almighty God for His guidance, mercy, love and in remembrance of my mum, Asantewaa Abena for her support and encouragement.

# KNUST



## Abstract

Clinoptilolite has been identified as a candidate for arsenic removal from water, but the exact adsorption sites, their relative stabilities and the characteristics of the environment where the arsenic is located within the zeolite framework still remains elusive. We investigated the arsenic acid  $\text{AsO}(\text{OH})_3$  and arsenous acid  $\text{As}(\text{OH})_3$  adsorption by Al(III)-modified natural zeolite clinoptilolite (CL) under vacuum and hydrated conditions using first-principles density functional theory calculations. Density functional theory (DFT) calculations within the generalized gradient approximation (GGA) were carried out using the plane-wave pseudopotential PWscf code in the Quantum-ESPRESSO package using ultrasoft pseudopotentials with the PBE functional. We also considered the effect of Si/Al ratio on the adsorption potentials of Al(III)-modified natural zeolite clinoptilolite. Essentially the adsorption energies for both arsenic and arsenous acids on dehydrated CL zeolite (Si/Al = 1.7 - 8) at all the adsorption sites are favorable (7 - 252 kJ/mol, exothermic) except at the 8 MR in the (100) plane (site 3) for  $\text{AsO}(\text{OH})_3$  at Si/Al ratio of 5 and the site locate between the 8MR in the (001) plane and the 8 MR in the (100) plane (site 4) for  $\text{AsO}(\text{OH})_3$  at Si/Al ratio of 6 and 8. However, in the hydrated CL, the exothermicity is maintained only in the 8 MR in the (001) plane (site 2) and site 4 with increase in the extent of exothermicity (32 - 161 kJ/mol) at these sites with an interatomic distance of the adsorption of single  $\text{AsO}(\text{OH})_3$  and  $\text{As}(\text{OH})_3$  molecules being 2.309 Å.

The unfavorableness of the adsorption in the hydrated systems increases with increasing water molecules added. We attribute this to the water molecules filling the pores in the zeolite, therefore leaving no space for the adsorbates to fit in. The strength of binding of the arsenic species is shown to depend sensitively on the Si/Al ratio in the Al(III)-modified CL zeolite, adsorption energies decreases (252 - 7 kJ/mol) as the Si/Al ratio increases (1.7 - 8), this is as a result of increase in the interaction between the framework cations and the arsenic species. The

calculated high adsorption energies indicated a great potential for Al(III)-modified clinoptilolite for arsenic immobilization. This preliminary work improves our understanding of the role that Al(III)-modified clinoptilolite zeolite may play in the remediation of Arsenic contaminated sites and may help the development of reliable forcefields that can be employed in classical MD simulations to simulate complex systems.

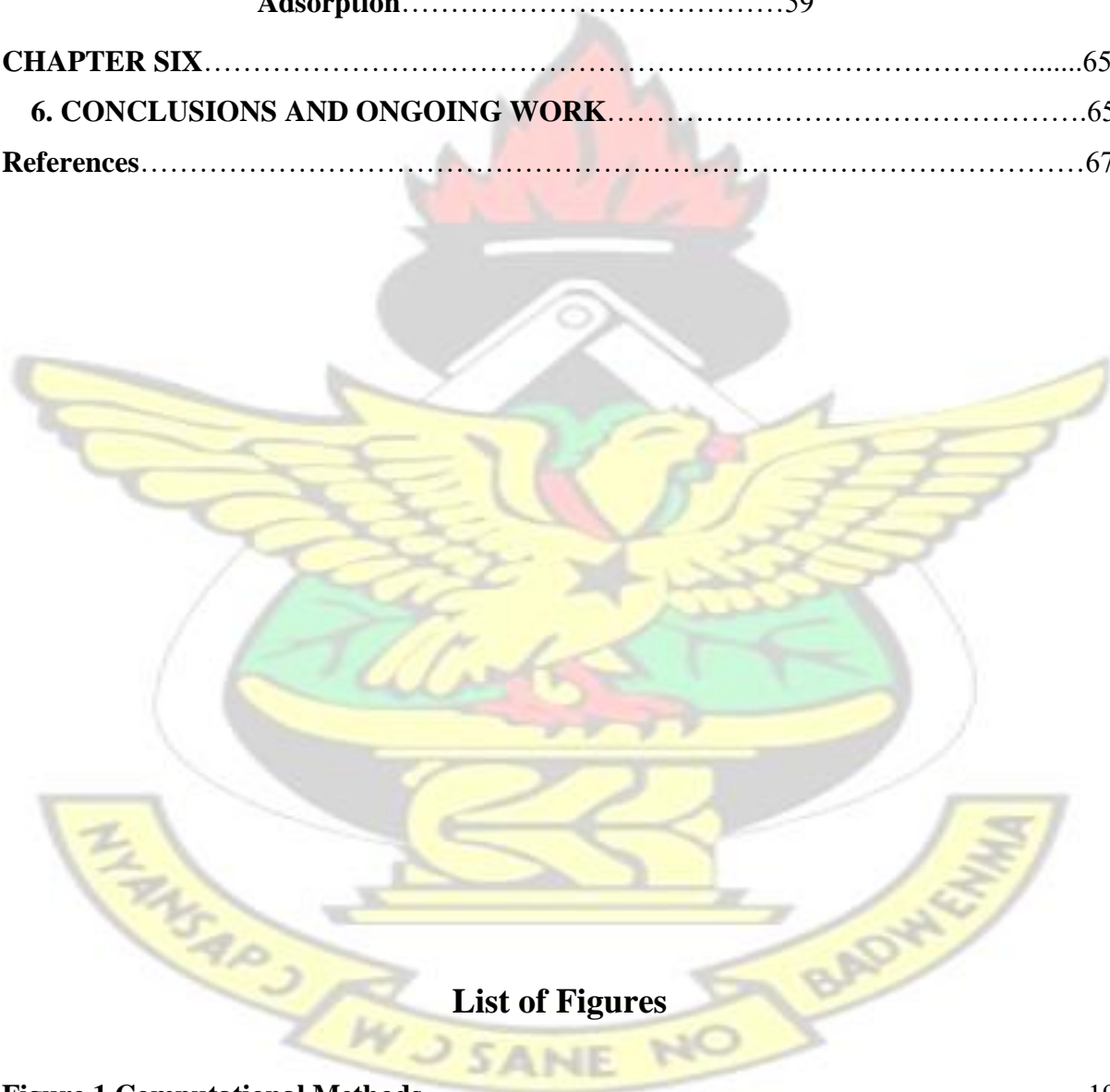


## Table of Contents

<b>Declaration .....</b>	<b>i</b>
<b>Acknowledgement.....</b>	<b>ii</b>
<b>Dedication.....</b>	<b>iii</b>
<b>Abstract .....</b>	<b>iv</b>
<b>List of Figures .....</b>	<b>viii</b>
<b>List of Tables.....</b>	<b>ix</b>
<b>List of Abbreviations .....</b>	<b>x</b>
<b>CHAPTER ONE.....</b>	<b>1</b>
<b>1. INTRODUCTION.....</b>	
1	
<b>1.1 Zeolites.....</b>	
.....1	
1.1.1 Natural Zeolites.....	1
1.1.2 Synthetic Zeolites.....	2
<b>1.2 Structure Description.....</b>	<b>3</b>
<b>1.3 Application of Zeolites.....</b>	<b>4</b>
1.3.1 Adsorption.....	5
1.3.2 Catalysis.....	6
1.3.3 Ion Exchange.....	10
<b>1.4 Arsenic Pollution.....</b>	<b>11</b>
<b>1.5 Objectives.....</b>	<b>13</b>
<b>CHAPTER TWO.....</b>	<b>14</b>

2. LITERATURE REVIEW.....	13
CHAPTER THREE.....	18
3. Computational Chemistry.....	18
3.1 Theoretical Background.....	19
3.1.1 Computational Methods.....	19
3.1.2 Electronic Methods.....	21
3.1.3 Wavefunction Methods.....	22
3.1.4 Density Functional Method.....	27
3.1.4.1 The Kohn-Sham Equations.....	28
3.1.5 Exchange-Correlation Functional.....	30
3.1.5.1 Local Density Approximation.....	30
3.1.5.2 Generalized Gradient Approximation.....	31
3.1.5.3 The Meta-GGAs.....	32
3.1.5.4 The Hybrid functionals.....	32
3.1.6 Basis Sets.....	34
3.1.7 The plane wave pseudopotential method.....	35
CHAPTER FOUR.....	36
4. COMPUTATIONAL METHODS.....	37
CHAPTER FIVE.....	39
5. RESULTS AND DISCUSSION.....	39
5.1 The Structure of Clinoptilolite.....	40
5.2 Al modified Clinoptilolite.....	41

5.2.1	<b>Hydrated Clinoptilolite</b> .....	42	Na <sup>+</sup>
5.2.2	<b>Dehydrated Clinoptilolite</b> .....	44	Na <sup>+</sup>
5.3	<b>Charge Density</b> .....	48	
5.4	<b>Adsorption Arsenic</b> .....	53	of
5.4.1	<b>Effect of Hydration Adsorption</b> .....	59	on Arsenic
<b>CHAPTER SIX</b> .....		65	
<b>6. CONCLUSIONS AND ONGOING WORK</b> .....		65	
<b>References</b> .....		67	



<b>Figure 1</b>	<b>Computational Methods</b> .....	19
<b>Figure 2</b>	<b>Sketch of the all-electron wave function and electronic potential plotted against distance from the atomic nucleus</b> .....	36
<b>Figure 3</b>	<b>The siliceous clinoptilolite framework</b> .....	40

Figure 4	The structure of hydrated clinoptilolite with different Si/Al ratios.....	43
Figure 5	The structure of dehydrated clinoptilolite with different Si/Al ratios.....	45
Figure 6	The isosurface of charge distribution inside the channels for a dehydrated and hydrated clinoptilolite.....	49
Figure 7	Adsorption of arsenic in adsorption site 1.....	54
Figure 8	Adsorption of arsenic in adsorption site 2.....	55
Figure 9	Adsorption of arsenic in adsorption site 3.....	56
Figure 10	Adsorption of arsenic in adsorption site 4.....	57
Figure 11	Adsorption energies of $AsO(OH)_3$ and $As(OH)_3$ as a function of Si/Al ratio at different adsorption sites of <i>dehydrated</i> and <i>hydrated</i> Na-clinoptilolite.....	59
Figure 12	The structure of clinoptilolite hydrated with 12 water molecules.....	60
Figure 13	The structure of clinoptilolite with 2 water molecules.....	62
Figure 14	Adsorption energies of $AsO(OH)_3$ and $As(OH)_3$ as a function of Si/Al ratio 5 at different adsorption sites of <i>hydrated</i> Na-clinoptilolite (12 water molecules).....	63
Figure 15	Adsorption energies of $AsO(OH)_3$ and $As(OH)_3$ as a function of Si/Al ratio 5 at different adsorption sites of <i>hydrated</i> Na-clinoptilolite (2 water molecules).....	64



### List of Tables

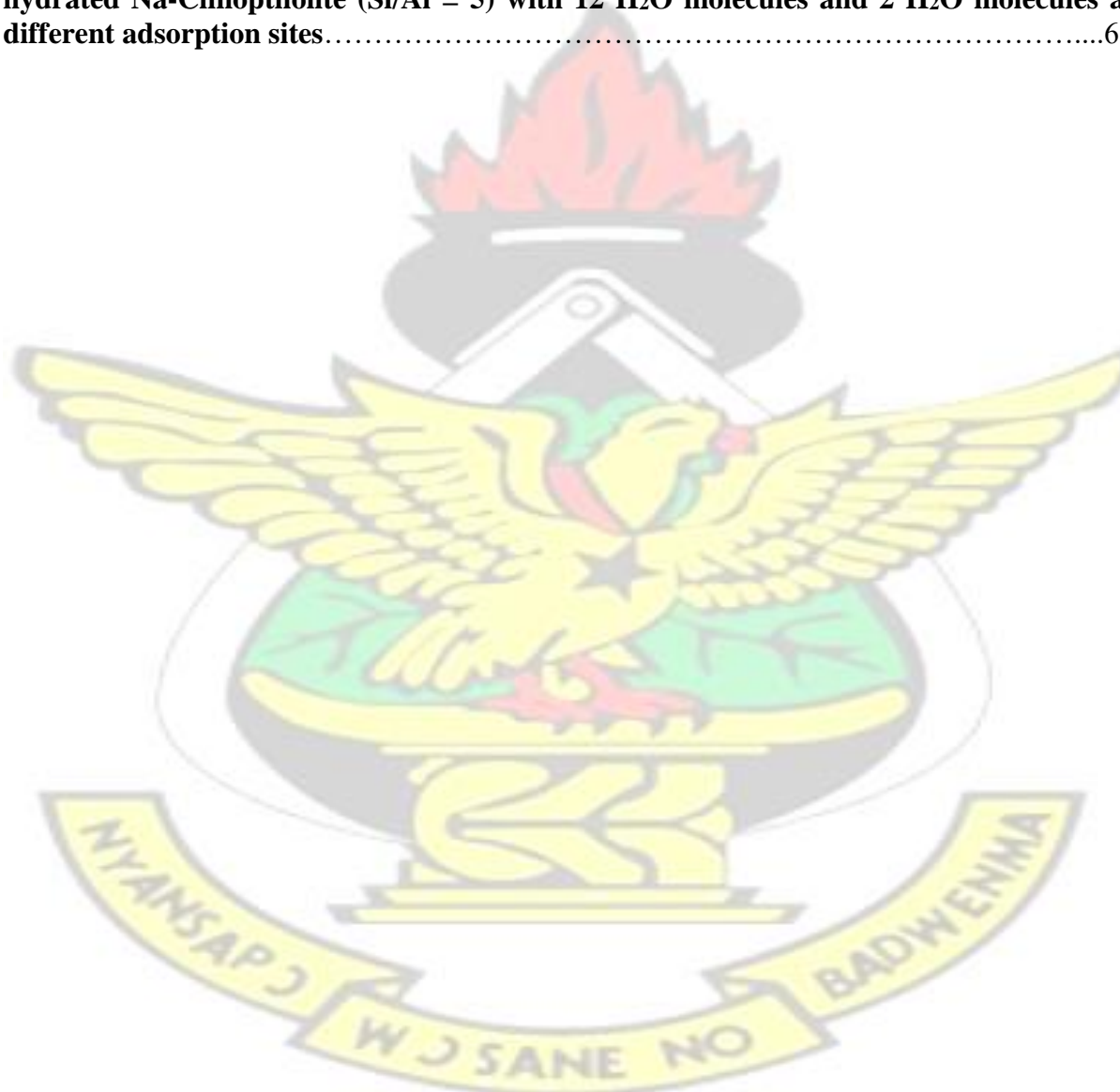
Table 1	Some strengths and limitations of computational methods.....	20
Table 2	Unit Cell Parameter, Si-O bondlength and bond angles at various T-sites in the siliceous clinoptilolite.....	41

**Table 3** The size of pores, angles between T-sites, Si-O, Al-O bondlength and Na<sup>+</sup>framework oxygen internuclear distances.....47

**Table 4** Adsorption energies (kJ/mol) for  $AsO(OH)_3$  and  $As(OH)_3$  on *dehydrated NaClinoptilolite* (Si/Al = 1.7, 5, 6 and 8) at different adsorption sites.....58

**Table 5** Adsorption energies (kJ/mol) for  $AsO(OH)_3$  and  $As(OH)_3$  on *hydrated NaClinoptilolite* (Si/Al = 1.7, 5, 6 and 8) at different adsorption sites.....58

**Table 6** Adsorption energies (kJ/mol) for two water molecules,  $AsO(OH)_3$  and  $As(OH)_3$  on hydrated Na-Clinoptilolite (Si/Al = 5) with 12 H<sub>2</sub>O molecules and 2 H<sub>2</sub>O molecules at different adsorption sites.....63



### List of Abbreviations

1. **CC** Computational Chemistry
2. **CMS** Computational Material Science

3. **DFT** Density Functional Theory
4. **HFSCF** Hartree-fock self-consistent field
5. **KS** Kohn Sham
6. **LDA** Local Density Approximation
7. **GGA** General Gradient Approximation
8. **PBE** Perdew Burke Ernzerhof
9. **XC** Exchange Correlation
10. **FCA** Frozen Core Approximation
11. **FD** Framework Density
12. **HEU** Heulandite
13. **CLI** Clinoptilolite



# CHAPTER ONE

## 1. INTRODUCTION

### 1.1 Zeolites

Zeolites are crystalline aluminosilicates of alkali or alkaline-earth metals, especially sodium, potassium, calcium, magnesium, strontium and barium. Structurally zeolites are micro-porous crystalline solids with well-defined micro-pores. Generally, the three constituents of zeolites are silicon, aluminium and oxygen in their framework, cations and water within their pores. The aluminosilicate framework is composed of infinitely extended three-dimensional network of  $\text{AlO}_4^-$  and  $\text{SiO}_4$  tetrahedra that form channels and interconnected voids roughly between 3 and 10 Å diameter. Owing to their unique poriferous properties, zeolites are used in a variety of applications within a global market of several millions tonnes per annum (TOP 2001, Kwakye-Awuah *et al.*, 2014), (Wong 2009).

#### 1.1.1 Natural Zeolites

The geologist Alex Fredrick Cronstedt (1722-1765) discovered a tectosilicate, called Stibillite, from the copper mine in Tornea, Sweden. In 1756 he published the article “Observation and description of an unknown species of rock, called “ZEOLITES”, in a Swedish magazine where he explained that this mineral visibly lost water when heated by a flame. By cooling the structure it could be rehydrated (Cronstedt 1756). Cronstedt gave these minerals an aptly descriptive name: “zeolite”, a term that etymologically comes from classic Greek zeo, which means to boil, and lithos which means stone. Therefore, these materials are literarily called “boiling stones.” At that time, it was impossible to imagine all the ways in which zeolites could be exploited. Zeolites can be found in a variety of geological environments containing siliceous materials (volcanic rocks, clays, feldspar, biogenic silica and other silica rocks).

These natural zeolites have a volcanic origin and are formed when flowing water of high pH and salt content interacts with volcanic ash, causing rapid crystal formation (Dyer. 1988). Many years ago, they were considered to only be museum pieces admired for their beauty and used exclusively in jewellery. Since the first zeolite was discovered by Cronstedt, around forty natural types have been found. The most abundant structures are mordenite, clinoptilolite, erionite, chabazite, phillipsite, stibillite and analcime.

### **1.1.2 Synthetic Zeolites**

Synthetic zeolites are created in the laboratory to mimic the behaviour and properties similar to natural conditions (Damour 1840). Von Schafhäütl performed the first trial of hydrothermal synthesis of a porous material with quartz in 1845. Some years later, in 1862, de St. Claire-Deville described the first hydrothermal synthesis of a zeolite: Levynita. At this time, techniques were not available to observe zeolites and there was not even information regarding atomic characterization (Claire-Deville 1862). Thus, these initial works were unable to provide information about the structure and suffered from low reproducibility. However, in 1930 the development of new experimental techniques like X-ray diffraction motivated Pauling to lead to experiments which made him able to describe the first structure of a zeolite. The adsorption was not limited to water.

In 1909, Grandjean observed that zeolites could adsorb other molecules, like hydrogen, ammonia or air. It was in 1948 when Barrer reported the first precise confirmation of hydrothermal synthesis of an analogue mordenite. As well, Barrer demonstrated that some zeolites could be synthesized in a form identical to their natural counterparts. Furthermore, Milton (Sánchez 2011) developed zeolite synthesis experiments to find new approaches for the separation and purification of mixture gases. Later on, together with Breck, their research produced a shift for industrial applications. That led to one of the most commercially successful zeolite that has no natural counterpart, Linde type A (LTA). In 1954, Union

Carbide, was the first company that commercialized zeolite for separation, purification of air and for drying refrigerant gas and natural gas (Sánchez 2011). Hydrothermal and solvothermal synthesis reactions have become the basis and core of the synthetic chemistry of microporous crystal, and have been widely used in the preparation and modification of porous materials. Hydro(solvo)thermal synthesis refers to the synthetic reactions conducted at appropriate temperature (100 ~ 1000 °C) and pressure (1 ~ 100 MPa) in aqueous or organic solvents within a specially sealed container or high pressure autoclave under subcritical or supercritical conditions. Under these conditions, the physical and chemical properties of reactants can be significantly changed (Xu *et al.*, 2009).

## 1.2 Structure Description

Zeolites with regular pore architectures comprise wonderfully complex structures and compositions. Their fascinating properties, such as ion-exchange, separation, catalysis and their roles as host in nanocomposite materials are essentially determined by their unique structural characters, such as the size of the pore, wide the accessible void space, the dimensionality of the channel system, and the numbers and sites of cations. The structural formula of a zeolite may be best by the idealized formula for a crystallographic unit cell, which is expressed as  $M_{x/n}[(AlO_2)_x (SiO_2)_y].wH_2O$ , where M is a framework cation with valence n and w is the number of water molecules. Describing the structure of a zeolite framework has always been a challenging task. Toward this end, many structural descriptors have been devised during the past decades. Meanwhile, the efficient calculation of complex structural features is also an important challenge in this field. Since the publication of the sixth edition of Atlas of Zeolite Framework Types in 2007 (Baerlocher *et al.*, 2007) many effort have been made to develop new structure descriptors and new methods for the calculation of complex porous structures. The framework density is defined as the number of T atoms per 1000 Å<sup>3</sup>. Isotypic materials with different chemical compositions may have different FDs (Baerlocher *et al.*, 1978). Each

T atom in a zeolite framework corresponds to a coordination sequence and a vertex symbol. The coordination sequence consists of a sequence of integers, where the *n*th integer represents the number of T atoms involved in the *n*th neighboring shell surrounding the original T atom. The vertex symbol indicates the size of the smallest ring associated with each of the six angles of a T atom (Baerlocher *et al.*, 2007, Baerlocher and McCusker 2012) The channel in a zeolite framework is a pore infinitely extended in one dimension and is large enough for guest species to diffuse along its length.

Similar to the definition of cavity, the opening of a channel has to be larger than 6-ring.

Channels may intersect to form two- or three-dimensional channel systems (Baerlocher *et al.*, 2007, McCusker *et al.* 2001, Baerlocher and McCusker 2012, Van Koningsveld 2007, Treacy and Foster 2009, Foster *et al.*, 2006).

### **1.3 Application of Zeolites**

The widespread use of zeolites is due to their unique adsorption, diffusion, and catalytic properties which, together with their pore size, allow perfect shape selectivity (Caro *et al.*, 2005, Watanabe *et al.*, 2004). For several decades, natural zeolites have been used for the treatment of various diseases in animals and humans. One of the most important is the use of Clinoptilolite as adjuvant in cancer therapy (Pavelic 2001, Zarkovic *et al.*, 2003).

The biggest advantage of zeolites is that their properties are easily modified for specific needs in many technological fields and environmental applications (Frising and Leflaive 2008). Due to their molecular sieve structure, zeolites can selectively adsorb components of gaseous or liquid mixtures according to their molecular size and the presence of non-framework cations (Frising and Leflaive 2008, Caro *et al.*, 2000). Most often, zeolites are used to make detergents, replacing the use of phosphates as water softening agents, since phosphates have irreversible adverse effects on lakes and rivers. Common uses are as cracking agents in the petrochemical

industry where complex organic molecules such as kerogens or heavy hydrocarbon are broken down into simpler molecules such as light hydrocarbons, by the breaking of carbon-carbon bonds in the precursors, and as ion-exchangers for water softening and purification. Because zeolites can adsorb relatively easily molecules within their pores, they are promising materials for immobilisation of toxic materials in the terrestrial and aquatic ecosystems. Several zeolites, such as Clinoptilolite (Bonnin 1997), Chabazite, SZP, 13x and 5A have been identified as potential candidates for arsenic removal from water (Shevade and Ford 2004). In published reports on arsenic removal using activated alumina, adsorption via ligand exchange has been identified as the removal mechanism (Stumm 1996). Clinoptilolite is a subject of numerous studies, because it is available as a natural zeolite in large deposits worldwide. It has the same topology as the mineral Heulandite, and thus belongs to the same structural group, denoted as HEU. The structure is a much opened one and possesses a two-dimensional network of intersecting channels in the [010] plane, with three main channels (Uzunova and Mikosch 2013b).

### **1.3.1 Adsorption**

Zeolites are unique adsorbent materials, characterized by 20% to 50% void volumes and internal surface areas of several hundred thousand square meters per kilogram. The adsorption of guest molecules can occur on the outer surface of crystallites or on the inner surface of the micropores, depending on the geometry and dimensions of the molecules, and on the diameter of the pores of the zeolite in question. Molecules of kinetic diameter larger than the diameter of the pores cannot pass through the windows and enter the canal system, which is why zeolites are also known as molecular sieves. The molecular sieve property may be affected by dehydration and heat. Heating can produce distortions in the lattice and increase the void volume of the channels, while dehydration causes a cation interchange and subsequent changes in charge distribution inside the structure. The size and shape of the channels in zeolites have

extraordinary effects on the properties of these materials for adsorption processes. One of the most interesting properties of zeolites, from the point of view of their possible applications, is their ability to adsorb certain molecules inside their structure (Sánchez 2011). Adsorption of a gas on a solid is the enrichment of molecules in an interfacial layer adjacent to a solid wall (Sing *et al.*, 1985). In the context of this thesis the solid wall refers to the inner surface of the zeolite pore accessible to gas molecules. The substance that is adsorbed is called adsorbate and the material taking on the adsorbate is the adsorbent. There are two kind of adsorption: physisorption or physical adsorption and chemisorption or chemical adsorption. The physical adsorption is a weak binding caused by van der Waals forces without a charge redistribution in the molecule and on the pore surface. There is no change in the chemical nature of the adsorbate in the physisorption. Chemical adsorption implies the creation of bonds and a change in the electron density between the adsorbent and the adsorbate. The nature of the link could be between ionic and covalent. The adsorption phenomena are characterized experimentally by measuring adsorption isotherms which represent the amount of adsorbed molecules in the adsorbate as a function of gas pressure or liquid outside (Sánchez 2011). Adsorption is by nature a surface phenomenon, governed by the unique properties of bulk materials that exist only at the surface due to bonding deficiencies. In some systems, adsorption is accompanied by absorption, where the adsorbed species penetrates into the solid. This process is governed by the laws of diffusion, a much slower mechanism, and can be readily differentiated from adsorption by experimental means.

### **1.3.2 Catalysis**

Zeolites have the ability to act as catalysts for chemical reactions which take place within the internal cavities. An important class of reactions is that catalysed by hydrogen-exchanged zeolites, whose framework-bound protons give rise to very high acidity. This is exploited in many organic reactions, including crude oil cracking, isomerisation and fuel synthesis.

Zeolites can also serve as oxidation or reduction catalysts, often after metals have been introduced into the framework. Examples are the use of titanium ZSM-5 in the production of caprolactam, and copper zeolites in NO<sub>x</sub> decomposition. The first use of molecular sieves in catalysis occurred in 1959 when zeolite Y was used as a catalyst for isomerization reactions. In 1962, the Mobil Company used zeolite X in the catalysis of cracking reactions. In 1969, Grace developed ultra-stable zeolite Y (USY) as a catalyst (Xu *et al.*, 2009). At that time, besides the catalysis of cracking and hydrocracking reactions, molecular sieves were also used for the isomerization of normal alkanes, C<sub>8</sub> aromatics, and the disproportionation of toluene in industry (Joo *et al.*, 2001). With increasing applications of molecular sieves in industry, the theories of acid catalysis, of B- and L-acids (Minachev and Ya.I. Isakov 1973), and on carbonium ion reaction mechanisms were established in the field of molecular sieve catalysis. At the same time, study on another important feature of molecular sieves, that is, catalytic shape-selectivity, was also carried out. The unique properties of mesoporous materials arise from their high specific surface areas (>1000 m<sup>2</sup>/g) and their uniform mesopores (diameters range from 2 to 50 nm) (Kresge *et al.*, 1992, Zhao *et al.*, 1998a, Corma 1997). In the past decade, mesoporous materials have been widely used in the field of catalysis, such as in petroleum processing, the fine-chemicals industry, and in reactions involving large molecules. For petroleum processing, the conventional catalysts are usually microporous zeolites, such as zeolite Y and ZSM-5. However, with the decrease of petroleum resources in the world and the increase of heavy components in crude oil, the applications of conventional zeolites are more and more restricted due to their small pores. Mesoporous materials have ordered mesopores which might have potential applications in the catalysis of heavy oil processing (Corma 1997). For example, Al-MCM-41 has shown better catalysis performance in hydrocracking, hydrodesulfurization, and hydrodenitrogenation reactions than do traditional microporous materials. In green oxidation reactions, zeolite TS-1 is the typical catalyst. Since the size of its

channels ranges from 5 to 6 Å, TS-1 can be used as the catalyst only for benzene and phenol conversion. However, ordered mesoporous titanium silicate materials have pores large enough for the catalytic reactions of bulkier molecules, and this is very important for the production of fine chemicals. For example, for the oxidation reaction of terpineol, Ti-MCM-41 performs much better than do microporous titanium silicate molecular sieves as a catalyst (Corma 1997). However, on the other hand, the hydrothermal stability and catalytic activity of ordered mesoporous materials are still lower than those of conventional microporous molecular sieves. In recent years, many measures have been taken to solve this problem, such as adding inorganic salts during the synthesis of mesoporous materials (Mokaya 1999), intensifying the post treatment (Ryoo *et al.*, 1999, 1997), using triblock copolymers as templates to obtain thicker channel walls of mesoporous materials (Zhao *et al.*, 1998b), using neutral surfactants to synthesize mesoporous materials (Corma 1997), using mixed templates (Karlsson *et al.*, 1999, Huang *et al.*, 2000, Kloetstra *et al.*, 1999), and synthesizing mesoporous materials at high temperatures (Han *et al.*, 2003). Although these methods more or less help enhance the hydrothermal stability of mesoporous materials, their catalytically active centers are still not comparable with those of conventional microporous molecular sieves. In recent years, scientists have tried to prepare novel ordered mesoporous materials through the self-assembly of nanoparticles consisting of microporous building units and surfactant micelles. Using this approach, both the hydrothermal stability and the catalytic activity of mesoporous materials have been enhanced (Zhang *et al.*, 2001a, Liu *et al.*, 2000). For instance, the novel mesoporous titanium silicate material, MTS-9, has shown better catalytic activity than have Ti-MCM-41 and TS-1 in the synthesis of an intermediate product of vitamin E (Zhang *et al.*, 2001b). Mesoporous materials have great application potential in novel and high-technology areas as well. They can be used for the stabilization or separation of enzymes and proteins, the degradation of organic wastes, the purification of water, and the transformation of exhaust gas.

They can also be used for energy storage. Many functional materials are able to be assembled into mesoporous materials. For example, advanced mesoporous optical materials may be prepared through assembly of laser-generating species or materials with optical activities (Xiao *et al.*, 2002, Marlow *et al.*, 1999, Scott *et al.*, 2001b). Ordered mesoporous conducting polymers may form through polymerization in ordered mesopores followed by chemical removal of the inorganic host (Scott *et al.*, 2001a). Ordered mesoporous carbon materials can be obtained through complete mixing of mesoporous materials and a glucoside followed by carbonization and dissolution of the inorganic species (Jang *et al.*, 2002). It has been demonstrated that the mesoporous carbon thus formed exhibits better performance than do conventional carbon materials when used as electrodes of fuel cells (Ryoo *et al.*, 1999). Through using the ordered channels in mesoporous materials as micro-reactors, fine nanoparticles and other quantum composite materials can be synthesized. Because of small size or quantum-size effects arising from the confinement of ordered channels, these composite materials exhibit unique optical, electrical, and magnetic properties. For example, it has been demonstrated that modified mesoporous zirconium oxides show unusual photoluminescence at room temperature.

In contrast with carbon nanotubes, mesoporous materials composed of silica and nonsilica species exhibit rich surface chemical activity. The ordered channels in mesoporous materials may act as micro-reactors to assemble nanometer-sized homogeneous guest materials, and, as a result, the application fields of mesoporous materials can be further broadened on the basis of the host–guest effects. Through using stable mesoporous materials as hosts, a variety of inorganic photoelectric nano-sized materials such as Si, BN, SiC, AgI, and AlN, and giant magneto-resistant transition metals such as Ni, Cu, and Co can be prepared. Assembly of some semiconductor clusters with a wide band-gap such as ZnO, ZnS, and CdS into mesoporous materials may greatly increase the fluorescence intensities of the former due to the host–guest

interactions and quantum-size effects, implying promising applications of these composites in the field of optoelectronics.

In view of the many applications in the fields of separation, purification, biology, medicine, chemical industry, catalysis, information, environment, energy, and advanced composite materials, it is believed that mesoporous materials will play more important roles in the 21st century as an increasing number of mesoporous materials with advanced functions are designed and synthesized (Xu *et al.*, 2009).

### 1.3.3 Ion Exchange

Another interesting property of zeolites is their ability to exchange cations (Breck 1974). This property, known as ion exchange, allows them to be used as water softeners, detergents and soaps. Hydrated cations within the pores of the zeolite are weakly attached and ready to exchange with other cations, when in an aqueous medium (Sánchez 2011). The reason for that are the trivalent aluminium ions that cause an imbalance in the structure characterized by an excess of negative charges. To compensate this excess, zeolites incorporate cations such as  $\text{Na}^+$ ,  $\text{K}^+$  and  $\text{Ca}^{2+}$  into structures (Breck 1974). These cations are easily interchangeable with others, which gives the zeolite a high ion exchange capacity. Through this exchange other metal cations can be introduced into the zeolite and thus modify their catalytic properties or molecular sieve properties. In general, by increasing the ratio of Al/Si, the exchange capacity of zeolites increases. Organic cations can also be introduced, for example in dye manufacturing (Ryder *et al.*, 2000). As its name implies, ion exchange describes a process by which ions are transferred from a solid phase to liquid phase simultaneously. Since ions undergo a phase change, ion exchange can be regarded as a sorption process. However, in contrast to other sorption process, ion exchange is necessarily stoichiometric. Each ion, which is removed from the solution is replaced by an equivalent amount of ion in the exchanger of the same sign by conserving electroneutrality. Thus ion exchange can be considered as a stoichiometric process. Ion

exchange phenomenon can be simply explained by sponge model. In this model, ion exchanger is thought as a sponge with counter ions (exchange ions) floating in the pores. When the sponge is immersed in a solution, counter ions can leave the pore and float out. However, to preserve electroneutrality, another counter ion from the solution enters the sponge and take its place in compensating of the framework charge (TOP 2001). As described in this picture, ion exchange concept can be given by the redistribution of ions. Cation exchange behaviour of zeolites depend on (1) the nature of the cation species, the cation size, both anhydrous and hydrated, and cation charge; (2) the temperature; (3) the concentration of the cation species in the solution; (4) the anion species associated with the cation in the solution; (5) the solvent ( most exchange has been carried out in aqueous solution, although some work has been in organic solvents); and (6) the structural characteristics of the particular zeolite (Breck 1974).

#### **1.4 Arsenic Pollution**

Arsenic occurs in many minerals, usually in conjunction with sulphur and other metals, and also as a pure elemental crystal or allotropes. In ground water, arsenic combines with oxygen to form inorganic pentavalent arsenate and trivalent arsenite. Unlike other heavy metalloids and oxyanion – forming elements, arsenic can be mobilized under a wide range oxidizing and reducing conditions at the pH values typically found in ground waters (pH 6.5 – 8.5). The toxicity of different arsenic species varies in the order arsenite > arsenate > monomethylarsenate > dimethylarsenite. Trivalent arsenic is about 60 times more toxic than arsenic in the oxidized pentavalent state, and inorganic arsenic compounds are about 100 times more toxic than organic arsenic compounds. The organic forms of arsenic are found mostly in surface waters or in area severely affected by industrial pollution. In general, ground waters exhibit higher concentrations of arsenic species that are more toxic than those found in surface waters. Over 300,000 people die of arsenic related diseases worldwide every year (Kwakye-Awuah *et al.*, 2014). Due to the presence in water, the natural method of human exposure is

through ingestion. The presence of arsenic trioxide and pentaoxide in the body can result in cancerous and non-cancerous health effects, such as stomach pain, nausea, vomiting, diarrhea and blindness (Shevade and Ford 2004). The World Health Organisation (WHO) has set the arsenic standard for drinking water at 0.10 parts per million (ppm) to protect consumers served by ground water systems from effects long-term, chronic exposure to arsenic. In many parts of the world, gold and base metals are associated with naturally occurring deposits of arsenic in what are commonly referred to as arsenopyritic ore bodies. Ghana, the former Gold Coast is richly mineralized with gold that is accompanied by arsenic mineralization. Norman et al (2010) studied 207 wells in the Upper Birimian rocks that cross Ghana for arsenic levels and detected arsenic in 52 of them, with concentration ranging up to 2000 ppb 25 wells had level greater than 5 ppb. They concluded that at least 10% of Ghana's rural boreholes wells have arsenic levels greater than the WHO recommended values (Norman and Nartey 2010).

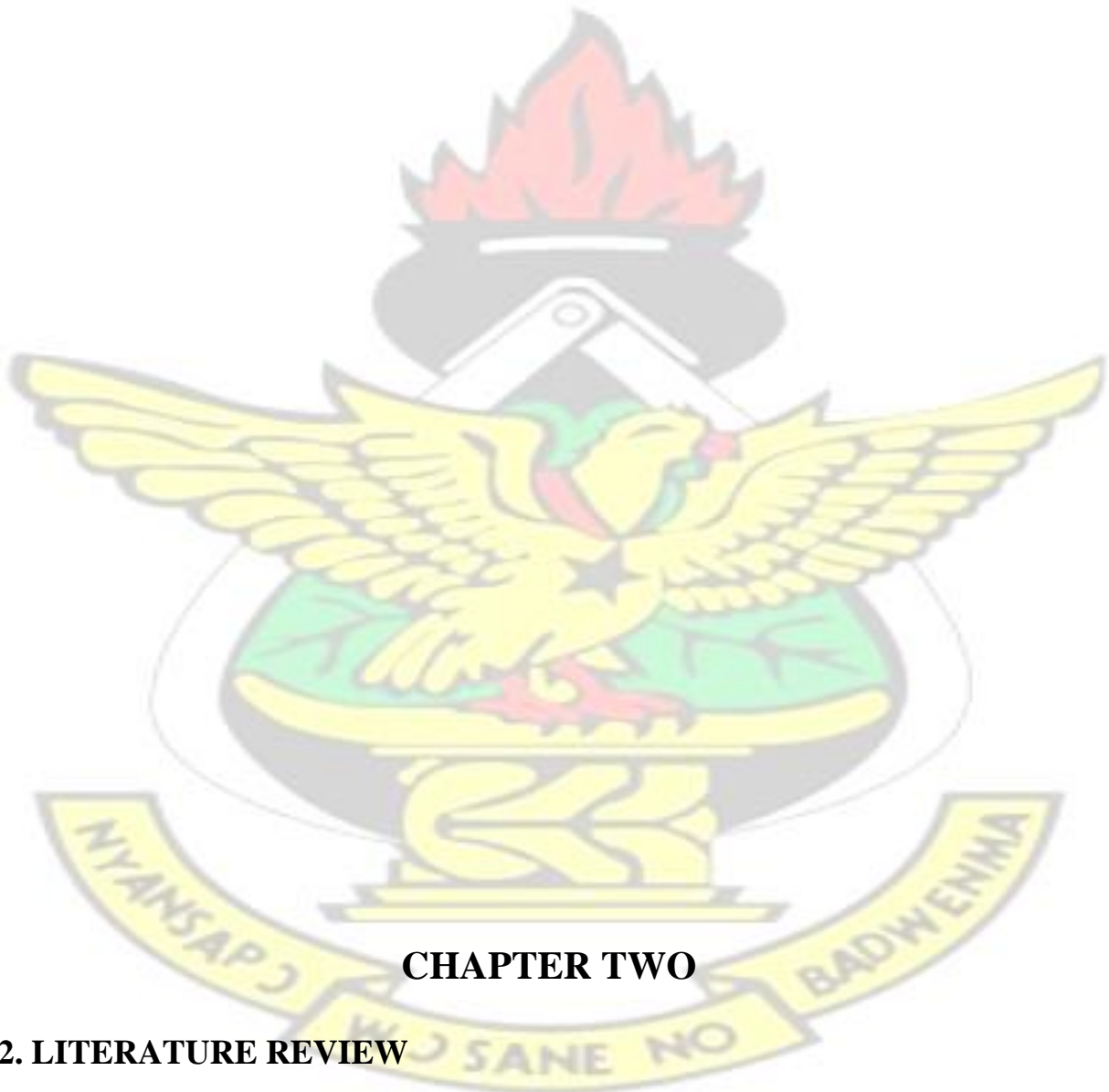
In general, experimental studies suggest that zeolites with a lower structural Si/Al ratio demonstrate greater capacity of arsenic removal due to the greater concentration of aluminol surface groups (Shevade and Ford 2004). Numerous studies so far have confirmed their excellent performance in the removal of metal cations from wastewaters (Baker *et al.*, 2009, Chojnacki *et al.*, 2004, Khachatryan 2014, Shaheen *et al.*, 2012). Current experimental methods provide an average picture of the zeolite. Complete information on local structure of zeolite clinoptilolite and reaction mechanism within the zeolite remain elusive (Ryder *et al.*, 2000).

## 1.5 Objectives

Though zeolite clinoptilolite has been identified as a candidate for arsenic removal from water, the exact adsorption sites, their relative stabilities and the characteristics of the environment where the arsenic species are located within the zeolite framework still remains unknown. The

distribution of the water molecules within the framework and their effect on adsorption also remains elusive. The current computer resources and first principles theoretical models make it possible to study these problems.

# KNUST



## **CHAPTER TWO**

### **2. LITERATURE REVIEW**

Zeolites have unique properties such as thermal stability, acidity, hydrophobicity / hydrophilicity of surfaces, ion-exchange capacity, low density and large void volume, uniform molecular size channels, adsorption for gas and vapor and catalytic properties. Adsorption of

the reactants is the key process for both separation and catalysis and this is the main focus of theoretical and experimental studies which target the design of new zeolites materials or modification of the available ones (Uzunova and Mikosch 2013b). The role of zeolites in the conversion of solid and liquid hazardous wastes into environmentally accepted products has also been demonstrated. Several zeolites namely Clinoptilolite, Chabazite, SZP, 13X and 5A have been identified as potential candidates for arsenic removal for water (Shevade and Ford 2004). Clinoptilolite has been the subject of numerous studies because it is available as natural zeolites in large deposits worldwide. Natural zeolites however find applications as ion-exchangers and adsorbents rather than catalysts because of their structure and pore sizes (Uzunova and Mikosch 2013b). It is known that dehydrated zeolites have excellent adsorption properties, and synthetic zeolites are widely used in drying and gas separation. Both mordenite-tuff and Clinoptilolite-tuff found in Japan were reported to show excellent adsorption properties compared with the commercial adsorbents silica and activated alumina (TOP 2001).

In 2004, Shevade and co-workers used synthetic zeolites (Y(6,40), ZSM-5(40), BETA(37.5), ferrierite(27.5)) in their  $H^+$  and  $NH_4^+$  form for arsenate removal from polluted water. It was found that  $H^+$ /Beta (HB) with Si/Al ratio 37.5,  $NH_4^+$ /Y (HY6) with ratio 6 and  $H^+$ /Y (HY6) with ratio 6 were very effective for removal of arsenate. In fact,  $NH_4^+$ /Y (NY6) removed arsenic to a concentration below 50 ppb, which is the current arsenic Minimum Contamination Level (MCL) established by the United State Environmental Protection Agency (USEPA).  $NH_4^+$ /Ferrierite (NFER)  $NH_4^+$ /ZSM-5 (NZ) and  $H^+$ /Y (HY40) were not effective in the arsenic removal reaction. This may be due to a higher concentration of terminal Al-OH species in low Si/Al ratio zeolite, which leads to a greater capacity for a ligand exchange reaction. This zeolite was stable over initial pH range 2-12 and showed a very effective arsenic removal over that pH range. The good performance of the NY6 zeolite over the wide initial pH range could be attributed to the pH buffering capacity of this zeolite. In general zeolites with lower structural

Si/Al ratio demonstrated greater capacity for arsenic removal due to the greater concentration of aluminol surface groups (Shevade and Ford 2004).

Li et al in 2007 reported a study on the sorption of arsenic by surfactant-modified zeolite and kaolinite that investigated the As sorption on SMZ and SMK as a function of As speciation (arsenate vs. arsenite), surfactant surface loading level, solution pH and ionic strength and counter ion desorption to elucidate the mechanism of As sorption on surfactant-modified minerals. It was found that when kaolinite was modified to 200% of its external cation exchange capacity (ECEC), the sorbed HDTMA molecules formed a bilayer surface configuration and reversed the surface charge to positive, resulting in sorption of anionic contaminants from water. In addition, the amine group in humid acids sorbed on kaolinite also contributed to the removal of arsenate from water. It was found that arsenate sorption is strongly affected by the surfactant surface coverage. With 0% surfactant surface coverage, the raw zeolite had no affinity for arsenate, which was different from the observation made earlier in which 70% of the input arsenic was removed. The difference could be attributed to Al content, an important factor for As sorption. The difference in sorption behavior between arsenate and arsenite could be attributed to different As sorption mechanism on the modified minerals. For arsenate sorption, the dominant mechanism is surface anion exchange, whereas surface complexation may be the mechanism for arsenite sorption. Therefore, the charge of surface charge had a minimal effect on arsenite sorption (Li *et al* 2007).

In 2004, Kucic et al. studied the sorption process for the removal of ammonium ions from aqueous solution using natural zeolite clinoptilolite at three different particle sizes (1-2mm, 2-4mm and 4-10mm). They reported that the adsorption capacity and removal efficiency rises with decreasing particle size of the zeolite. This is because the smaller the particle size, the greater the specific surface area, which promotes external surface adsorption. It was shown by

their work that clinoptilolite can be used as an adsorbent for removal of ammonia ions from aqueous solution but the adsorption mechanism was not known (Kucic *et al* 2012).

Arsenic has many allotropic forms, it is regularly present as yellow, black, or grey solids. Although its presence is not uniform around the world, countries which have levels high enough to cause concern include USA, China, Chile, Bangladesh, Taiwan, Mexico, Argentina, Poland, Canada, Hungary, Japan, India (Landau 1937) and Ghana. Arsenic contamination of underground drinking water sources has been a health risk for many parts of the world. Consequently, there is an urgent need to develop cost-effective methods for As removal from groundwater and wastewater (Li *et al* 2007). Arsenic exist in nature as As(III) in the form of arsenite or as As(V) in the form of arsenate depending on the ambient redox potential. Since As(III) is more mobile and more toxic than As(V) and is predominant in many ground waters, active remediation of As often require conversion of As(III) to As(V), and immobilization of both species. Sorption of arsenate and arsenite on clays and zeolites has been studied extensively in recent years. The mobility of arsenate As (V) and arsenite As (III) through porous media is controlled primarily by sorption reaction with metal hydroxides and aluminosilicates (Redman *et al* 2001).

Current experimental methods provide an average picture of zeolites; hence complete information on local structure and reaction mechanism within the zeolite remain elusive.

Computational methods have emerged as a powerful complementary tool to experimental methods. Using electronic structure calculations, one can obtain information pertinent to the local electronic and structural properties of the zeolite, and the potential energy hypersurface characterizing interactions with host molecules (Ryder *et al* 2000). A well-designed computer simulation can predict thermodynamic properties and can be a substitute for experiments. Molecular simulation can also provide data that is inaccessible through experimental methods or when experiment has components that are too dangerous or too expensive (Sánchez 2011).

In 2013, Mikosch and coworkers examined ethane adsorption in transition metal exchanged Clinoptilolite with cations Fe-Cu and also Pd by density functional theory with B3LYP functional, using the embedded cluster method in ONIOM. The periodic calculations were performed with Gaussian 09 using PBE density functional. They investigated the cation sites of clinoptilolite and reported four cation sites as also reported by Takeuchi and Kayomo (Koyama and Takeuchi 1977). They found that the ethene adsorption complex in Cu (I) MFI zeolites showed much higher adsorption energies of 175-194 kJmol<sup>-1</sup>. It can be expected that adsorption energies for cation-exchanged Clinoptilolite should be higher than those for FAU (80 – 100kJmol<sup>-1</sup>), because Clinoptilolite lacks six-membered rings where cations could be strongly confined and also because the adsorption energies of small hydrocarbons are known to increase with decreasing pore size (Uzunova and Mikosch 2013b).

## CHAPTER THREE

### 3. Computational Chemistry

Computational chemistry is a field of chemistry where mathematical theories incorporated in computer algorithms to help solve interesting chemical problems (Cramer 2013). It is an interdisciplinary subject, implying the synergy of quantum, classical and statistical mechanical physics, of chemistry and even biochemistry (to study biological systems) (Greeley 2002). Computational Chemistry generally complements experimental investigations and in some few cases replace them, when experiment is not practicable. Computational Chemistry is crucial in a number of cases:

1. Computational Chemistry is crucial in elucidating important mechanistic details that are difficult, if not impossible, to determine experimentally due to transient transition states that cannot be measured or detected experimentally.
2. In some cases, calculation is much simpler than experiment. An example is an important fundamental property of a surface such as the surface energy. It is very difficult to measure, and currently the best source of surface energies is calculations. It is very simple to change the lattice constant of a metal in a calculation and bring out the effect of strain on the reactivity without concern about the problems associated with straining a crystal in real life.
3. In certain cases, calculation is cheaper than experiment due to expensive or scarce chemicals or materials but computational chemistry is not so important in the interpretation of experimental results.
4. To predict and interpret the outcome of experimental results

The scope of applicability of Computational Chemistry is constantly expanding as theories and algorithms as well as hardware capabilities keep improving, from a qualitative to quantitative accurate account of experimental results. Apart from its application to molecular studies, it can also be used now to study more dense systems like materials, and surface reactions.

Computational Materials Science is a young discipline of condensed matter physics, which investigates several microscopic properties of materials, like structure properties (bond lengths and angles, crystal lattice parameters, surface reconstructions, structural phase transitions), electronic and transport properties, mechanical properties (bulk modulus, elastic constants), reactivity of surfaces, charge transfer, magnetic properties. Computational Materials Science is now an integral part for the study of materials at the atomistic scale towards the design of efficient materials with desired applications and an important new tool for researchers in the

fields of surface science and catalysis (Greeley 2002). Crystalline materials mostly occur in nature with defects which can now be mimicked in computer modeling.

### 3.1 Theoretical Background

#### 3.1.1 Computational Methods

There are two types of computational methods

1. Non-Quantum Chemistry/ Force Field methods
2. Quantum Chemistry Methods/ Electronic Structure methods
  - a. Semi-empirical Methods
  - b. Ab-initio Methods

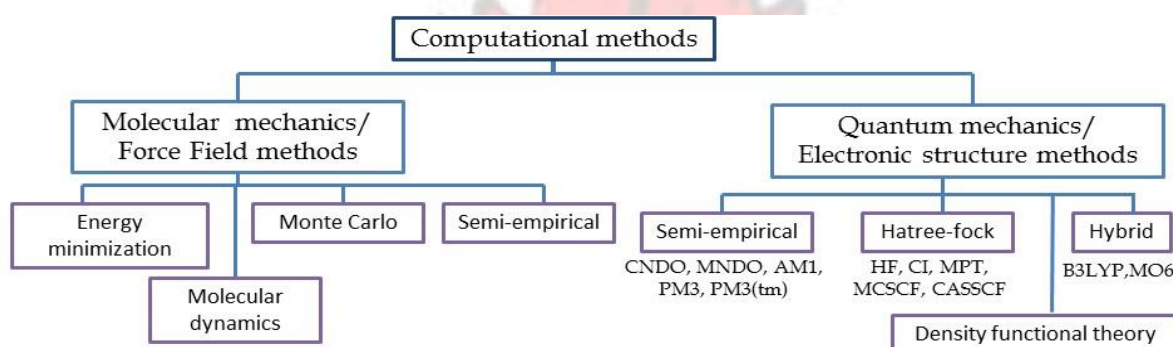


**Figure 1** Computational Method

**Table 1.** Some Strengths and Limitations of Computational Methods

Method	Advantages	Advantages	Disadvantages	Best for
MM	<ul style="list-style-type: none"> <li>•uses classical physics</li> <li>•relies on force-field with embedded empirical parameters</li> </ul>	<ul style="list-style-type: none"> <li>•Computationally least intensive - fast and useful with limited computer resources</li> <li>•can be used for molecules as large as enzymes</li> </ul>	<ul style="list-style-type: none"> <li>•particular force field applicable only for a limited class of molecules</li> <li>•does not calculate electronic properties</li> <li>•requires experimental data (or data from ab initio) for parameters</li> </ul>	<ul style="list-style-type: none"> <li>•large systems (thousands of atoms)</li> <li>•systems or processes with no breaking or forming of bonds</li> </ul>

Semi-Empirical	<ul style="list-style-type: none"> <li>•uses quantum physics</li> <li>•uses experimentally derived empirical parameters</li> <li>•uses approximation extensively</li> </ul>	<ul style="list-style-type: none"> <li>•less demanding computationally than ab initio methods</li> <li>•capable of calculating transition states and excited states</li> </ul>	<ul style="list-style-type: none"> <li>•requires experimental data (or data from ab initio) for parameters</li> <li>•less rigorous than ab initio)methods</li> </ul>	<ul style="list-style-type: none"> <li>•medium-sized systems (hundreds of atoms)</li> <li>•systems involving electronic transitions</li> </ul>
Ab Initio	<ul style="list-style-type: none"> <li>•uses quantum physics</li> <li>•mathematically rigorous, no empirical parameters</li> <li>•uses approximation extensively</li> </ul>	<ul style="list-style-type: none"> <li>•useful for a broad range of systems</li> <li>•does not depend on experimental data</li> <li>•capable of calculating transition states and excited states</li> </ul>	<ul style="list-style-type: none"> <li>•computationally expensive</li> </ul>	<ul style="list-style-type: none"> <li>•small systems (tens of atoms)</li> <li>•systems involving electronic transitions</li> <li>•molecules or systems without available experimental data ("new" chemistry)</li> <li>•systems requiring rigorous accuracy</li> </ul>

Computational Quantum Chemistry Methods calculate both energy and electronic structure while Non-Quantum Chemistry Methods calculate only energy and ignore the electronic structure of the system because nuclear and electronic constituents of the atoms are ignored and molecules are treated as a collection of hard balls linked by springs.

### 3.1.2 Electronic Structure Methods

The electronic structure methods attempt to solve the non-relativistic time independent Schrödinger equation

$$\hat{H}\Psi(\{R_A\}, \{r_i, \sigma_i\}) = E\Psi(\{R_A\}, \{r_i, \sigma_i\}) \quad (3.1)$$

For a system containing M nuclei and N electrons the many-body wave-function ( $\Psi$ ) is a function of all the spatial coordinates of nuclei ( $\{R_A\}$ ,  $A = 1, \dots, M$ ) and spatial and spin coordinates of electrons ( $\{r_i, \sigma_i\}$ ,  $i = 1, \dots, N$ ). The Hamiltonian ( $\hat{H}$ ) is a sum of all possible interactions between electrons and nuclei. In atomic units (energy in Hartree and length in Bohr),  $\hat{H}$  is given by:

$$\hat{H} = -\sum_{i=1}^N \frac{\nabla_i^2}{2} + \sum_{A=1}^M \frac{\nabla_A^2}{2M_A} + \sum_{i=1}^N \sum_{j>i}^N \frac{1}{|r_i - r_j|} + \sum_{i=1}^N \sum_{A=1}^M \frac{Z_A}{|r_i - R_A|} - \sum_{A=1}^M \sum_{B>A}^M \frac{Z_A Z_B}{|R_A - R_B|} \quad (3.2)$$

In the equation above,  $M_A$  is the ratio of the mass of nucleus A to the mass of an electron and  $Z_A$  is the atomic number of nucleus A. The  $\nabla_i^2$  and  $\nabla_A^2$  are the Laplacian operators. The first two terms in equation (3.2) represent the kinetic energies of all the electrons and nuclei respectively. Equation (3.1) is deceptively simple by its form but enormously complex to solve and hence several approximations are made to make it solvable for many body systems. The first is the Born-Oppenheimer approximation which simplifies the full equation into nuclear and electronic equations, where the nuclear part is a constant. The Born-Oppenheimer approximation relies on the fact that atomic nuclei move thousands of times slower than electrons, which allows the dynamics of the electrons and nuclei to be decoupled and nuclei considered to be static relative to electrons. Hence for a given nuclear configuration the electrons are assumed to remain in their instantaneous ground state. As a result, the second term in equation (3.2) can be neglected and the fourth term, the repulsion between nuclei, can be treated as a constant for a fixed configuration of the nuclei. The remaining terms in equation (3.2) are called the electronic Hamiltonian ( $\hat{H}_e$ ),

$$\hat{H}_e = -\sum_{i=1}^N \frac{\nabla_i^2}{2} + \sum_{i=1}^N \sum_{j>i}^N \frac{1}{|r_i - r_j|} - \sum_{i=1}^N \sum_{A=1}^M \frac{Z_A}{|r_i - R_A|} \quad (3.3)$$

The full electronic Schrödinger equation becomes,

$$\hat{H}_e \Psi_e(\{R_A\}, \{r_i, \sigma_i\}) = E_e \Psi_e(\{R_A\}, \{r_i, \sigma_i\}) \quad (3.4)$$

The electronic wave function ( $\Psi_e$ ) depends on nuclear coordinates ( $\{R_A\}$ ) only parametrically now, thus for fixed configuration of nuclei  $\{R_A\}$  is suppressed. Furthermore, for simplicity electronic spatial and spin coordinates ( $\{r_i, \sigma_i\}$ ) are put together in to one variable  $\{x_i\}$

(i.e.,  $\{x_i\} = \{r_i, \sigma_i\}$ ) and equation (4) is rewritten as,

$$\hat{H}_e \Psi_e(\{x_i\}) = E_e \Psi_e(\{x_i\}) \quad (3.5)$$

The total energy for some fixed configuration of the nuclei will then be a sum of the electronic energy from equation (3.5) and the constant nuclear repulsion term leading to,

$$E_{total} = E_e + \sum_{A=1}^M \sum_{B>A}^M \frac{Z_A Z_B}{|R_A - R_B|} \quad (3.6)$$

The Born-Oppenheimer approximation enables the construction of the potential energy surfaces (PES's), where for a given electronic configuration the solution of the time independent Schrödinger equation (TISE) for many different nuclear arrangements permits the construction of potential energy surfaces (PES's). For systems of interest with more than two electrons, the many body electronic problem is difficult to solve analytically leading to further approximations. There are two basically different approaches to the calculation of the electronic structure and total energies of molecules and solids; the wave-function-based methods and the density functional theory (DFT) methods (Koch and Holthausen 2001).

### 3.1.3 Wavefunction Methods

The wave function methods are based on the Hartree-fock self-consistent field (HFSCF) approximation. The Hartree-fock methods are variational methods and the first step to determination of the many electron wave function  $\Psi$ , is often by a simple educated guess and then reliance on the variational principle. The variational principle shows that the expectation value of the electronic Hamiltonian  $H_e$  of any guessed or trial wave function is always upper bound than the electronic ground state energy  $E_0[\Psi_0]$  and the equality will hold only when the wavefunction is in the true ground state  $\Psi_0$ , i.e., ( $E[\Psi] \geq E_0[\Psi_0]$ ). The advantage of the variational principle is that starting with a trial wave function one can approach towards the ground state energy  $E_0[\Psi_0]$  by variationally improving the quality of the wave function. In the HFSCF approach, the many electron wave-function of N-electrons  $\Psi(\{x_i\})$  can be approximately described with a single Slater determinant. A Slater determinant is a linear combination of the product of independent electron wave functions ( $\{\varphi_i x_i\}$ ) (also known as

spin orbitals) with all possible combinations of the permutations of their coordinates. Also the Slater determinant satisfies the anti-symmetric property of the electronic wave function, which is essential because the electrons are fermions and obey the Pauli's exclusive principle. For the N-electron system the HF wave-function is,

$$\Psi(\{x_i\}) \approx \Psi^{HF}(\{x_i\}) = \frac{1}{\sqrt{N!}} \begin{bmatrix} \varphi_i(x_i) & \varphi_j(x_i) & \cdots & \varphi_N(x_i) \\ \vdots & \vdots & \ddots & \vdots \\ \varphi_i(x_N) & \varphi_j(x_N) & \cdots & \varphi_N(x_N) \end{bmatrix} \quad (3.7)$$

In the Slater determinant each of the columns are labeled by spin orbitals and exchange of two electron coordinates will interchange the two columns inside the determinant, thus satisfying the anti-symmetric requirement. The anti-symmetric property of the Slater determinant can be simply realized considering a two-electron system:

$$\Psi(x_1, x_2) = \frac{1}{\sqrt{2!}} [\varphi_1(x_1)\varphi_2(x_2) - \varphi_2(x_1)\varphi_1(x_2)] = -\Psi(x_2, x_1) \quad (3.8)$$

Now using the HF wave function the electronic energy can be rewritten as;

$$\begin{aligned} E_{HF} &= \langle \Psi_{HF} | \hat{H}_e | \Psi_{HF} \rangle \\ &= \sum_{i=1}^N \int \varphi_i^*(x_i) \left[ -\frac{\nabla_i^2}{2} + V^{ext}(x_i) \right] \varphi_i(x_i) dx_i \\ &\quad + \frac{1}{2} \sum_{i=1}^N \sum_{j=1}^N \int \int \varphi_i^*(x_i) \varphi_j^*(x_j) \frac{1}{|r_i - r_j|} \varphi_j(x_j) \varphi_i(x_i) dx_i dx_j \\ &\quad - \frac{1}{2} \sum_{i=1}^N \sum_{j=1}^N \int \int \varphi_i^*(x_i) \varphi_j^*(x_j) \frac{1}{|r_i - r_j|} \varphi_j(x_i) \varphi_i(x_j) dx_i dx_j \end{aligned} \quad (3.9)$$

The above equation can be treated as energy functional,  $E^{HF}[\{\varphi_i^*(x_i)\}, \{\varphi_i(x_i)\}]$ , and can be minimized variationally by applying Lagrange undetermined multiplier subject to the constraints that the independent electron wave function  $\{\varphi_i(x_i)\}$  are orthonormal i.e.,  $\langle$

$\varphi_i(x_i)\varphi_j(x_j) > = \delta_{ij}$ . This leads to a mapping from a complex N-electron Schrödinger equation in to effective one-electron Schrödinger-like equations

$$F_i\varphi_i(x_i) = \epsilon_i\varphi_i(x_i),$$

$$\hat{F}_i = -\frac{\nabla^2}{2} + V^{ext}(x_i) + V^{Hartree}(x_i) + V_i^{Exchange}(x_i) \quad (3.10)$$

$\hat{F}_i$  represents a one-electron Hamiltonian, known as the Fock operator.  $\epsilon_i$  and  $\varphi_i$  are the corresponding eigenvalues and eigenvectors, respectively. The first two terms in  $F_i$  are, respectively, the kinetic energy of n independent electron and the external potential. The external potential,  $V^{ext}(x_i)$ , is the coulomb attraction on the  $i^{th}$  electron due to all the nuclei. The third and fourth terms approximately account for the many body electron-electron interactions.  $V^{Hartree}(x_i)$  is the Hartree potential, which is the Coulomb repulsion between the  $i^{th}$  electron and the electron density produced by all electrons

$$V^{Hartree}(x_i) = \int \frac{n(x_j)}{|r_i - r_j|} dx_j,$$

$$n(x_j) = \sum_{j=1}^N |\varphi_j(x_j)|^2 \quad (3.11)$$

The fourth term solely appears from the antisymmetric nature of the wave function and is known as exchange potential ( $V_i^{Exchange}(x_i)$ ).

Unlike  $V^{ext}(x_i)$  and  $V^{Hartree}(x_i)$ ,  $V_i^{Exchange}(x_i)$  does not have any classical analogy, and it can only be written as an integral operator

$$V_i^{Exchange}(x_i)\varphi_i(x_i) = \left[ \sum_{j=1}^N \int \varphi_j^*(x_j) \frac{1}{|r_i - r_j|} \varphi_j(x_j) dx_j \right] \varphi_i(x_j) \quad (3.12)$$

As evident from the above equation,  $V_i^{Exchange}(x_i)$  leads to an exchange of the variable in the two spin orbitals. Furthermore, the exchange operator  $V_i^{Exchange}(x_i)$  is said to be a nonlocal

operator, as the results of  $V_i^{Exchange}(x_i)$  operating on the spin orbitals  $\varphi_i(x_i)$  will depend on the value of  $\varphi_i(x_i)$  throughout all space. Also when  $i = j$ , the last two terms in equation (3.9) cancel each other, and so by construction the HF method is self-interaction free. Equation (3.10) is the usual form of the HF equation, which is a linear eigenvalue problem and must be solved self-consistently. The HF method treats the exchange interaction between electrons with the same spin exactly and is an exact exchange approach. The HF method is applied extensively to study various materials science problems, such as adsorption, defects in solids and electronic structure of insulators.

A major drawback lies in the effective mean field treatment of the Coulomb repulsion between electrons, which provides an inaccurate description of the spatial separation of the electrons as it would be in a completed many-electron interaction. This missing part is widely designated as electron correlation. The difference between the ground state HF energy and the exact ground state energy is used as a standard definition of the correlation energy in quantum chemistry. The correlation energy is typically a small fraction of the total energy. However, it can be a very important contribution to many systems of physical and chemical interest.

An iterative scheme is used to solve the equation above. It involves the choice of initial guesses for the one-electron wave-functions (usually written as linear combinations of basis functions), the calculation of an average electron-electron interaction energy (which depends on all of the one-electron orbitals) from these wave-functions, the insertion of this interaction energy term as part of  $v$  in Equation (3.4), and the solution of Equation (3.4) for improved one-electron orbitals. This process is repeated until orbital convergence (self-consistency) is obtained. Full self-consistency in the HFSCF method requires  $N^4$  calculations, where  $N$  is the number of basis functions used.

Although this solution technique is appealing in its simplicity, the HFSCF approach gives very inaccurate molecular energies. The problem stems primarily from the lack of explicit electron correlation (EC) effects in the technique. Only correlation exchange effects imposed by the anti-symmetric wave function are accounted for; the neglect of other correlation energies can give very poor results. Good methods of correcting for this deficiency do exist, but they are generally extremely computationally expensive e.g. Configuration interaction (CI), Moller-Plesset perturbation theory, and Coupled Cluster. CI methods make use of unoccupied (virtual) states to account for correlation effects. The mechanics of the technique are very similar to the HFSCF technique, but additional (unoccupied) one-electron wave functions are used to construct the total wave function. This procedure essentially allows the incorporation of excited electron configurations into the wave function. The result of CI calculations is an accurate solution of the TISE but at extreme computational cost (the HFSCF method requires calculations per basis function, while CI methods can require more than  $N$  calculations per basis function). Typically, excitations beyond the triple excitation level are infeasible computationally, and the method is truncated at that point.

Quantum Monte Carlo (QMC) techniques present an alternative to CI methods for the incorporation of electron correlation effects into electronic structure calculations. These techniques use random sampling approaches to calculate energies for many-electron systems. In the Variational Monte Carlo method, for example, random sampling is used to evaluate integrals that arise naturally during CI calculations. In the Diffusion Monte Carlo method, on the other hand, the Schrödinger equation is recast into an integral Green's function form, and the Green's function is approximated by successive Monte Carlo sampling. QMC techniques are computationally expensive, but they are beginning to be applied to realistic solid-state systems. These techniques have many attractive features; they offer the possibility of obtaining exact solutions to the TISE, and they are well suited to describe systems where electronic

interactions are particularly important, such as superconductors, materials with large low-temperature-specific heat coefficients, and systems where van der Waals forces play a significant role. The computational burden of the exact calculation of correlation effects make sit highly desirable to use an approximate scheme for evaluating such effects (Greeley 2002).

### 3.1.4 Density Functional Theory Method

There are two basically different approaches to the calculation of the electronic structure and total energies of molecules and solids; the wave function-based methods and the density functional theory methods. The former, which can be accurate if high level of configuration interactions is included, is currently limited to 10 – 100 electrons. This generally makes these methods unattractive for routine treatments of complex systems needed to be modelled (Hammer and Nørskov 2000). An important advantage of using electron density over the wave function is the much reduced dimensionality. Regardless of how many electrons one has in the system, the density is always three dimensional. This enables DFT to readily be applied to much larger systems, hundreds or even thousands of atoms become possible. Partly for this reason, DFT has become the most widely used electronic structure approach today, particularly in the condensed matter physics community. Density functional theory describes how the ground state electron-density and total energy can be obtained by solving a set of one-electron Schrödinger equations (Kohn-Sham equations) instead of the complicated many electron Schrödinger equation. This results in an enormous computational simplification, and systems with more than 1000 electrons can be treated (Parr *et al.*, 1989, Parr 1980, Parr and W. Yang 1989, Jones and O. Gunnarsson 1989, Geerlings *et al.*, 2003, Ziegler 1991).

First, the electron density is defined as

$$n(r) = N \int \dots \int |\varphi(x_1, x_2 \dots x_N)|^2 d\sigma_1 dx_2 \dots dx_N \quad (3.13)$$

where  $\{x_i\}$  represent both spatial and spin coordinates.  $n(r)$  determines the probability of finding any of the  $N$  electrons within the volume  $r$  but with arbitrary spin while the other  $N-1$  electrons have arbitrary positions and spin in the state represented by  $\psi$ . This is a nonnegative simple function of three variables  $x$ ,  $y$  and  $z$ , integrating to the total number of electrons,

$$N = \int n(r) dr \quad (3.14)$$

### 3.1.4.1 The Kohn-Sham Equations

In 1965, Kohn and Sham published a paper which transformed density functional theory into a practical electronic structure theory. Kohn and Sham recognized that the failure of Thomas-Fermi theory mainly resulted from the bad description of kinetic energy. To address this problem (similar to the Hartree-Fock approaches) they re-introduced the idea of noninteracting electrons moving in an effective field.

The functional form of  $F_{HK}[n(r)]$  is written as a sum of the kinetic energy of non-interacting electrons ( $T_s$ ), the Hartree energy ( $E^{Hartree}$ ), and all the many-body quantum effects are put together in to the exchange and correlation energy ( $E_{xc}$ ). Thus the energy functional is

$$E[n] = \int n(r)v(r)dr + F_{HK}[n(r)] \quad (3.15)$$

where  $F_{HK}$  is a universal functional of  $n(r)$ ,

$$F_{HK}[n(r)] = \int n(r)v(r) + T_s[n(r)] + E^{Hartree}[n(r)] + E_{xc}[n(r)] \quad (3.16)$$

$$v_{eff} = \frac{\delta \{ \int n(r)v(r)dr + T_s[n(r)] + E^{Hartree}[n(r)] + E_{xc}[n(r)] \}}{\delta n(r)}$$

$$= v(r) + \int \frac{n(r')}{|r-r'|} dr' + v_{xc}(r) \quad (3.17)$$

where  $v_{xc}(r)$  is the exchange-correlation potential defined as;

$$v_{xc}(r) = \frac{\delta E_{xc}[n(r)]}{\delta n(r)} \quad (3.18)$$

This leads to the central equation in Kohn-Sham DFT which is the one-electron Schrodinger like equation expressed as;

$$[-\frac{1}{2}\nabla^2 + V^{eff}]\phi_i = \epsilon_i \phi_i \quad (3.19)$$

here  $\{\phi_i\}$  are the Kohn-sham one-electron orbitals and the electron density is defined as

$$n(r) = \sum_{i=1}^N |\phi_i|^2 \quad (3.20)$$

The  $\epsilon_i$ 's are the energies of the Kohn-Sham one-electron orbitals. Clearly, this is a HartreeFock like single particle equation which needs to be solved iteratively. Finally, the total energy can be determined from the resulting density through

$$E = \sum_{i=1}^N \epsilon_i - \frac{1}{2} \iint \frac{n(r)n(r')}{|r-r'|} + E_{xc}[n] - \int v_{xc}(r)n(r)dr \quad (3.21)$$

Equations (3.17), (3.19) and (3.20) are the celebrated Kohn-Sham equations. The  $V^{eff}$  depends on  $n(r)$  through (3.20). So the Kohn-Sham equation must be solved self-consistently. The general procedure is to begin with an initial guess of the electron density, construct the  $V^{eff}$  from (3.17), and then get the K-S orbitals. Based on these orbitals, a new density is obtained from (3.20) and the process is repeated until convergence is achieved. Finally, the total energy will be calculated from the equation (3.21) with the final electron density. If each term in the K-S energy functional was known, we would be able to obtain the exact ground state density and total energy. Unfortunately, there is one unknown term, the exchange – correlation (xc) functional ( $E_{xc}$ ). Exc includes non-classical aspects of the electron-electron interaction along with the component of the kinetic energy of the real system different from the fictitious non-

interacting system. Since Exc is not known exactly, it is necessary to approximate it (Sc. Biswajit Santra 2010).

### 3.1.5 Exchange-Correlation Functional

The two exchange-correlation functionals that are the local density approximation (LDA) and the generalized gradient approximation (GGA), which are both approximations to the exact and unknown exchange-correlation functional (Filippi *et al* 1996). The local density approximation makes the assumption that the exchange and correlation contributions to the energy as a function of density at a point are exactly the same as a homogeneous system with the same density. The generalized gradient approximation attempts to improve LDA by including the magnitude and direction of the gradient. GGA improves upon LDA for the calculation of atomic and molecular total energies, and the lattice parameters of solids. In general, the overestimation of the lattice constants using GGA is much less than the underestimation of the lattice constants using LDA (Cassandras *et al* 1998, Perdew *et al* 1996).

#### 3.1.5.1 Local Density Approximation

The local density approximation (LDA) is the first approximation to the exchange-correlation energy. This approximation is based on the assumption that the exchange correlation energy of a real system behaves locally as in a uniform electron-gas having the same density. Within the LDA, the exchange-correlation ( $E_{xc}$ ) has the form:

$$E_{xc}[\rho(r)] = \int \rho(r) \varepsilon_{xc}^{LDA}(r) dr \quad (3.22)$$

where  $\varepsilon_{xc}^{LDA} = \varepsilon_{xc}^{hom}[\rho(r)]$  is the exchange-correlation energy density of the homogeneous system assumed.

A formulation of the exchange-correlation functional depending only on the total electron density should give an exact description of real systems (A. Malashevich 2009), however, the treatment of magnetic systems is much easier if the exchange-correlation energy functional is

explicitly considered as dependent on the two spin populations separately. Then, LDA is extended to include spin polarization and results in what is known as the local spin density approximation LSDA, which is the most general local approximation. It can be formulated in terms of either the two spin densities  $\rho^\uparrow(r)$  and  $\rho^\downarrow(r)$  or the total density  $\rho(r)$  and the fractional spin polarization  $\xi = \frac{\rho^\uparrow(r) - \rho^\downarrow(r)}{\rho(r)}$ . In the LSDA, the Kohn-Sham equations are solved independently for electrons with different spin orientation.

LDA, because of the assumption of slowly varying density, works very well for free electronlike metals and is strictly valid only if the charge density is slowly varying. Considerable effort has been exerted to cure some of the deficiencies. Now, many extensions are available which give improved accuracy for systems with strongly correlated electrons, such as the manganites (Madsen and Novák 2005).

### 3.1.5.2 Generalized Gradient Approximation

There are different techniques that go beyond the homogeneous electron gas approximation so as to overcome some of the deficiencies of the LDA. As a first alternative, but connected approach, is to build a “semi-local” functional that depends not only on the density at  $r$  but also on its gradient, or on higher order gradient extensions. Different forms have been proposed that are summarized under the label of Generalized Gradient Approximations. They are all based on a functional of the type (Filippi *et al* 1996, Perdew *et al* 1996).

$$E_{xc}^{GGA}[\rho] = \int \rho(r) \epsilon_{xc}^{GGA}[\rho(r); |\nabla\rho(r)|] dr \quad (3.23)$$

By including the gradient of the density in the exchange-correlation functional some nonlocality is introduced to the previously local functional.

Standard DFT approximations (LDA, LSDA, GGA) often fail to correctly describe strongly correlated systems (M. Cococcioni 2002, Baroni *et al* 2001, Ravindran *et al* 2004, Anisimov *et*

al 1997). These systems contain localized, atomic-like electronic states, typically originating from d or f atomic states, together with delocalized, band-like states originating from s and p states. The electrons in a strongly correlated system are localized in the same shell and subjected to strong Coulomb repulsion. In a homogeneous-gas treatment, the LDA does not distinguish electrons as separate entities in the electron gas, and the effects of localization of electrons are not reproduced. The LDA+U method, which takes into account the orbital dependence of the Coulomb and exchange interactions, is quite efficient to study the band structures of strongly correlated systems (Anisimov *et al* 1997).

### 3.1.5.3 The Meta-GGAs

These are the third generation functionals (third rung of Jacob's ladder) and use the second derivative of the density,  $\nabla^2 n(r)$ , and/or kinetic energy densities,  $\tau_\sigma(n) = \frac{1}{2} \sum_i |\nabla \varphi_i(n)|^2$ , as additional degrees of freedom. In gas phase studies of molecular properties meta-GGAs such as the TPSS functional have been shown to offer improved performance over LDAs and GGAs.

### 3.1.5.4 The hybrid functionals

These fourth generation functionals add “exact exchange” calculated from the HF functional to some conventional treatment of DFT exchange and correlation. The philosophy behind the hybrid functional is rooted in the “adiabatic connection” equation, which is a rigorous *ab initio* equation for the exchange-correlation energy of DFT. One conventional expression of this equation is:

$$E_{xc} = \int_0^1 U_{xc}^\lambda d\lambda, \quad (3.24)$$

where  $\lambda$  is an inter electronic coupling strength parameter that switches on the  $\frac{1}{|r_i - r_j|}$  coulomb repulsion between electrons, and  $U_{xc}^\lambda$  is the potential energy of exchange and correlation at  $\lambda$ . This equation connects the non-interacting reference system with the fully interacting one at

density  $n(r)$ . Recognizing that the non-interacting  $\lambda=0$  limit is nothing more than HF exchange, it is expected that exact exchange must play a role in “better” of exchange correlation functionals and thus LDA and GGA exchange and correlation functionals are mixed with a fraction of HF exchange.

The most widely used, particularly in the quantum chemistry community, is the B3LYP functional which employs three parameter,  $a_{1-3}$  (determined through fitting to experiment) to control the mixing of the HF exchange and density functional exchange and correlation. It has the following form:

$$E_{xc} = E_{xc}^{LDA} + a_1(E_x^{HF} - E_x^{LDA}) + a_2\Delta E_x^{GGA} + a_3\Delta E_c^{GGA}. \quad (3.25)$$

Here B88 and LYP are used as GGA exchange and correlation. Reformulating this to eliminate two parameters leads to an equation of the form

$$E_{xc} = E_x^{GGA} + a(E_x^{HF} - E_x^{GGA}) \quad (3.26)$$

And setting  $a=1/4$  (based on the grounds of perturbation theory) leads to a class of functionals with only as many parameters as their underlying GGAs. If PBE is the GGA used in equation (3.26) then the hybrid PBE0 functional is obtained. Another popular hybrid functional is BH&HLYP, which has 50% HF exchange. Such functionals have been shown to offer noticeably improved performance over LDA and GGA functionals for the calculation of gas phase properties of molecules and solids.

In the fourth rung are the hybrid meta-GGA functionals, which is a combination of metaGGA and hybrid functionals with suitable parameters fitted to various molecular databases.

Among many, MPWB1K and PW6B95 have been used in this thesis.

Beyond these few rungs of Jacob’s ladder, there are other XC functionals of increasing complexity. However, adding complexity by climbing higher on Jacob’s ladder or by obeying more and more constraints does not necessarily bring improved performance in total energies (Hamann 1997).

LDA calculations often produce poor estimates of binding energies and molecular structures. State-of-the-art GGA calculations (together with suitable models for the surface structure, discussed below), however, can give much better values. Bond lengths and solid lattice constants, for example, are reproduced to within several hundredths of an angstrom, and vibrational frequencies are calculated with an accuracy of 5%. Comparison of calculated adsorption energies with experimental values (which are obtained most accurately from Single-Crystal Adsorption Calorimetry) demonstrates that these energies can be found to within 0.15 eV (Greeley 2002).

### **3.1.6 Basis Sets**

Essentially, almost all electronic structure methods today rely on an expansion on the unknown wave function in terms of a set of basis functions. There are two types of basis sets, localized (e.g. gaussians, atomic orbitals, linearized muffin tin orbitals (LMTOs), etc.) and delocalized i.e. Plane waves (including augmented plane waves (LAPWs), etc.) The choice depends on preference and the kind of problem studied. Localized functions are the usual choice in cluster-type models, whereas both localized (LMTOs) and plane waves are used in slab-type calculations. The slab models require the use of a periodic basis set to match the boundary conditions; plane waves are often used for this purpose. This basis works well for periodic systems, although convergence can be slow where there are sharp electron density gradients. The inclusion of some atomic orbitals (exactly represented with plane waves) has been shown to speed convergence for some systems.

### **3.1.7 The plane wave pseudopotential method**

The plane wave pseudopotential (PWPP) method is one of the most widely used implementations of DFT (Hill 2002, Martin 2005). In the PWPP method, plane wave basis set is used to expand the electronic wave functions and pseudopotentials to model the electron-ion

interactions. Plane waves have many attractive features. They are simple to use, orthogonal by construction, and unbiased by atomic positions. PW basis set, in principle, is only complete in the limit of infinite number of plane waves. However, in practical calculations, we deal with a finite number of plane-waves and choose those contained in a sphere of maximum energy  $E_{cut}$ .

$$-\frac{1}{2}\nabla^2|K + G|^2 \leq E_{cut} \quad (3.27)$$

Unlike calculations based on localized (atomic-like) basis sets, those made with plane waves can be simply checked for convergence by increasing the size of the basis set, as given by the kinetic energy cutoff. The energy cutoff is the only parameter in the theory, which controls the accuracy of the description of our system. The accuracy of the calculations can be improved by increasing the value of the energy cutoff and studying the convergence of the properties we are interested in. The especially important advantage of using PW basis set lies in the fact that the Pulay (Giannozzi 2007) terms are absent in the calculation of the derivatives of the energy. As a consequence, the Hellmann-Feynman expressions for force and force constants are valid without any correction (Giannozzi 2007, Baroni *et al.*, 2001). Plane waves are used in conjunction with pseudopotentials. Pseudopotential is an effective potential constructed to replace the atomic all-electron potential such that the core states are eliminated and the valence electrons are described by nodless pseudo-wavefunctions. The pseudopotential approximation, which is based on the assumption that the most relevant physical properties of a system are brought about by its valence electrons only, treats each nucleus together with its core electrons as a frozen core that doesn't change in response to changes in its environment. The valence electrons thus move in the effective external field produced by these inert ionic cores and the pseudopotential tries to reproduce the interaction of the true atomic potential on the valence states without explicitly including the core states in the calculations. This provides a rational way to isolate the fundamental role of electrons in the electronic structure problem.

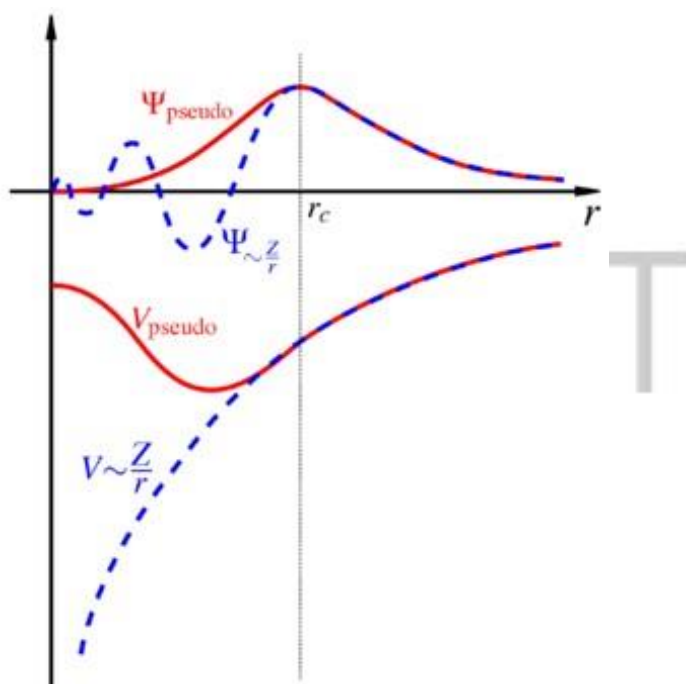


**Figure 2.** Sketch of the all-electronic wave function and electronic potential (solid lines) plotted against distance from the atomic nucleus. The corresponding pseudo wave function and potential (dashed lines) are plotted. Outside a given radius,  $r_c$ , the all-electron and pseudo electron values are identical.

## CHAPTER FOUR

### 4. COMPUTATIONAL METHODS

The structure optimization and total free energy calculations were performed using the density functional theory method (DFT) with plane wave basis and the ultra-soft (Vanderbilt) pseudopotential within the Quantum opEN Source Package for Research in Electronic Structure, Simulation, and Optimization (Espresso). This is an open source full ab-initio package implementation of electronic structures and energy calculation, linear response methods (to calculate phonon dispersion curves, dielectric constants and Born effective

charges) and third-order anharmonic perturbation theory. It uses both norm-conserving pseudopotentials (PP) and ultrasoft pseudopotentials (US-PP), within the DFT (Anon 2008).

The periodic calculation were performed with the generalized gradient approximation (GGA) using the Perdew-Burke Ernzerhof (PBE) exchange-correlation functional to represent the potential of the nuclei and core electrons of atoms, and a plane-wave basis with an energy cutoff of 30 Ryd to represent Kohn-Sham wavefunctions. GGA for the exchange correlation energy improve upon the local spin density (LSD) description of atoms, molecules and solids. The functional form is adopted, which ensures the normalization condition and that the exchange hole is negative definite. This leads to an energy functional that depends on both the density and its gradient. GGAs tend to improve total energies, atomization energies, energy barriers and structural energy differences. PBE exchange correlation is a simplification and improvement of Perdew-Wang 1991 (PW91), which yields almost identical numerical results with simpler formulas from a simpler derivation. Improvement over PW91 include an accurate description of the linear response of the uniform electrons gas, correct behavior under scaling, and a smoother potential. Integration over the Brillouin zone is carried out using the Monkhorst–Pack scheme (Pack and Monkhorst 1977) with a 1 x 1 x 1 mesh of k-points, and occupation numbers are treated according to the Methfessel–Paxton scheme (Methfessel and Paxton 1989) with a broadening of 0.003 Ry. Structural relaxation is carried out in each case to minimize the energy using the Broyden–Fletcher–Goldfarb–Shanno (BFGS) based method (Fletcher 2013).

The unit cell of the purely siliceous clinoptilolite was modelled in the monoclinic (space group) structure consisting of 108 atoms with general formula  $\text{Si}_{36}\text{O}_{72}$ . A full optimization was performed on the initial siliceous zeolite to obtain the relaxed unit cell parameters and the interatomic bond distances and angles. Having obtain the relaxed structure of the purely siliceous clinoptilolite zeolite, the Si/Al ratio in the range 1.7-8 were examined. Thus, for a

given Si/Al ratio, the algorithm first randomly substitutes the required number of some of the Si atoms with Al, beginning from the Si atoms at the tetrahedral sites in the pores. Additional constraints were applied, the most useful being that of the Löwenstein's rule (Koyama and Takéuchi 1977), where no Al-O-Al linkage are permitted and Dempsey's rule for maximum separation of negative framework charges (Uzunova and Mikosch 2013a). Extra framework cations were then inserted to compensate each Al by placing it in the same plane as the Al and two randomly selected oxygen to which the Al is bonded. These structures were visualized using the XCrysSDen (Kokalj and Causà 2000) package for proper choice of bravais lattice which will ensure utilization of symmetry to reduce computation time significantly. The structural rearrangement which was done using p4Vasp package became critical as the number of Al and cations increased. For example, the presence of a single Al in the framework will be compensated by a cation that will coordinate directly to the oxygen atoms adjacent to the Al. However, when multiple Al sites are close together, it becomes more difficult to envisage how to incorporate multiple cations within the pores of the material (French *et al* 2011).

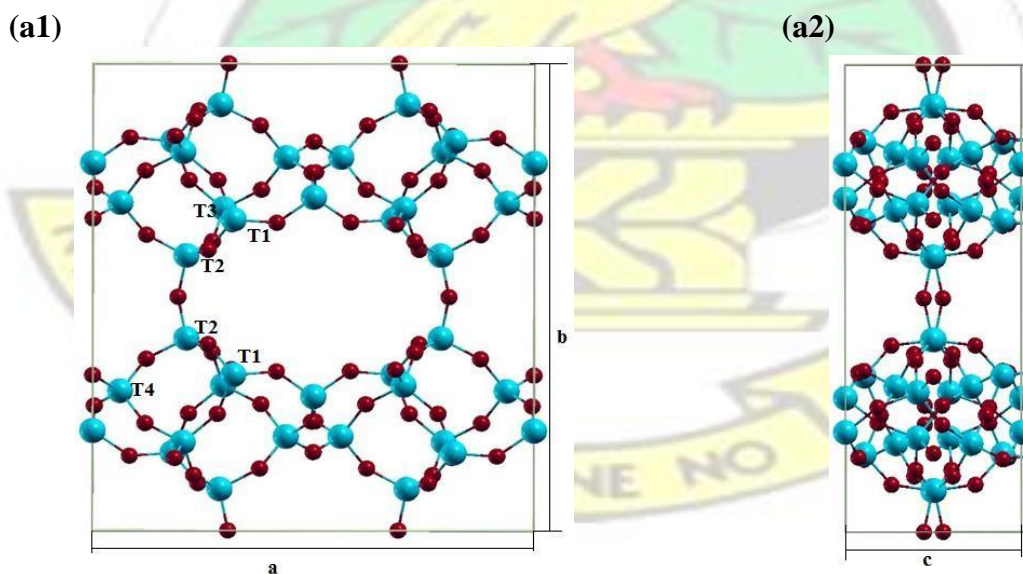
## CHAPTER FIVE

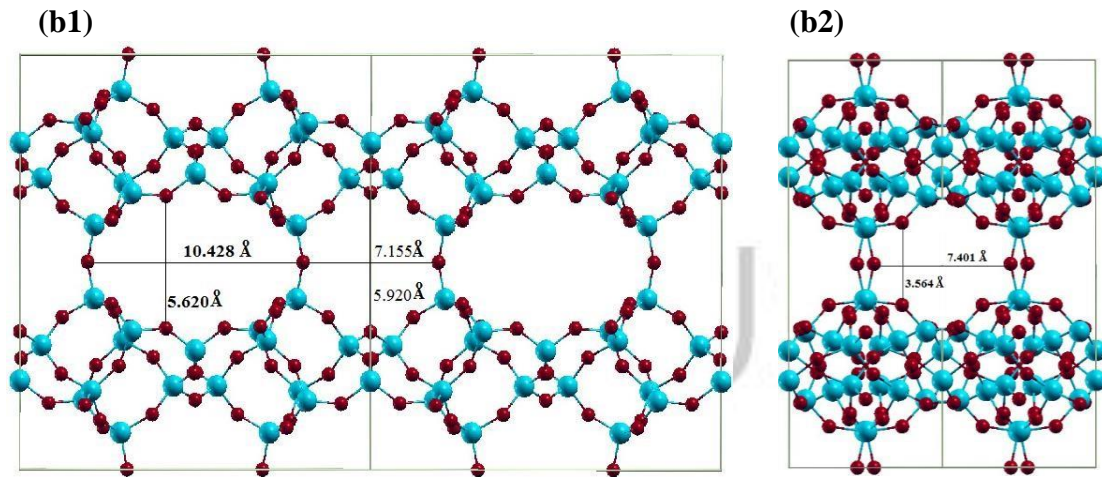
### 5. RESULTS AND DISCUSSION

#### 5.1 The Structure of Clinoptilolite

The structure of clinoptilolite is monoclinic (space group  $C2/m$ ) whose secondary building unit can be described by 4-4-1 type (Gottardi and E. Galli 1985) and consist of four- and five-member rings; eight- and ten-member rings define the channel system (Uzunova and Mikosch 2013a). The framework density of clinoptilolite is low,  $17.7T/1000\text{\AA}$  with five tetrahedral sites. It has the same topology as the mineral Heulandite, and thus belongs to the same structural group, denoted as HEU. A view of a purely siliceous clinoptilolite structure is

represented in Figure 3. The HEU framework contains three sets of intersection channels all located in the (010) plane. Two of the channels are parallel to the c-axis; the channels A are formed by strongly compressed ten-member rings and channels B are confined by eight-member rings (Godelitsas and Armbruster 2003). The monoclinic structure of clinoptilolite consisting of four- and five-member rings with eight- and ten-member rings defining the channel system (Alberti 1972). The structure comprises of three types of pores. Two of them are located in the (001) plane, an eight-member ring (8MR) which is composed of eight tetrahedral and eight oxygen atoms and a ten-member ring which is composed of ten tetrahedral and ten oxygen atoms. The third pore is an eight-member ring located in the (100) plane. Figure 1b1 & b2 show the calculated pore sizes of the purely siliceous framework which was deformed after Al  $\rightarrow$  Si substitution was done. Our estimates of the lattice parameters and the interatomic bond distances and angles of the purely siliceous CL are summarized in Table 2, and they show excellent agreement with experimental data. The secondary building unit (SBU) of HEU is 4-4 = 1 with a cage number of 2 (Baerlocher *et al* 2007). The structure is a much opened one and possesses a 2D net of intersecting channels in the (010) plane (Uzunova and Mikosch 2013a).





{[001] **10** 3.1 x 7.5+ **8** 3.6 x 4.6} [100] **8** 2.8x 4.7 (variable due to considerable flexibility of framework) Baerlocher, R. H. *Atlas of Zeolites Framework Types*, 6<sup>th</sup> Revised Edition, Elsevier Science: London, **2007**

**Figure 3** The Siliceous Clinoptilolite framework identifying the lattice parameters, the tetrahedral sites (a1) and the three types of pores (b1 & b2) viewed along the [001] (a2 & b2) and [100] (a1 & b1). (Si = light blue, O = red)

**Table 2** Unit cell Parameter (a, b and c) (nm), Si-O Bond Length (Å) and Bond Angles (Si-O-Si, deg) at various T-sites in the siliceous Clinoptilolite, as calculated using the PBE density functional.

	<b>This work</b>	<b>Experiment**</b>
<i>a</i>	17.52	17.50
<i>b</i>	17.64	17.60
<i>c</i>	7.40	7.40
Si-O	1.61	1.62
T2-O-T2	153.47	156.59
T2-O-T3	147.20	148.53
T2-O-T1	137.24	140.48

\*\*Experimental unit cell parameters, Si-O bondlength and bond angles are from Refs. (Baerlocher *et al* 2007, Uzunova and Mikosch 2013a, Alberti 1972, Koyama and Takéuchi 1977)

## 5.2 Al modified Clinoptilolite

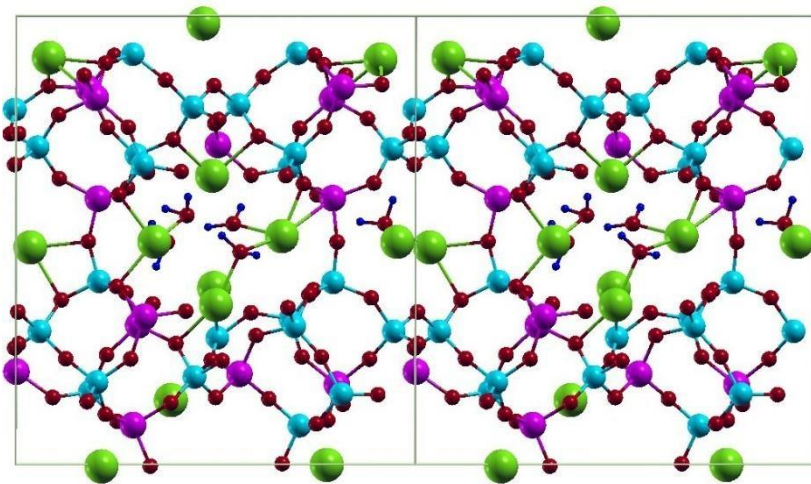
Substituting some of the tetrahedral site Si atoms by Al creates negatively charged frameworks and thus requires charge-compensation by extra framework cations within the cages and channels, typically of alkali metal and alkaline earth elements (e.g., Na<sup>+</sup>, K<sup>+</sup>, Ca<sup>2+</sup>, Ba<sup>2+</sup>, Sr<sup>2+</sup>, Cs<sup>+</sup>, and Mg<sup>2+</sup>) (Koyama and Takéuchi 1977). In this study, Na<sup>+</sup> is used to compensate for the negative charge resulting from the Al → Si substitution. Different Al/Si ratios were considered (1.7–8.0) and, in each composition, five water molecules are added (to reduce computational cost) in the extra-framework positions yielding the general formula (A<sup>z</sup>)<sub>y/z</sub>(Al<sup>3+</sup>)<sub>y</sub>(Si)<sub>x</sub>O<sub>2(x+y)</sub>·nH<sub>2</sub>O where A represents extra framework cations, z is the charge on the extra framework cations, n is the number of moles of molecular water, and x and y are the stoichiometric coefficients for Al<sup>3+</sup> and Si<sup>4+</sup> in tetrahedral sites, respectively. In Table 3, we report the optimized structural parameters of different Si/Al ratios of CL, for both the hydrated and dehydrated compositions. From the optimized structures, as the cations increases in the framework, they only imitate the known cation sites that is M1, M2, M3 and M4 that had been determined in early crystallographic studies of mineral samples and were summarized by Takéuch and Koyama (Koyama and Takéuchi 1977) for alkali and alkaline-earth cations.

### 5.2.1 Hydrated Na<sup>+</sup> Clinoptilolite

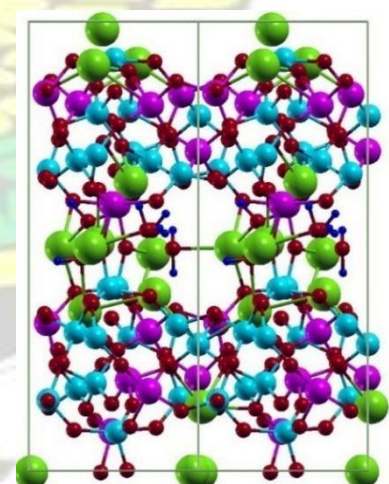
In the hydrated framework, the main Na<sup>+</sup> cation positions in this structure are; M1, which is located in channel A, coordinated by oxygen atoms from the side 10-membered ring and at least one H<sub>2</sub>O molecule. Three Na<sup>+</sup> cations occupy this site for the clinoptilolite with Si/Al ratio of 5. From the Figure 4, M1a is located close to the T2-O-T2 linkage while the both M1b and

M1c are located close to T5 with a bond length of 2.96Å between them and sharing one H<sub>2</sub>O molecule. This site also preferred by Ca<sup>2+</sup> (TOP 2001). M2 is located in the channel B coordinated by oxygen atoms from the 8-member ring. This site is occupied by two Na<sup>+</sup> cations, M2a and M2b. The site M2b is slightly shifted to the center of the ring. M2 is occupied basically by Na<sup>+</sup> and Ca<sup>2+</sup> [1]. M3 is located in channel C, is coordinated by framework oxygen and one H<sub>2</sub>O molecule. This site is preferably occupied by K<sup>+</sup> (TOP 2001, Uzunova and Mikosch 2013a). M4 is the fourth sites which is located in the center of channel A different from M1. The occupancy of this site is low, and provided by Mg<sup>2+</sup> (Arcoya *et al.*, 1996). M4 was not occupied by the Na<sup>+</sup> cation.

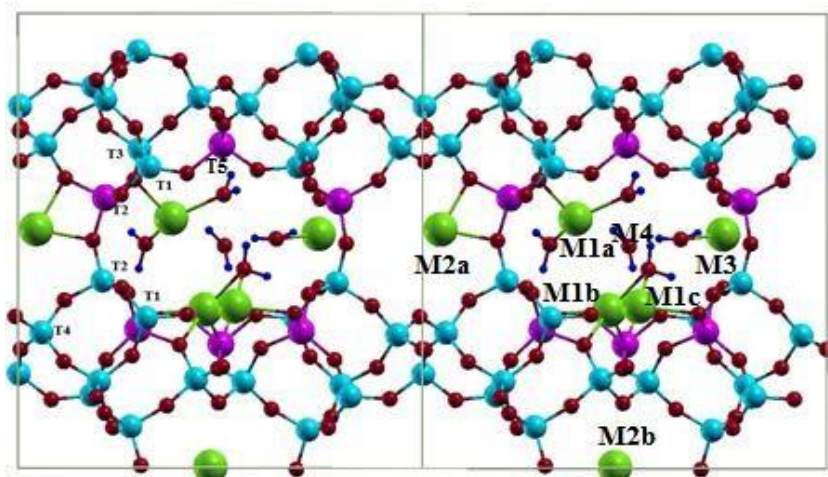
(a1)



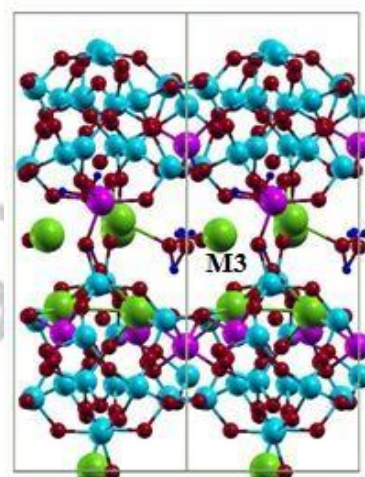
(a2)



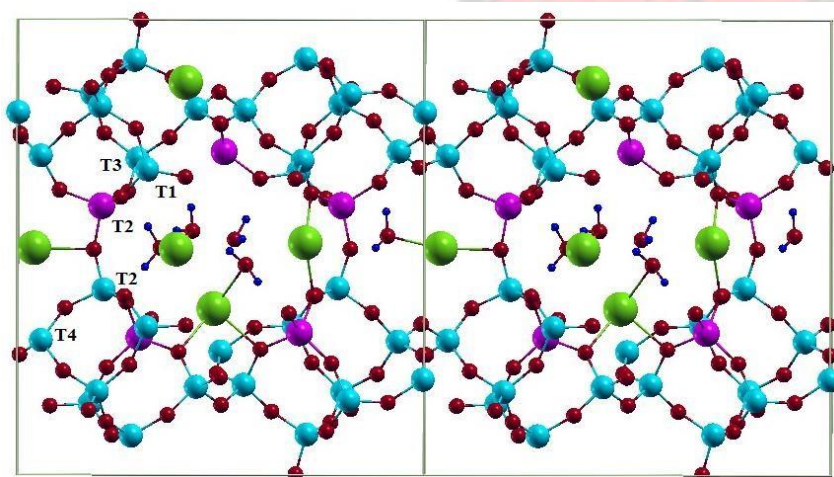
(b1)



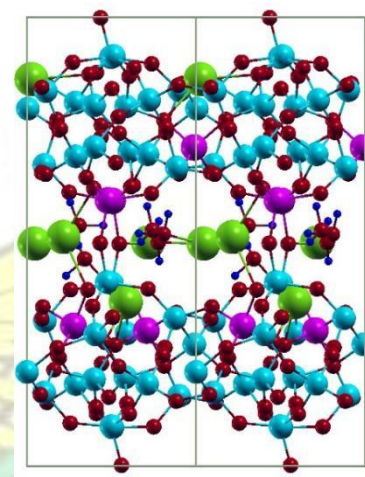
(b2)



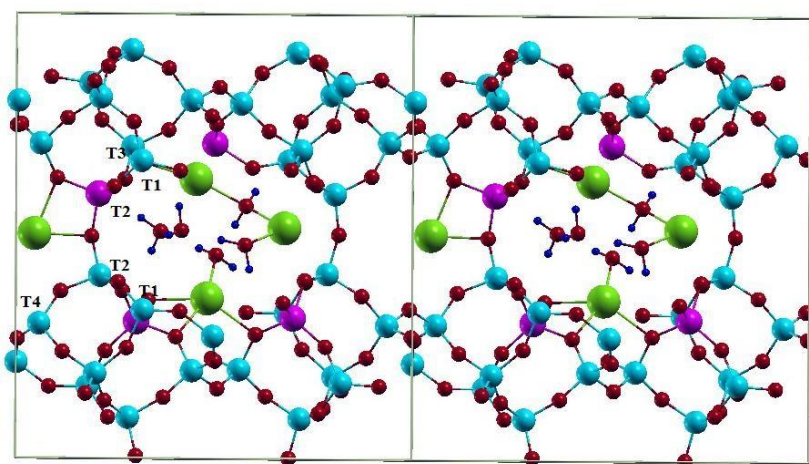
(c1)



(c2)



(d1)



(d2)

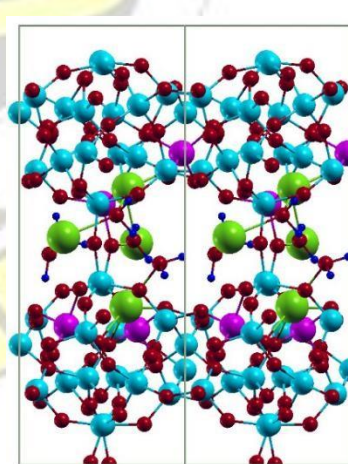
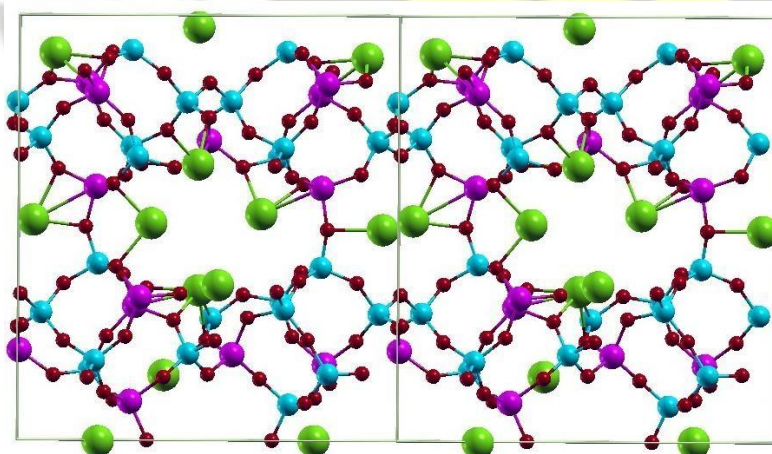


**Figure 4** The structure of hydrated clinoptilolite with Si/Al ratio 1.7(a), 5(b), 6(c) and 8(d) viewed along [001] (a1, b1, c1 & d1) and [100] (a2, b2, c2 & d2) showing the Na<sup>+</sup> cation preference sites. (Si = light blue, O = red, Al = violet, Na = green, H = dark blue)

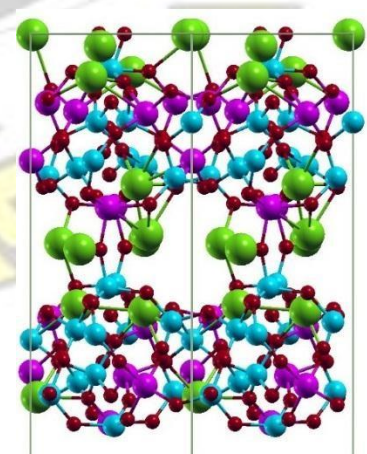
### 5.2.2 Dehydrated Na<sup>+</sup> Clinoptilolite

The distribution of the Na<sup>+</sup> cations in the dehydrated system is different from that of the hydrated system, though the sites are the same. The distribution is as a result of the absence of water which affects the mobility of the cations, serves as charge distributor in the channels and pores and also minimizes the electrostatic repulsion between framework oxygen (Higgins *et al* 2002, Johnson *et al* 2003). In the absence of water, the Na<sup>+</sup> cations tend to cluster relatively closer (distance of 2.34 Å) to the negatively charged framework oxygen. In the absence of H<sub>2</sub>O molecules, the Na<sup>+</sup> cation located at M1a in the hydrated system moves into the channel C to occupy the M3 sites resulting in two atoms occupying that site for the Si/Al ratio 5. The angles TOT in proximity to cation sites undergo strong deformation (see Table 3), and it is consistent with an earlier DFT result of Uzunova and co-workers in 2013 (Uzunova and Mikosch 2013a).

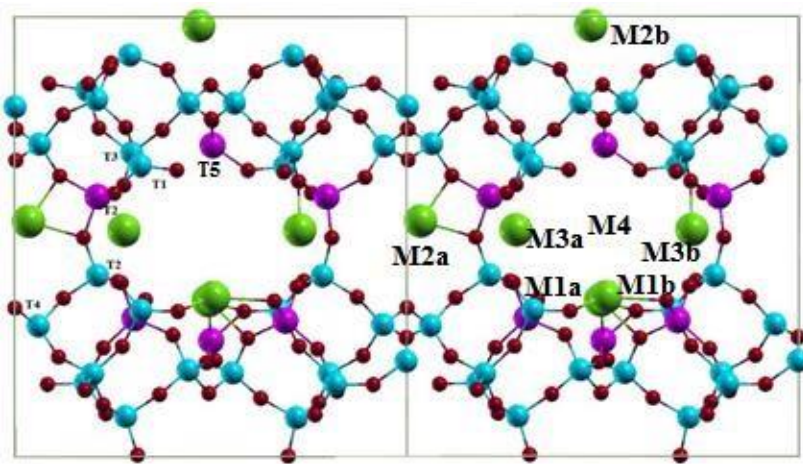
(a1)



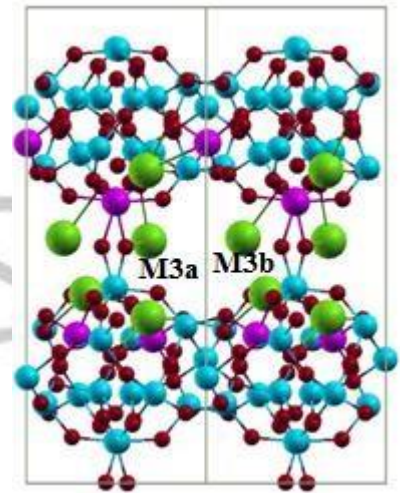
(a2)



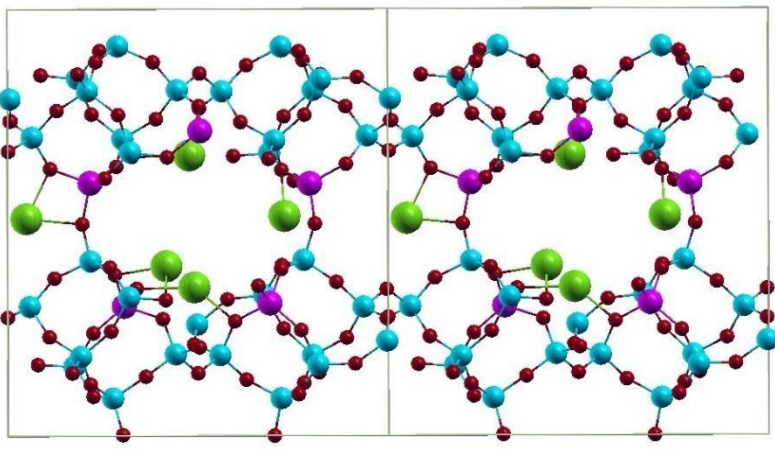
(b1)



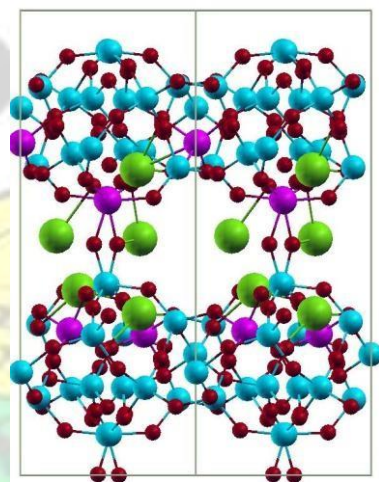
(b2)



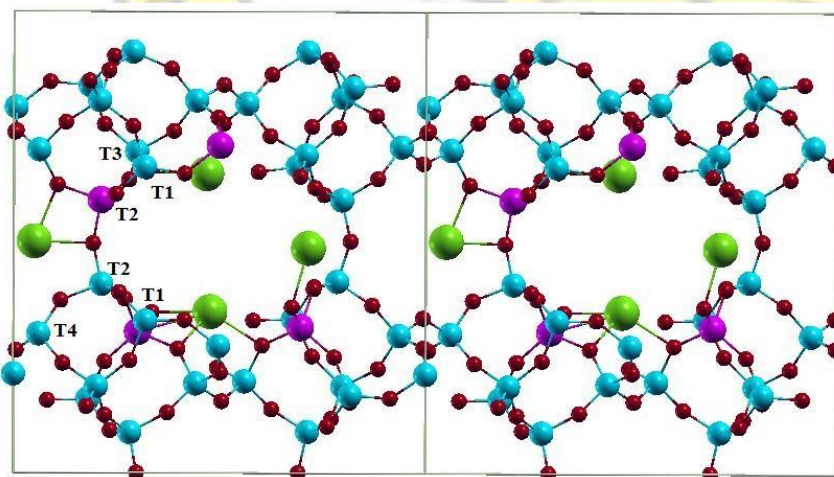
(c1)



(c2)



(d1)



(d2)

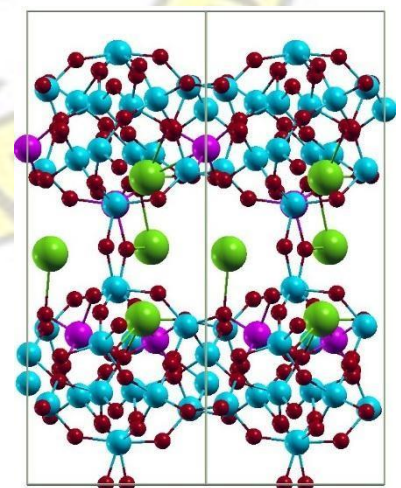


**Figure 5** The structure of dehydrated clinoptilolite with Si/Al ratio 1.7(a), 5(b), 6(c) and 8(d) viewed along [001] (a1, b1, c1 & d1) and [100] (a2, b2, c2 & d2) showing the Na<sup>+</sup> cation preference sites. (Si = light blue, O = red, Al = violet, Na = green, H = dark blue)

# KNUST



**Table 3** The sizes of pores (Å), angles between tetrahedral sites (Deg), Si-O, Al-O bond lengths (Å) and Na<sup>+</sup>-framework oxygen internuclear distance before adsorption (R<sub>MO</sub>/Å) and after adsorption (R<sub>MOA</sub>/Å) for Na-Clinoptilolite at different Si/Al ratios

	Na-Clinoptilolite (Si/Al=1.7)		Na-Clinoptilolite (Si/Al=5)		Na-Clinoptilolite (Si/Al=6)		Na-Clinoptilolite (Si/Al=8)		Uzunova et al
	Dehyd.	Hyd.	Dehyd.	Hyd.	Dehyd.	Hyd.	Dehyd.	Hyd.	
10MR	10.69 x 5.25	10.49 x 5.49	10.66 x 5.66	10.55 x 5.47	10.33 x 5.90	10.72 x 5.75	10.61 x 5.61	10.61 x 5.59	-
8MR	6.96 x 5.79	7.13 x 5.79	6.98 x 5.29	7.08 x 6.03	7.27 x 5.72	6.87 x 6.08	6.98 x 5.91	6.98 x 6.07	-
8MR (100)	7.40 x 3.66	7.40 x 3.61	7.40 x 3.59	7.40 x 3.45	7.40 x 3.55	7.40 x 3.79	7.40 x 3.54	7.40 x 3.88	-
T2-O-T2	143.8	150.0	139.6	147.7	151.4	154.5	152.0	152.9	147.2
T2-O-T3	138.4	137.5	138.9	143.2	146.2	143.5	150.7	142.6	140.5
T2-O-T1	130.0	131.9	126.5	125.3	128.7	136.9	129.1	131.5	135.2
Si-O	1.643	1.648	1.612	1.614	1.591	1.602	1.600	1.721	1.656
Al-O	1.777	1.761	1.748	1.745	1.744	1.722	1.723	1.609	1.763
R <sub>MO</sub>	2.320	2.234	2.439	2.367	2.339	2.365	2.340	2.391	2.325
R <sub>MOA</sub>	2.338	2.345	2.445	2.383	2.377	2.366	2.326	2.389	-

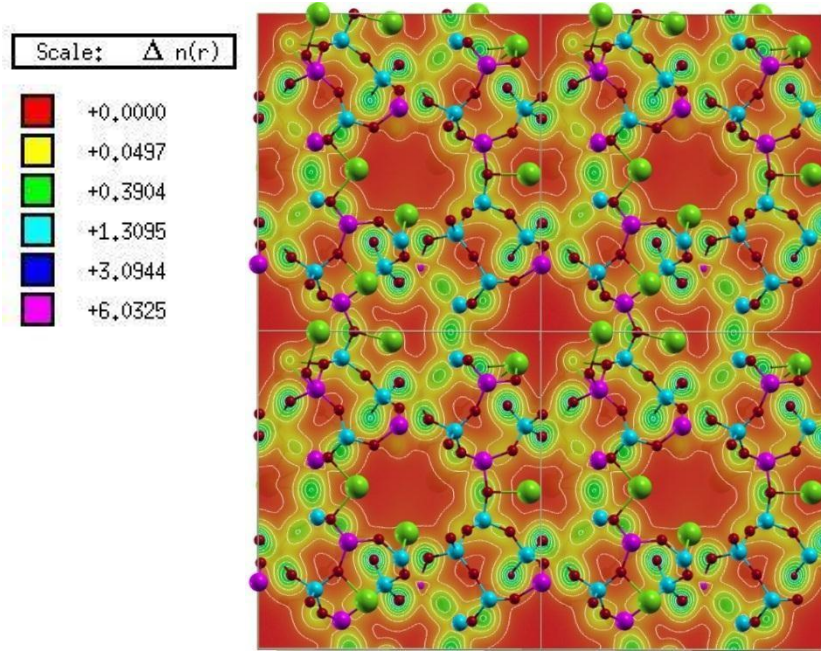


### 5.3 Charge Density

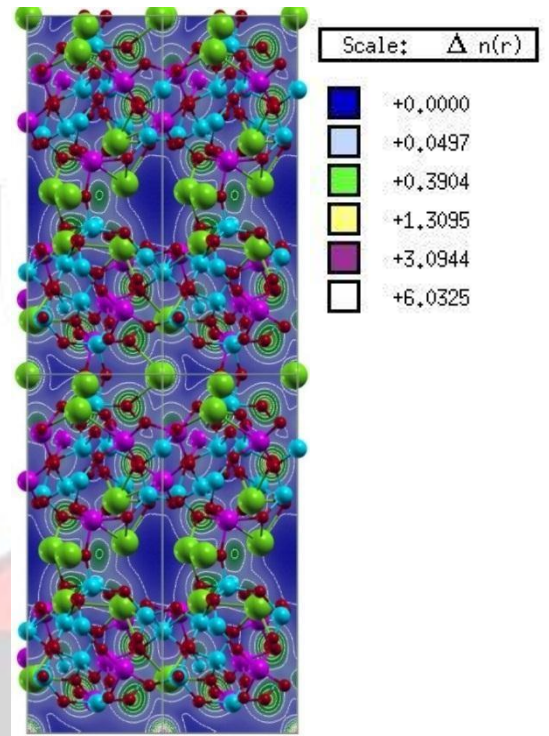
Charge density refers to the distribution of the charge over the volume of a molecule, atom or ion. Adsorption selectivity highly depends on polarity of both adsorbent and adsorbate. In the case of zeolites, the parameter that governs the polarity is the Si/Al ratio. The polarity determines the molecules that can be adsorbed in the zeolite. For a low Si/Al ratio, the polarity increases and the zeolite is hydrophilic. Then, more polar molecules occupy the sites with high charge density within the lattice (Sánchez 2011). This analysis of the electronic density based on DFT calculation of clinoptilolite reveals the important electronic density depletion around the silicon atoms to the benefit of the oxygen atom (Rozanska and Santen 2003). Shown in Figure 6 is the isosurface of the charge density of the hydrated and dehydrated Al-modified CL zeolite with Si/Al ratio of 5. Compared to the dehydrated case, the charge density distribution within the pores is reduced in the hydrated frameworks (see Figure 6), consequently the presence of water in the CL zeolites framework appears to serve as a charge delocalizer. Charge density affects the location of molecules in the lattice, more polar molecules occupy the sites with high charge density within the lattice.



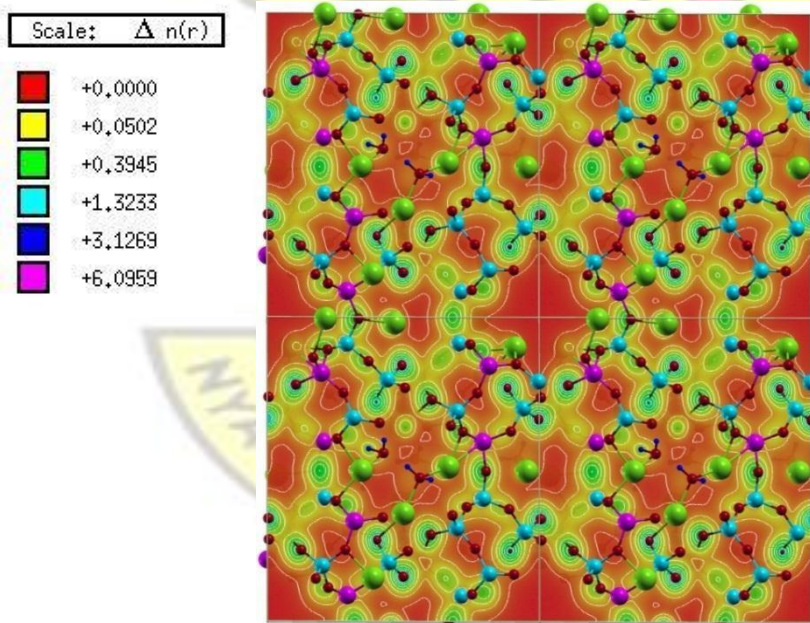
(a1)



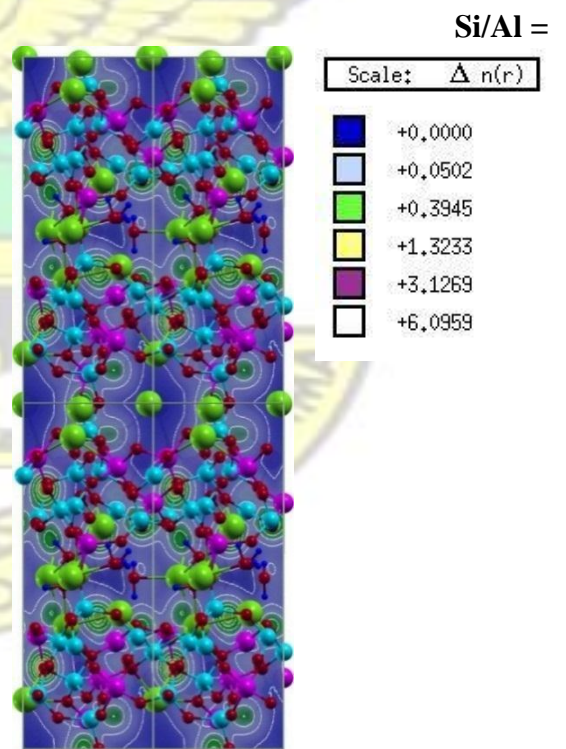
(a2)



(b1)



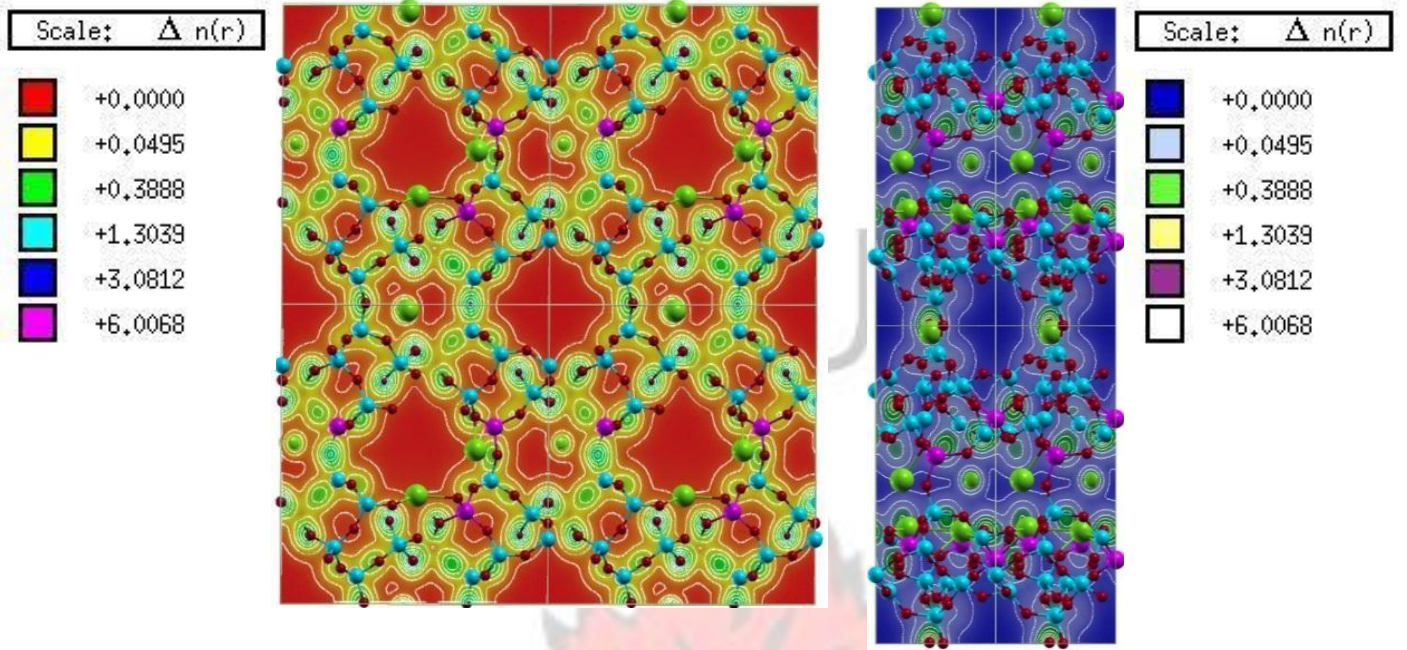
(b2)



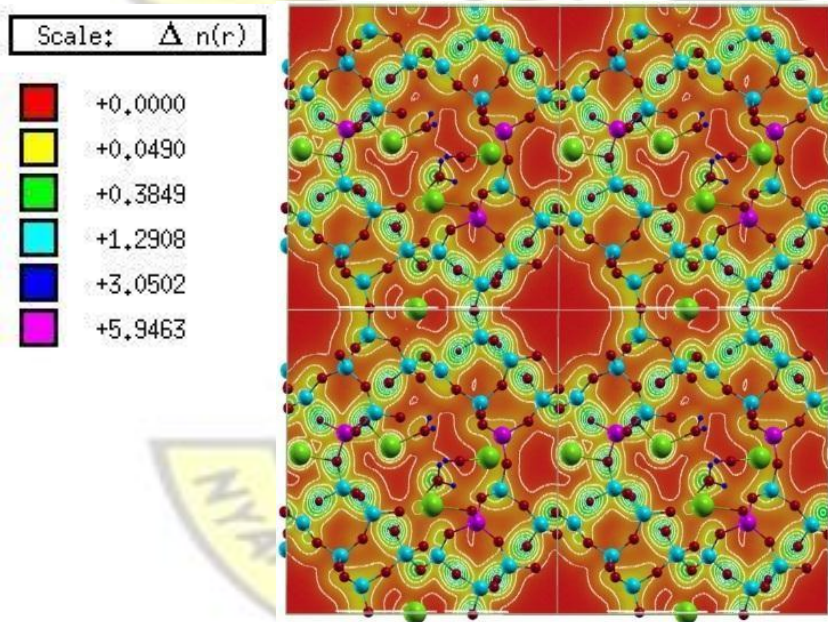
1.7

(a2)

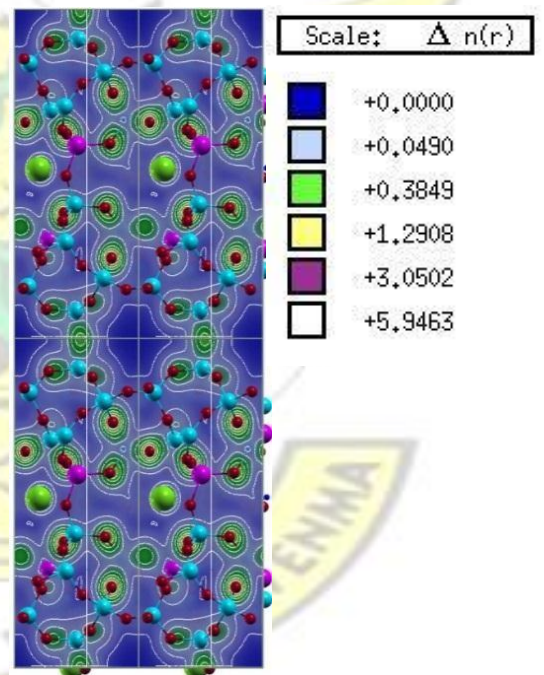
(a1)



(b1)

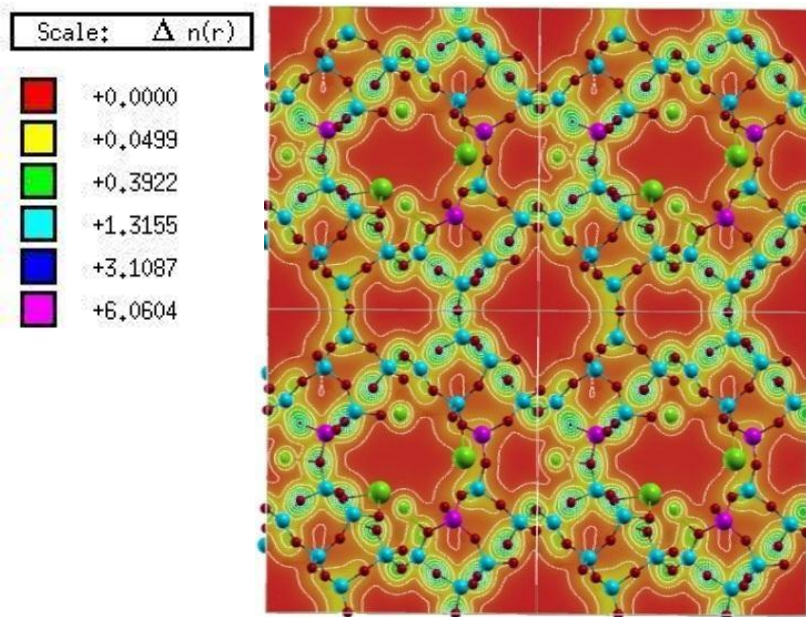


(b2)

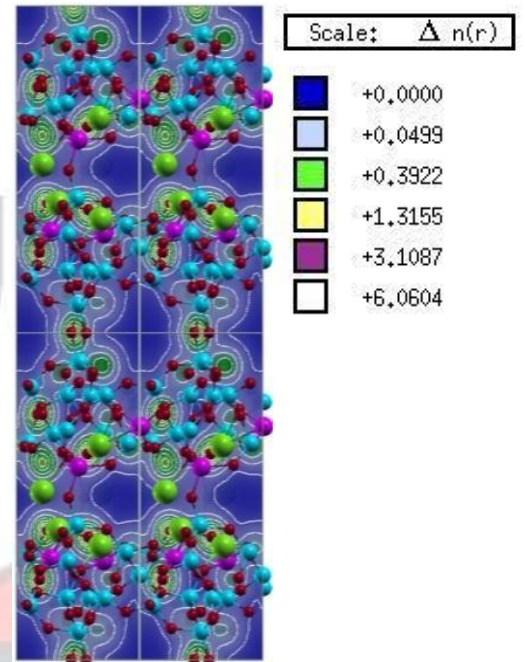


Si/Al = 5

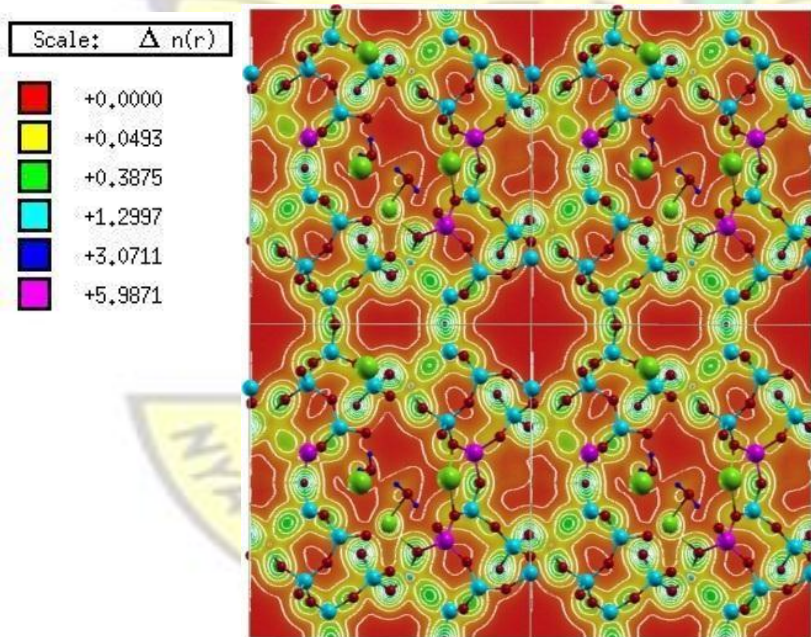
(a1)



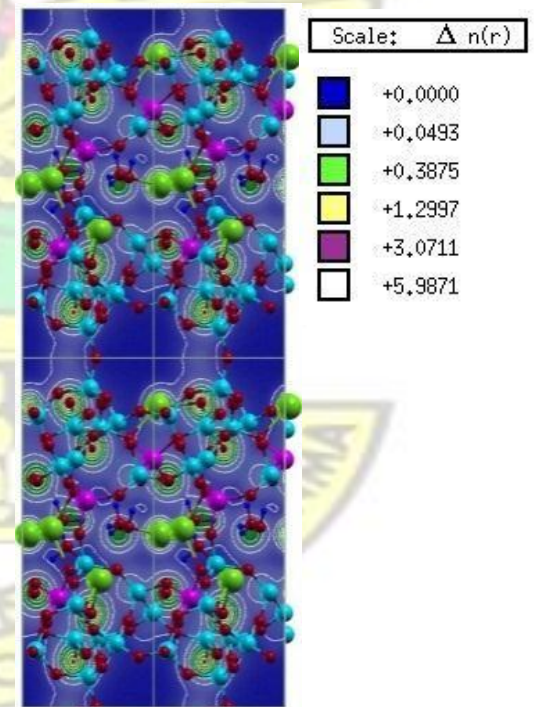
(a2)



(b1)



(b2)



Si/Al = 6

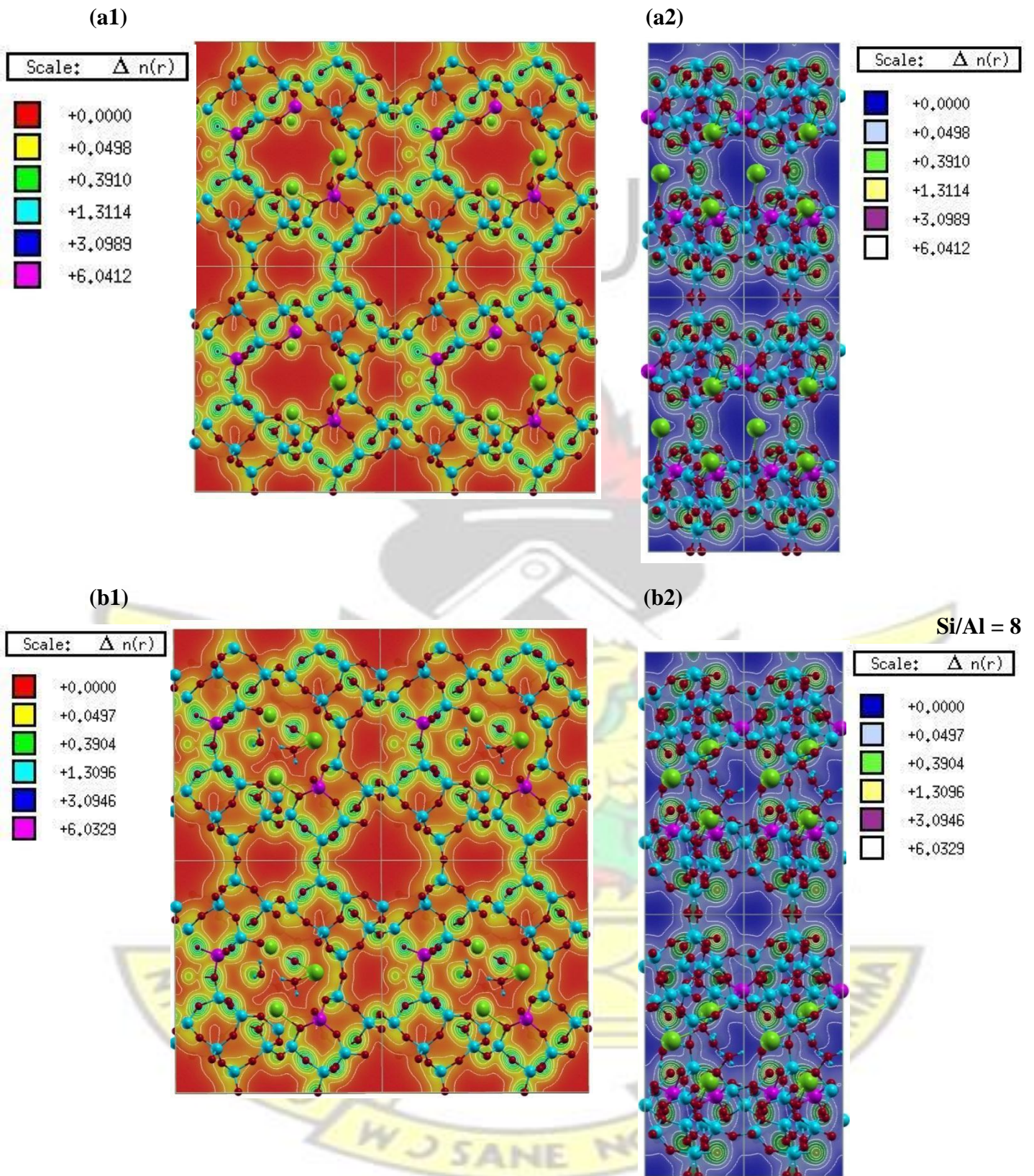


**Figure 6** The isosurface of the charge density distribution inside channels A, B (a1 & b1) and channel C (a2 & b2) for a dehydrated clinoptilolite (a) at different Si/Al ratios and a hydrated clinoptilolite structure (b) (Si = light blue, O = red, Al = violet, Na = green, H = dark blue).

## 5.4 Adsorption of Arsenic

The molecular adsorption process results in an exothermic attachment of the molecule to the surface of the voids and it is characterized by a high order of specificity (Flank 1980). Clinoptilolite has a high ability of adsorbing certain molecules because of the effective anionic framework and mobile cations. We now discuss the adsorption characteristics of  $\text{AsO}(\text{OH})_3$  and  $\text{As}(\text{OH})_3$  by the hydrated and dehydrated Al-modified clinoptilolite zeolites.

The adsorption energies in kJ/mol at different adsorption sites as a function of Si/Al ratio (Si/Al = 1.7, 5, 6 and 8) are summarized in Tables 4 and 5, for the dehydrated and hydrated compositions respectively. Essentially the adsorption energies for both arsenic and arsenous acids on dehydrated CL zeolite (Si/Al = 1.7 - 8) at all the adsorption sites are favorable (7 – 252 kJ/mol, exothermic) except at the 8 MR in the (100) plane for  $\text{AsO}(\text{OH})_3$  at Si/Al ratio of 5 and the site located at the intersection of the 8MR in the (001) plane and the 8 MR in the (100) plane for  $\text{AsO}(\text{OH})_3$  at Si/Al ratio of 6 and 8. However, in the hydrated (5  $\text{H}_2\text{O}$  molecules) CL, the exothermicity is maintained only in site 4 with increase in the extent of exothermicity (32 - 161 kJ/mol) at these sites. We observed that the adsorption of arsenic in Site 1 is much preferred in the dehydrated framework. The adsorption site 1 (Figure 7) is located in the ten-membered ring (Channel A) containing two cation preference sites (M1 and M4). Prior to adsorption, the  $\text{Na}^+$  cation located at site M3a and M1a shift towards the adsorbate to form an Na-O bond. This results in the elongation of the M-O bond (+0.02 Å). Both adsorbates also undergo deformation respectively. The As-O bond after adsorption undergoes elongation. Though the adsorption stabilities are high (- 56.50 – 250.55 kJ/mol), it is only favorable in the dehydrated CL zeolite. The adsorption of the arsenic species in Site 1 does not only depend on the state of the framework but also on the Si/Al ratio. The interaction between the  $\text{Na}^+$  cations and the adsorbates increases when the dehydrated CL is aluminium rich. As a result, the exothermicity of the adsorption energies increases. Both  $\text{AsO}(\text{OH})_3$  (56.50 – 250.55 kJ/mol)

and  $\text{As}(\text{OH})_3$  (123.61 – 226.34 kJ.mol) were adsorbed associatively and exothermically at this site (Figure 11a & c). The strongest interaction (226.34 kJ/mol) for  $\text{As}(\text{OH})_3$  is recorded at this site. For the hydrated framework, we observed that, the water molecules in the framework have a destabilization effect on the adsorption of both  $\text{AsO}(\text{OH})_3$  and  $\text{As}(\text{OH})_3$ .

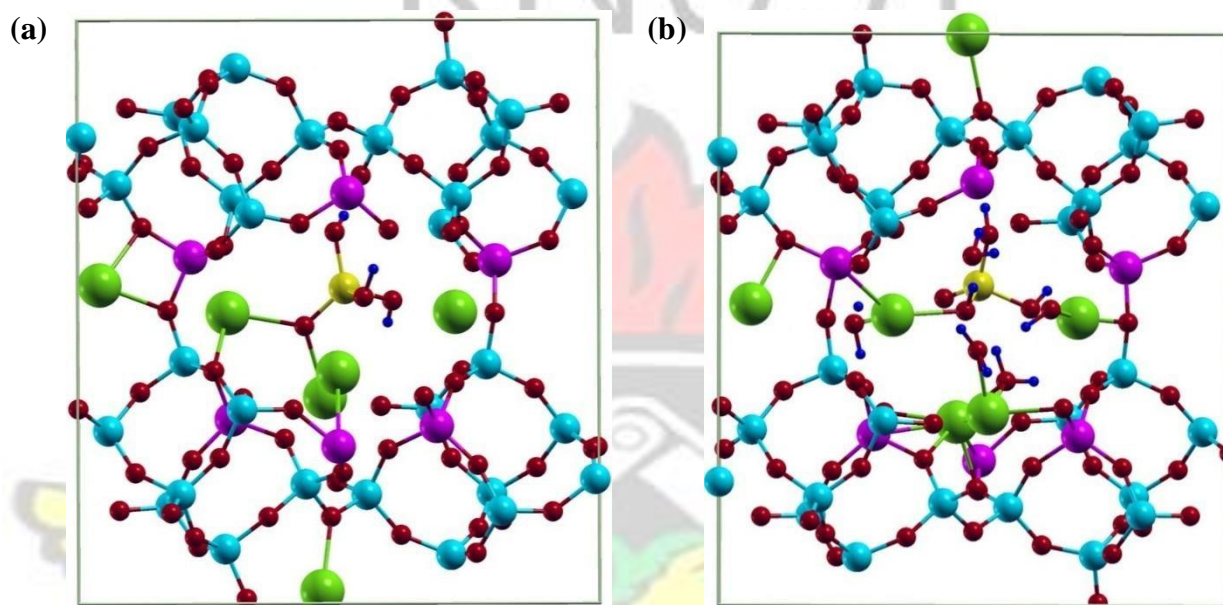


**Figure 7** Adsorption of arsenic in adsorption site 1. (a) Dehydrated framework and (b) Hydrated framework (Si = light blue, O = red, Al = violet, Na = green, H = dark blue, As = Yellow)

Site 2 (Figure 8) is located in the eight membered ring in the (001) plane (channel B). This site contains one cation preference site that is M2. We observed that this site is a favorable adsorption site for both arsenic species in both hydrated and dehydrated CL zeolite. However, for Si/ Al ratio 1.7, the adsorption was unfavorable for  $\text{AsO}(\text{OH})_3$ . At this site, the two  $\text{Na}^+$  cations were bonded to a water molecule while bonded to the  $\text{AsO}(\text{OH})_3$ , hence the interaction between the  $\text{Na}^+$  cations and  $\text{AsO}(\text{OH})_3$  is weakened by the water molecule. The  $\text{Na}^+$  cation located at M2 moves slightly towards the center of the channel to form a Na-As bond with the adsorbate. This results in the elongation of the bond distance (from 2.373 to

2.414 Å) between the Na<sup>+</sup> cation and the framework oxygen. The adsorption energies of both AsO(OH)<sub>3</sub> and As(OH)<sub>3</sub> in hydrated (113.24 kJ/mol) clinoptilolite is higher than that of the dehydrated (109.23 kJ/mol) in sites 2 (Figure 11). The behaviour of the two adsorbates are the same in the eight member ring, that is they are adsorbed associatively and exothermically but the exothermicity of AsO(OH)<sub>3</sub>(124.34 kJ/mol) is higher than the As(OH)<sub>3</sub>(92.02 kJ/mol). Similarly both adsorbates experience a slight lengthening of As-O (from 1.745 Å to 1.774 Å) and O-H bonds (from 0.981 Å to 1.000 Å).

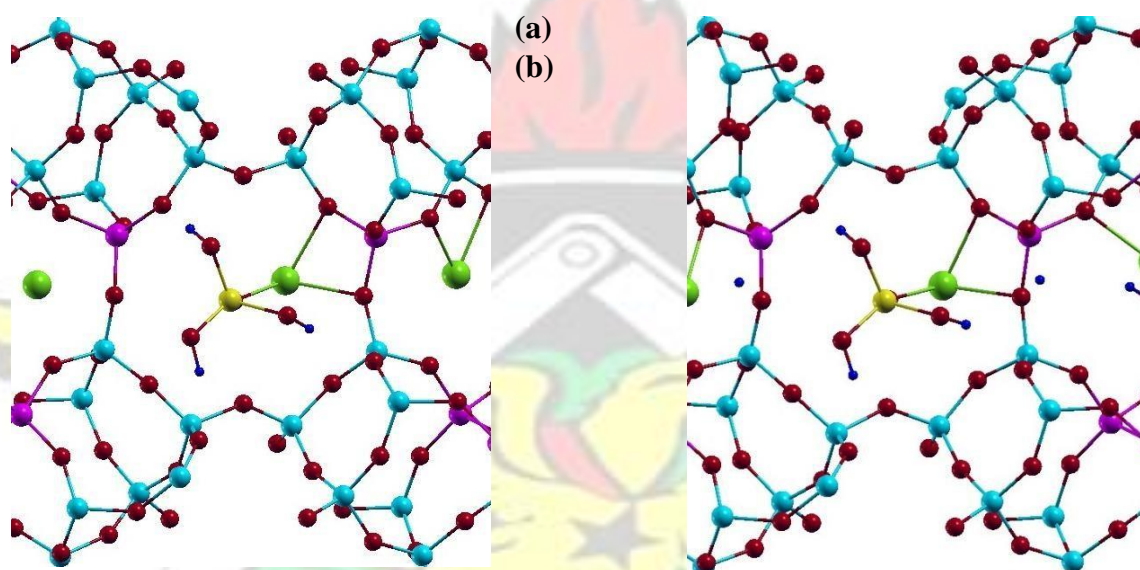


**Figure 8** Adsorption of arsenic in adsorption site 2. (a) Dehydrated framework and (b) Hydrated framework (Si = light blue, O = red, Al = violet, Na = green, H = dark blue, As =Yellow)

It is worth noting that the Site 3 and Site 2 have the same member rings. The difference being that, Sites 3 (Figure 9) is located in the (100) plane and also smaller in size compared to that of Site 2. This site consists of one cation preference site (M3) and lies perpendicular to the (001) plane. Similar to the Site 1, this adsorption site is favorable for adsorption of both  $\text{AsO}(\text{OH})_3$  and  $\text{As}(\text{OH})_3$  only in dehydrated state with  $\text{AsO}(\text{OH})_3$  (171.78 – 252.39 kJ/mol) having a stronger interaction than  $\text{As}(\text{OH})_3$  (116.56 – 158.82 kJ/mol). At low Si/Al ratios (1.7 and 5), the  $\text{Na}^+$  cations increase in number causing the pore size to decrease and also increasing the number of adsorption sites, as a result the arsenic acid undergoes dissociation, the O-H bond breaks away from the  $\text{AsO}(\text{OH})_3$  and get adsorbed to the inner surface of the framework. The  $\text{As}(\text{OH})_3$  only dissociate at Si/Al ratio of 1.7. In the dehydrated CL zeolite the strongest interaction (252.39 kJ/mol) for  $\text{AsO}(\text{OH})_3$  is observed at site 3 for Si/Al ratio of 1.7

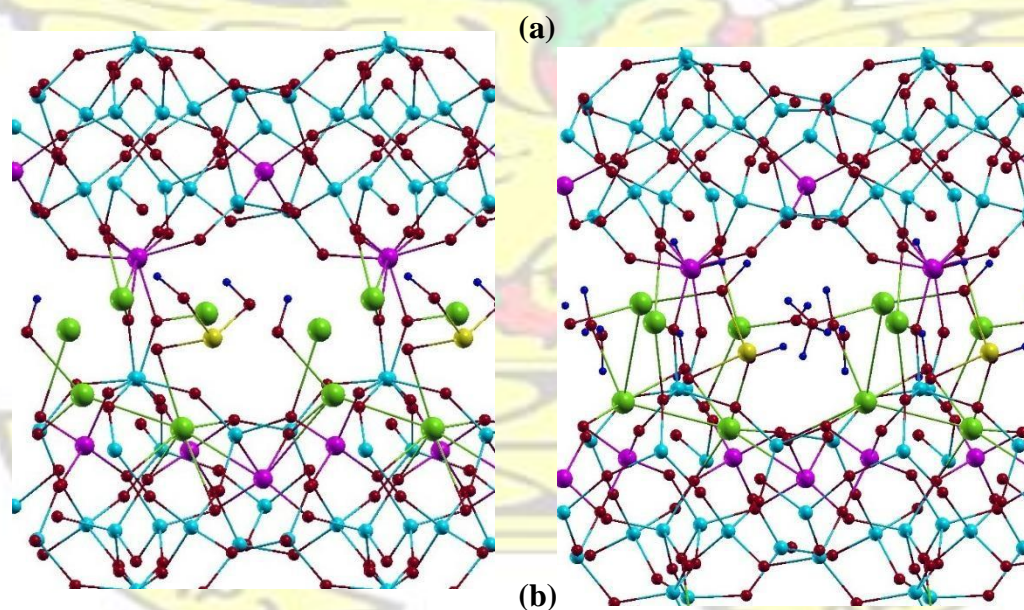


**Figure 9** Adsorption of arsenic in adsorption site 3. (a) Dehydrated framework and (b) Hydrated framework (Si = light blue, O = red, Al = violet, Na = green, H = dark blue, As =Yellow)

The adsorption of the arsenic species in Site 4 (Figure 10) is almost the same as that in Site 2. Site 4 is located in between the 8 member ring in the (001) plane and the 8 member ring in the (100) plane. This site contains one cation sites (M2). The  $\text{Na}^+$  cation is bonded to two framework oxygen prior to the adsorption of the adsorbates. After adsorption, the cation shifts towards the adsorbates to form a Na-O bond resulting in the elongation of the M-O bond length (Table 13). Similar to Site 2, this adsorption site proves stable for adsorption of both  $\text{AsO}(\text{OH})_3$  and  $\text{As}(\text{OH})_3$  in both dehydrated and hydrated states except the energies are lower than in the Site 2. At low Si/Al ratio (1.7), the site was stable for the adsorption of  $\text{AsO}(\text{OH})_3$  in both dehydrated and hydrated states while at high ratios (6 and 8) the sites was unstable in the dehydrated state. At this site, it was found that there was a strong interaction between  $\text{As}(\text{OH})_3$  and the zeolite than  $\text{AsO}(\text{OH})_3$ . In the hydrating (5  $\text{H}_2\text{O}$  molecules) CL, the strongest interaction (161.12 kJ/mol) was observed at site 4 for Si/Al ratio 1.7. This site contains two  $\text{Na}^+$  cations and no water molecule, hence the strong interaction was as a result of the two  $\text{Na}^+$  cations bonding with two oxygen atoms of the As ( $\text{OH})_3$  and the absence of a water molecule to reduce the interaction.

These results reveals that the adsorption of  $\text{AsO}(\text{OH})_3$  and  $\text{As}(\text{OH})_3$ , does not only depend on the Si/Al ratio and cation but also on the location inside the zeolite framework as well as its state.

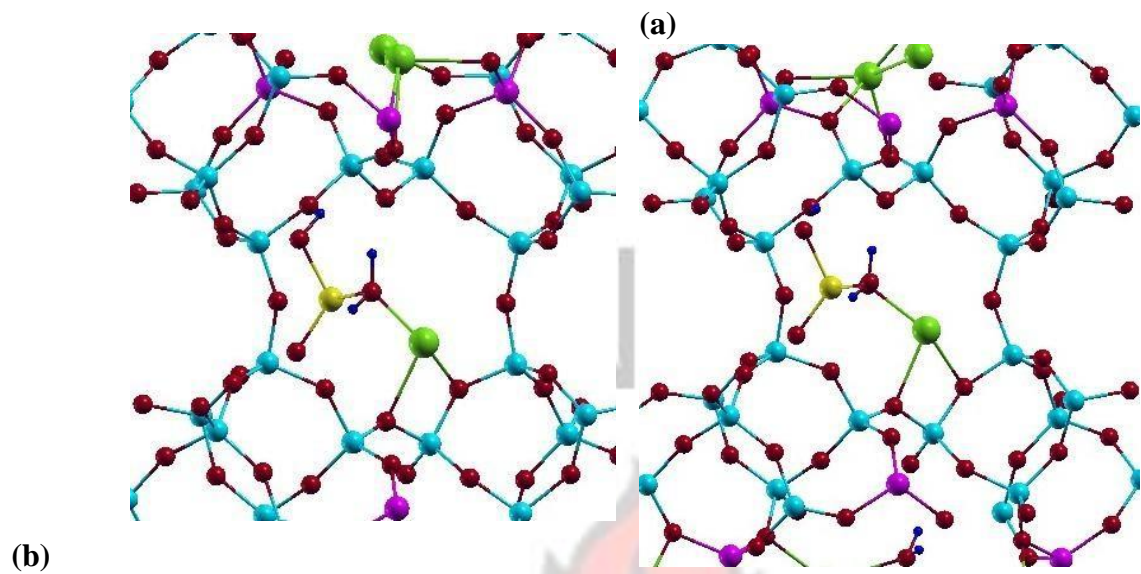


**Figure 10** Adsorption of arsenic in adsorption site 4. (a) Dehydrated framework and (b) Hydrated framework (Si = light blue, O = red, Al = violet, Na = green, H = dark blue, As = Yellow)

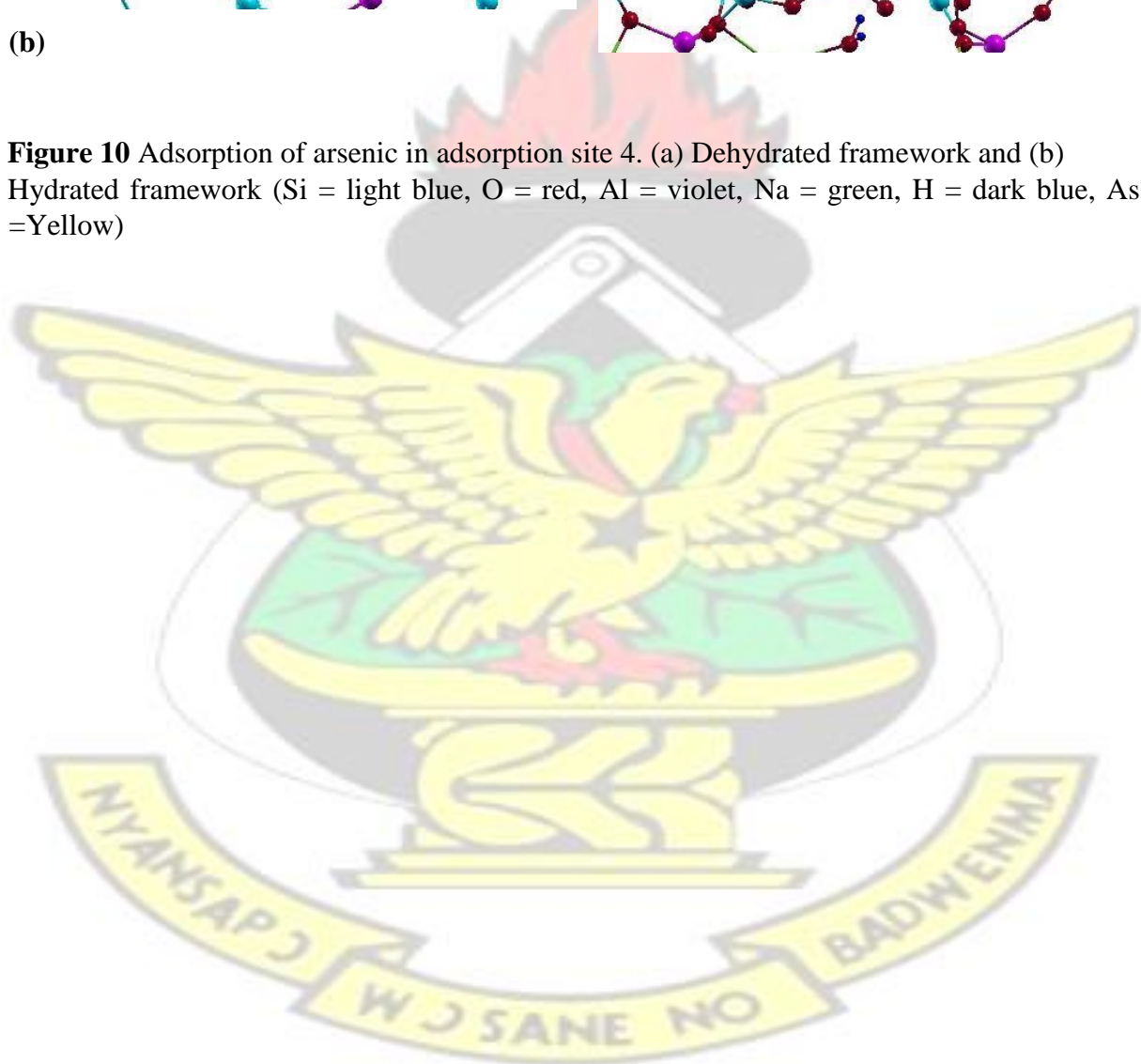


**Table 4** Adsorption energies (**kJ/mol**) for  $AsO(OH)_3$  and  $As(OH)_3$  on *dehydrated Na-Clinoptilolite* (Si/Al = 1.7, 5, 6 and 8) at different adsorption sites.

	<b>DEHYDRATED</b>							
	<b>Arsenic acid</b>				<b>Arsenous acid</b>			
	<b>1.7</b>	<b>5</b>	<b>6</b>	<b>8</b>	<b>1.7</b>	<b>5</b>	<b>6</b>	<b>8</b>
<b>Site 1(10 MR [001])</b>	-250.55	-200.09	-97.35	-56.50	-226.34	-131.87	-163.92	-123.61
<b>Site 2 (8 MR [001])</b>	-177.96	-124.84	-123.36	-98.47	-108.19	-77.15	-91.50	-72.39
<b>Site 3 (8 MR [100])</b>	-252.39	2.21	-171.78	-143.88	-158.82	-127.57	-116.59	-117.13
<b>Site 4 (8 MR)</b>	-104.36	-8.19	0.08	4.87	-125.34	-70.21	-33.98	-7.99

**Table 5** Adsorption energies (**kJ/mol**) for  $AsO(OH)_3$  and  $As(OH)_3$  on *hydrated (5 H<sub>2</sub>O molecules) Na-Clinoptilolite* (Si/Al = 1.7, 5, 6 and 8) at different adsorption sites.

	<b>HYDRATED</b>							
	<b>Arsenic acid</b>				<b>Arsenous acid</b>			
	<b>1.7</b>	<b>5</b>	<b>6</b>	<b>8</b>	<b>1.7</b>	<b>5</b>	<b>6</b>	<b>8</b>
<b>Site 1(10 MR [001])</b>	260.22	38.96	214.01	243.83	365.23	7.62	123.65	314.10
<b>Site 2 (8 MR [001])</b>	118.34	-156.76	-104.86	-144.09	-69.67	-138.96	-63.62	-114.70
<b>Site 3 (8 MR [100])</b>	193.52	150.32	173.63	205.20	64.68	-6.05	32.26	585.75
<b>Site 4 (8 MR)</b>	-58.45	-59.24	-32.43	-51.02	-161.12	-129.29	-68.78	-61.45

# KNUST

58



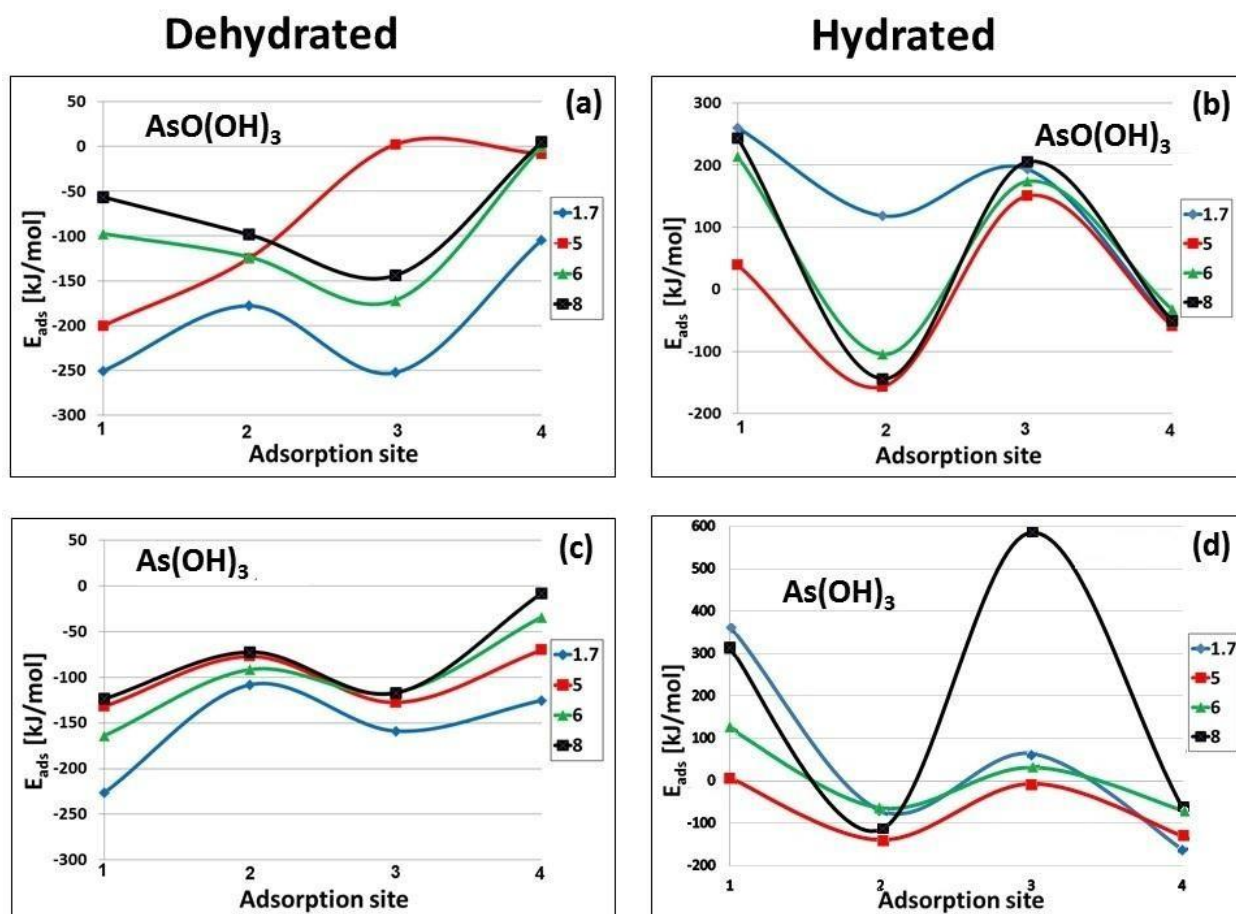
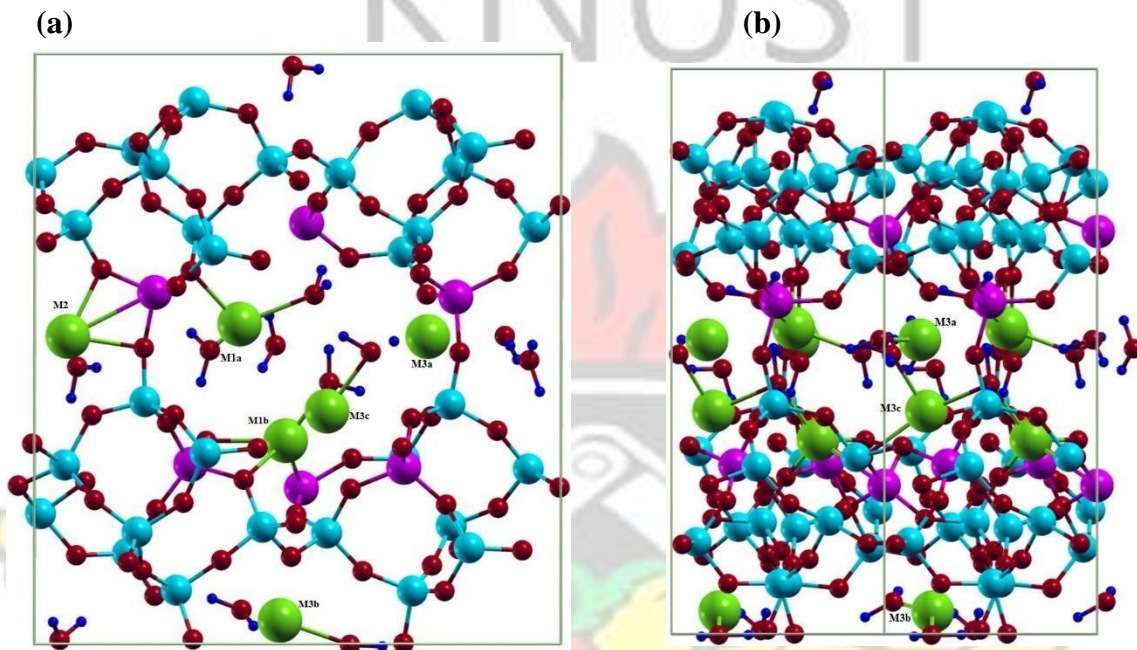


**Figure 11** Adsorption energies of  $AsO(OH)_3$  and  $As(OH)_3$  as a function of Si/Al ratio (1.7, 5, 6 and 8) at different adsorption sites of *dehydrated* and *hydrated* Na-clinoptilolite.

### 5.4.1 Effect of Hydration on Arsenic Adsorption

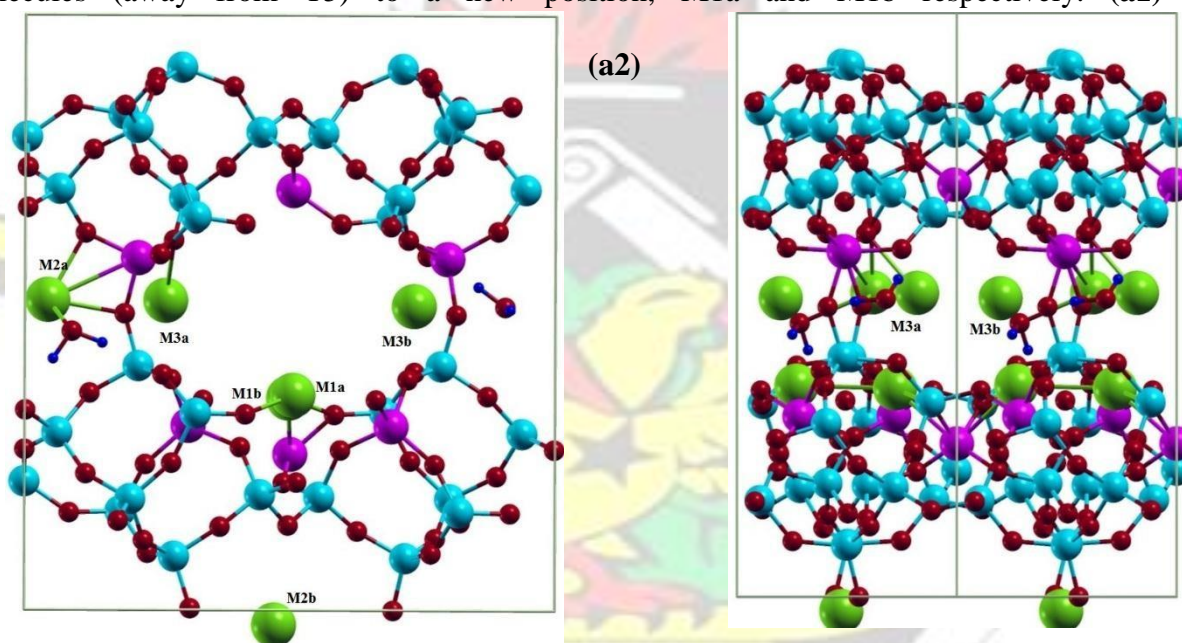
We next varied the amount of water molecules in the Na-clinoptilolite structure, in order to investigate the effect of water on the adsorption sites and relative stabilities. A number of different configurations were studied where 12 water molecules were added around the adsorbates at different locations (Figure 12). In contrast to the dehydrated modified CL zeolite, the introduction of water molecules in the framework is found to have a destabilization effect on the adsorption of both  $AsO(OH)_3$  and  $As(OH)_3$ . This is as a results of the water molecules filling the pores, leaving no space for the adsorbates to fit in. We observed that when extra framework cations are strongly hydrated, they are reluctant to move to sites where they are required to shed some or all of their coordinated water molecules. In view of this, most of the

$\text{Na}^+$  cations do not migrate towards the adsorbates to enhance their adsorption. Hydrating the framework with 12 water molecules loosened the Na-Na bonding causing them to break apart. From Table 6, we observed that increasing the water molecules destabilized the adsorption sites rendering them not preferred (see Figure 14).



**Figure 12** The structure of clinoptilolite hydrated with 12 water molecules viewed along [001] (a) and [100] (b) showing the  $\text{Na}^+$  cation preference sites. (Si = light blue, O = red, Al = violet, Na = green, H = dark blue)

We then reduced the water molecules to 2, these 2 were placed at three different locations, namely in the ten ring-window (channel A) (Figure 13b), eight ring-window (Channel B) (Figure 13a) and one water molecule in channel A and channel B (Figure 13c). The most stable adsorption site for the two water molecules (Table 6) was found in the channel A with the least being found in the channel B. When two water molecules were placed in the ten-ring window, the cations sites remained similar to when five water molecules were added. The difference was the located at M1a, M1b and M1c positions. M1a shifted from its initial position towards the channel C to occupy the M3a position. M1b and M1c also moved towards the water molecules (away from T5) to a new position, M1a and M1b respectively. (a1)



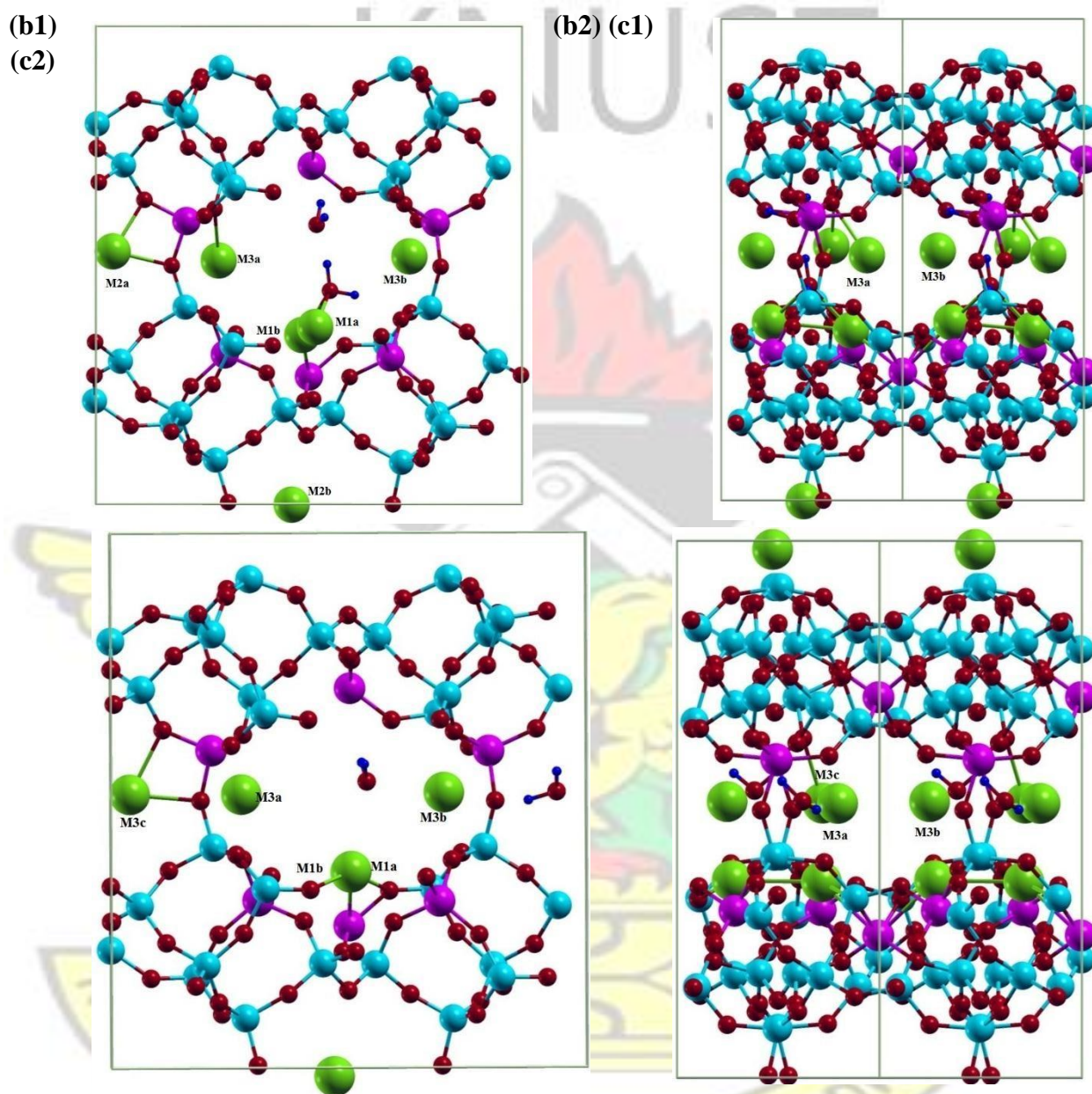


**Figure 13** The structure of clinoptilolite hydrated with 2 water molecules (a) all in 8 ring window, (b) all in the 10 ring window and (c) one in each ring window viewed along [001] (a1, b1 & c1) and [100] (a2, b2 & c2) showing the  $\text{Na}^+$  cation preference sites. (Si = light blue, O = red, Al = violet, Na = green, H = dark blue)

The adsorption sites under this condition all tend out to be favorable for the adsorption of both arsenic species except at Site 3 for  $\text{AsO}(\text{OH})_3$  (Figure 15). The adsorption energies of  $\text{AsO}(\text{OH})_3$  (42.04 – 186.57 kJ/mol) were higher than that of  $\text{As}(\text{OH})_3$  (72.86 – 159.83 kJ/mol) except at Site 4, where the energies of  $\text{As}(\text{OH})_3$  (84.82 – 121.87 kJ/mol) were higher than that of  $\text{AsO}(\text{OH})_3$  (11.43 – 64.36 kJ/mol). Putting all the two water molecules in channel B, the cation sites in channel a remained the same as the dehydrated state. In channel B, the  $\text{Na}^+$  cations was coordinated by the water molecules and an additional Al-Na bond was form at T2. When one water molecule was placed in channel A and another in channel B, the cation sites were almost the same as that of the dehydrated framework. The presence of the water caused the  $\text{Na}^+$  cation at M3b to move away from the lattice oxygen causing the Na-O in increase by 0.05Å. Similar to when all the water molecules were in channel A, all the adsorption sites proved favorable for adsorption of both  $\text{AsO}(\text{OH})_3$  and  $\text{As}(\text{OH})_3$  except at Site 3 for  $\text{AsO}(\text{OH})_3$  (103.09 kJ/mol, endothermic). In this condition, the energies were higher than when all the two water molecules were placed in channel A and lower than when all the water were placed in channel B (Table 6) These results shows that the adsorption properties of zeolites depends on the amount of water molecules in the framework and also their locations in the framework.

**Table 6** Adsorption energies (kJ/mol) for two water molecules,  $\text{AsO}(\text{OH})_3$  and  $\text{As}(\text{OH})_3$  on hydrated Na-Clinoptilolite (Si/Al = 5) with 12  $\text{H}_2\text{O}$  molecules and 2  $\text{H}_2\text{O}$  molecules at different adsorption sites

	12 $\text{H}_2\text{O}$ Molecules		2 $\text{H}_2\text{O}$ Molecules					
	Arsenic acid	Arsenous acid	One $\text{H}_2\text{O}$ molecule in One pore		All $\text{H}_2\text{O}$ molecules in 10MR		All $\text{H}_2\text{O}$ molecules in 8MR	
Arsenic acid			Arsenous acid	Arsenic acid	Arsenous acid	Arsenic acid	Arsenous acid	
			-142.42		-172.47		-108.17	
Site 1(10 MR [001])	458.74	209.97	-151.58	-137.82	-119.69	-50.80	-186.57	-167.51
Site 2 (8 MR [001])	440.36	410.02	-152.31	-132.93	-128.66	-76.49	-42.04	-72.86
Site 3 (8 MR [100])	155.70	100.00	52.20	-117.46	103.09	-60.17	-44.40	-159.83
Site 4 (8 MR)	51.02	-18.52	-40.78	-97.36	-11.43	-84.82	-64.67	-121.87

### Hydrated (12 H<sub>2</sub>O molecules)

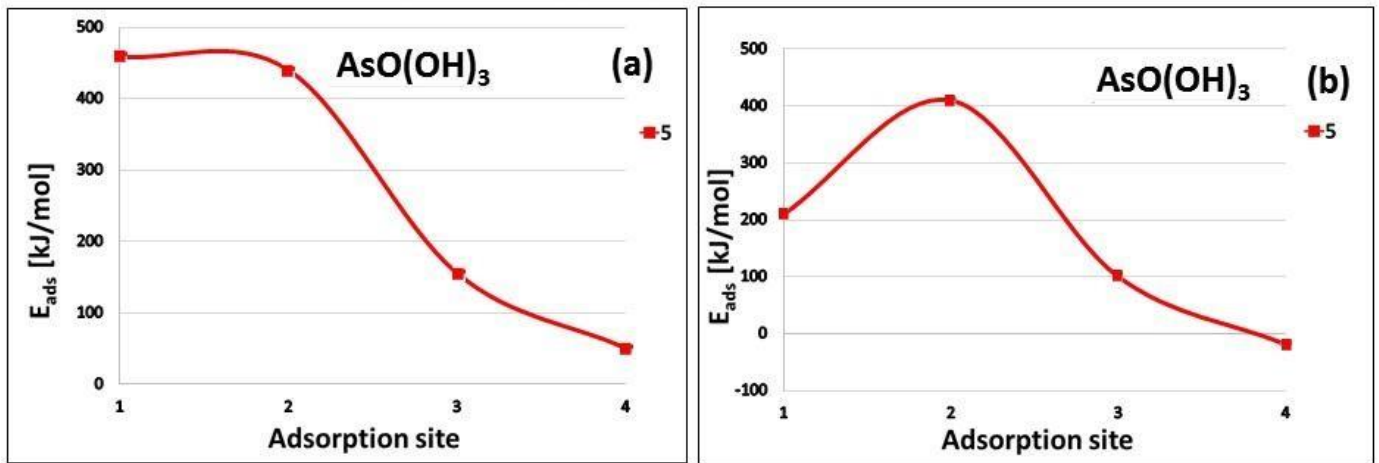


**Figure 14** Adsorption energies of  $\text{AsO(OH)}_3$  and  $\text{As(OH)}_3$  as a function of Si/Al ratio 5 at different adsorption sites of *hydrated* Na-clinoptilolite (12 water molecules).

### Hydrated (2 H<sub>2</sub>O molecules)

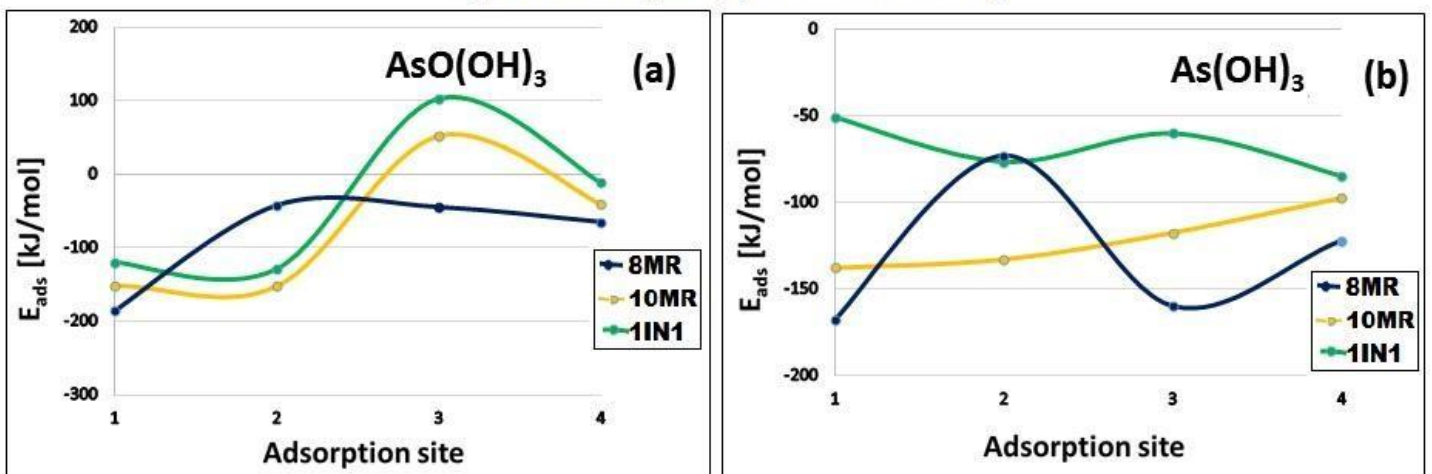


**Figure 15** Adsorption energies of  $\text{AsO(OH)}_3$  and  $\text{As(OH)}_3$  as a function of Si/Al ratio 5 at different adsorption sites of *hydrated* Na-clinoptilolite (2 water molecules).

# KNUST

## CHAPTER SIX

### 6. CONCLUSION AND ONGOING WORK

We have employed first-principles DFT calculations to evaluate the adsorption capacity of the Al(III)-modified clinoptilolite zeolite for  $\text{AsO}(\text{OH})_3$  and  $\text{As}(\text{OH})_3$  under vacuum and aqueous condition. We have shown from calculations that, when present, the framework water molecules coordinate with the cations present in the CL zeolites pores, and they act to reduce the charge density distribution within the pores (Figure 6), in good agreement with the theoretical prediction of Higgins *et al.* (Higgins *et al* 2002). The calculated structural parameters and the cation preference sites agree well with theoretical values obtained by Uzunova *et al.*, 2013 (Uzunova and Mikosch 2013a). The average bondlength of the  $\text{Na}^+$  cation with the hydrated framework oxygen was calculated at  $2.361\text{\AA}$  due to the interaction between the water molecules oxygen ions to the framework silicon and aluminium ions and extra framework cations. From the calculated adsorption energies and characteristics, we show that

both species of arsenic adsorb preferentially in the dehydrated Al(III)-modified CL zeolite (associative and exothermic) than in the hydrated case (dissociative and endothermic). The results of our calculation showed that, in general, the adsorption site 2 which is an eightmember ring (channel B) was the most energetically favorable (-113.24 kJ/mol) site for the adsorption of arsenic in the hydrated state and site 1 (channel A) being the most favorable (156.28 kJ/mol) site for adsorption of arsenic in the dehydrated state. Upon adsorption of arsenic, there was lengthening of the O-H bond (+0.019 Å) as well as the As-O bond (+0.029 Å) of the adsorbates. The adsorption sites 3 (eight member-ring in (100) plane) was found to be the most energetically favorable (-189.35 kJ/mol) adsorption site for arsenic acid but in the dehydrated framework and in the hydrated framework, site 2 was found (-135.24 kJ/mol). Alternatively, site 1 was the most energetically favorable site (-161.44 kJ/mol) for arsenous acid adsorption in the dehydrated state and site 4 favourable in the hydrated structure (105.16 kJ/mol).

Our calculation identified channel A as the energetically most favourable adsorption site for the two water molecules. These results of our calculation show the importance of including the effects of hydration when studying adsorption in zeolites. Dehydrated zeolites retain some water adsorbed within the lattice and we have shown that even a small number of water molecules can influence the preferred adsorption position of the extra framework cations. We also shown the importance of including the effects of the amount of aluminium in the zeolite framework.

These results demonstrate a great potential for Al(III)-modified clinoptilolite for arsenic immobilization. Moreover, our calculated structures for the adsorption of the single  $\text{AsO}(\text{OH})_3$  and  $\text{As}(\text{OH})_3$  molecules in this study could serve towards the development of reliable forcefields that can be employed in classical MD simulations to simulate complex systems.

# KNUST

## References

- Alberti, A., 1972, On the crystal structure of the zeolite heulandite; *Tschermaks Mineral. und Petrogr. ...* **146**
- Anisimov V.I. Aryasetiawan, F, and Lichtenstein, A. I., 1997, *J. Phys.:Condens. Matter* **9**
- Anon 2008 Developer's Manual for QUANTUM ESPRESSO(v.5.1.0) Online: [http://www.quantum-espresso.org/wp-content/uploads/Doc//developer\\_man/](http://www.quantum-espresso.org/wp-content/uploads/Doc//developer_man/)
- Arcoya, A. Gonzalez, J.A. Llabre, G. Seoane, X.L. and Travieso, N., 1996, Role of Counteractions on the Molecular Sieve Properties of Clinoptilolite, *Microporous Mater.* **7** 1–13
- Baerlocher, C. and Hepp, A., 1978, DLS-76, a program for the simulation of crystal structures by geometric refinement, *Lab. f. Kristallographie* (ETH Zürich)
- Baerlocher, C. and McCusker, L.B., 2012, Database of Zeolite Structures, Online: <http://www.iza-structure.org/databases/>.
- Baerlocher, C. Mccusker, L.B. and Olson, D.H., 2007, *Atlas of Zeolite Framework Types* ed C B L B M D H Olson (Amsterdam, The Netherlands: Elsevier)
- Baker, H. Massadeh, A.H.Y., 2009, Natural Jordanian zeolite: removal of heavy metal ions from water samples using column and batch methods, *Environ. Monit. ...* **157** 319–30
- Baroni, S. Girincoli, S.d. and Corso, A.D., 2001, *Rev. of Mod. Phys.* **73**
- Bonnin, D., 1997, Proceedings of the Annual Conference on American Water Works Association p 421

- Breck, D.W., 1974, *Zeolite Molecular Sieves*. (Wiley)
- Caro, J. Noack, M. Kolsch, P. and Schafer, R., 2000, *Microporous and Mesoporous Materials* **38** 3–24
- Caro, J. Noack, M. and Kolsch, P., 2005, *Adsorption J. Int. Adsorpt. Soc.* **11** 215–27
- Cassandras, C.G, Pepyne, D.L. and Wardi, Y., 1998, Generalized gradient algorithms for hybrid system models of manufacturing systems, *Proc. 37th IEEE Conf. Decis. Control (Cat. No.98CH36171)* **3**
- Chojnacki, A. Chojnacka, K. Hoffmann, J.H. G., 2004, The application of natural zeolites for mercury removal: from laboratory tests to industrial scale, *Miner. Eng.* **17** 933–7
- Claire-Deville, M.H de St., 1862, *Compt. Rend. Compt. Rend.* **54**
- Cococcioni, M., 2002, *A LDA+U study of selected iron compounds* (Trieste, Italy)
- Corma, A., 1997, From Microporous to Mesoporous Molecular Sieve Materials and Their Use in, Catalysis. *Chem. Rev.* **97**, 2373–420
- Cramer, C.J., 2013, *Essentials of computational chemistry: theories and models*. (John Wiley & Sons)
- Cronstedt, A.F., 1756, *Svenska Vetenskaps Akademiens Handlingen Stockholm* **18** **18**
- Damour, A., 1840, *Annales des Mines*, **17**, 191–202
- Dyer, A., 1988, *An Introduction to Zeolite Molecular Sieves*. (John Wiley & Sons Ltd)
- Filippi, C. Gonze, X. and Umrigar, C. J., 1996, Generalized gradient approximations to density functional theory: comparison with exact results, *Elsevier* 1–32
- Flank, W., 1980, *Adsorptio Exchang with Synthetic Zeolites* (United States: ACS symposium series)
- Fletcher, R., 2013, *Practical methods of optimization*. (John Wiley & Sons)
- Foster, M.D. Rivin, I.J. Delgado T.M.M. Friedrichs, O., 2006, *Microporous Mesoporous Mater.* **90**
- French, S.A. Coates, R. Lewis, D.W. and Catlow C.R.A., 2011, Probing the structure of complex solids using a distributed computing approach—Applications in zeolite science *J. Solid State Chem.* **184**, 1484–91
- Frising, T. and Leflaive, P., 2008, *Microporous and Mesoporous Materials.* **114**, 27–63
- Geerlings, P. Proft, F.D. and Langenaeker W., 2003, *Chem. Rev.* **103**

- Giannozzi, G., 2007, *Numerical methods in electronic structure* (Italy: University of Udine)
- Godelitsas, A. and Armbruster, T., 2003, HEU-type zeolites modified by transition elements and lead *Microporous Mesoporous Mater.* **61**, 3–24
- Gottardi, G. and Galli E., 1985, *Natural Zeolites* (Berlin: Springer-Verlag)
- Greeley, J., 2002, Electronic structure and catalysis on metal surfaces. *Annu. Rev. Phys. Chem.* **53**, 319–48
- Hamann, D.R., 1997, H<sub>2</sub>O hydrogen bonding in density-functional theory. *Phys. Rev. B* **55** R10157
- Hammer, B. and Nørskov, J., 2000, Theoretical surface science and catalysis—calculations and concepts. *Adv. Catal.* **45**
- Han, Y. Li, D. Zhao, L. Song, J. Yang, X. Li, N. Di, Y. Li, C. Wu, S. Xu, X. Meng, X. Lin, K. and Xiao, F., 2003, High-temperature Generalized Synthesis of Stable Ordered Mesoporous Silica- based Materials using Fluorocarbon-Hydrocarbon Mixtures. *Angew. Chem., Int. Ed.* **42**, 3633–7
- Higgins, F.M. De Leeuw, H.N. and Parker, S.C., 2002, Modelling the effect of water on cation exchange in zeolite A. *J. Mater. Chem.* **12**, 124–31
- Hill, N. A., 2002, *Annu. Rev. Mater. Res.* **32**, 1–37
- Huang, L. Guo, W. Deng, P. Xue, Z. and Li, Q., 2000, Investigation of Synthesizing MCM41/ZSM-5 Composites. *J. Phys. Chem. B.* **104**, 2817–23
- Jang, J. Oh, J.H. and Stucky, G.D., 2002, Fabrication of Ultrafine Conducting Polymer and Graphite Nanoparticles. *Angew. Chem., Int. Ed.* **41**, 4016–9
- Johnson, M. O'Connor, D. Barnes, P., Catlow, C. R. A. Owens, S. L. Sankar, G. Bell, R. Teat, S. J. and Stephenson, R., 2003, Cation Exchange, Dehydration, and Calcination in Clinoptilolite: In Situ X-ray Diffraction and Computer Modeling *J. Phys. Chem. B.* **107**, 942–51
- Jones, R. O. and Gunnarsson, O., 1989, *Rev. Mod. Phys.* **61**
- Joo, S. H. Choi, S. J. Oh, I. Kwak, J. Liu, Z. Terasaki, O. and Ryoo, R., 2001, Ordered Nanoporous Arrays of Carbon Supporting High Dispersions of Platinum Nanoparticles. *Nat.* **414**, 470
- Karlsson, A. Stocker, M. and Schmidt R., 1999, Composites of Micro- and Mesoporous Materials: Simultaneous Syntheses of MFI/MCM-41-like Phases by a Mixed Template Approach. *Microporous Mesoporous Mater.* **27**, 181–92
- Khachatryan, S., 2014, Heavy metal adsorption by Armenian natural zeolite from natural aqueous solutions, *Chem. Biol.* **2**, 31–5

- Kloetstra, K.R. Bekkum, H. V. and Jansen, R.J., 1999, Mesoporous Material containing Framework Tectosilicate by Pore-wall Recrystallization. *Chem. Commun.* 2281–2
- Koch, W. and Holthausen, M. C., 2001, *A Chemist 's Guide to Density Functional Theory* vol 3, (Wiley-VCH Verlag GmbH)
- Kokalj, A. and Causà, M., 2000, Scientific Visualization in Computational Quantum Chemistry, Proceedings of High Performance Graphics Systems and Applications European Workshop (Bologna, Italy) pp 51–4
- Van Koningsveld, H., 2007. *Compendium of Zeolite Framework Types: Building Schemes and Type Characteristics* (Amsterdam, The Netherlands: Elsevier)
- Koyama, K. and Takéuchi, Y., 1977, Clinoptilolite: the distribution of potassium atoms and its role in thermal stability. *Z. Krist.* **145**, 216–39
- Kresge, C. T. Leonowicz, M. E. Roth, W. J. Vartuli, J. C. and Beck, J. S., 1992, Ordered mesoporous molecular sieves synthesized by a liquid- crystal template mechanism. *Lett. to Nat.* **359**, 710–2
- Kucic, D. Marki, M. and Briski, F., 2012, Ammonium Adsorption on Natural Zeolite ( Clinoptilolite ): Adsorption Isotherms and Kinetics. *Holist. Approach to Environ.* **2**, 145–58
- Kwakye-Awuah, B. Labik, L. Nkrumah, I. and Williams, C., 2014, Removal of Arsenic in River Water Samples Obtained From A Mining Community in Ghana Using Laboratory Synthesized Zeolites *Int. J. Adv. Sci.* **4**, 304–15
- Landau, L., 1937, Use of adsorption in removal of arsenic from drinking water. *Zhurnal Eksp. i Teor. Fiz.* 1–28
- Li, Z. Beachner, R. McManama, Z. and Hanlie, H., 2007, Sorption of arsenic by surfactantmodified zeolite and kaolinite. *Microporous Mesoporous Mater.* **105**, 291–7
- Liu, Y. Zhang, W. and Pinnavaia, T.J., 2000, Steam-stable Aluminosilicate Mesostructures assembled from Zeolite Type Y Seeds. *J. Am. Chem. Soc.* **122**, 8791–2
- Madsen, G. K. H. and Novák, P., 2005, Charge order in magnetite; An LDA+ U study *Europhys. Lett.* **69**, 777–83
- Malashevich, A., 2009, *First-principles study of electric polarization in piezoelectric and magnetoelectric materials* (Rutgers University, New Jersey, USA)
- Marlow, F. McGehee, M. D. Zhao, D. Y. Chmelka, B. F. and Stucky G.D., 1999, Doped Mesoporous Silica Fibers: A New Laser Material. *Adv. Mater.*, **11**, 632–6
- Martin, R. M. 2005, *Electronic Structure: Basic Theory and Practical Methods* (England: Cambridge University Press,)
- McCusker, L. B. Liebau, F. and Engelhardt, G., 2001, *Pure Appl. Chem.* **73**

- Methfessel, M. P. A. T. and Paxton, A. T., 1989, High-precision sampling for Brillouin-zone integration in metals. *Phys. Rev. B* **40**, 3616
- Minachev, K. M. and Ya, I. I., 1973, Catalytic Properties of Zeolites – A General in Review *Mol. Sieves- ed. W.M. Meier J.B. Uytlerhoeven, ACS Symp. Ser.* **121**, 451–60
- Mokaya, R., 1999, Ultrastable Mesoporous Aluminosilicates by Grafting Routes. *Angew. Chem., Int. Ed.* **38** 2930–4
- Norman, D. and Nartey, I., 2010, *Arsenic In Ghana, West Africa, Ground Waters* Online: [http://www.brr.cr.usgs.gov/projects/GWC\\_chemtherm/FinalAbsPDF/norman.pdf](http://www.brr.cr.usgs.gov/projects/GWC_chemtherm/FinalAbsPDF/norman.pdf)
- Pack, J. D. and Monkhorst, H. J., 1977, Special points for Brillouin-zone integrations —a reply. *Phys. Rev. B* **16**, 1748
- Parr, R. G., 1980, Density functional theory of atoms and molecules *Proc.Int.Congr.Quantum Chem.* **3rd.** 5–15
- Parr, R. G. and Yang W., 1989, *Density-Functional Theory of Atoms and Molecules* (New York: Oxford University Press)
- Parr, R. W. Yang, W. Breslow, R. Goodenough, J. B. Halpern, J. and Rowlinson, J. S., 1989, *Density-Functional Theory of Atoms and Molecules* vol 58 (Oxford University Press)
- Pavelic K 2001 *Journal of Molecular Medicine* **78**, 708–20
- Perdew, J. Burke, K. and Ernzerhof, M., 1996, Generalized Gradient Approximation Made Simple. *Phys. Rev. Lett.* **77**, 3865–80
- Ravindran, P. Vidya, R. Fjellag H. and Kjekshus, A., 2004, *J. of Crystal Growth.* **268**
- Redman, A. D. Macalady, D. L. and Ahmann. D., 2001, *A Preliminary Study of Various Factors Influencing Arsenic Mobility in Porous Media* (Colorado)
- Rozanska, X., and van Santen, R., 2003, Reaction mechanisms in zeolite catalysis ... *of zeolite science and technology* (The Netherlands: Marcel Dekker, Inc.)
- Ryder, J. A. Chakraborty, A. K. and Bell, A. T., 2000, Density Functional Theory Study of Proton Mobility in Zeolites: Proton Migration and Hydrogen Exchange in ZSM-5 *J. Phys. Chem. B* **104**, 6998–7011
- Ryoo, R. Joo, H. and Jun, S., 1999, Synthesis of Highly Ordered Carbon Molecular Sieves via Template-mediated Structural Transformation. *J. Phys. Chem. B* **103**, 7743–6
- Ryoo, R. Jun, S. Kim, J. M. and Kim, M. J., 1997, Generalised Route to the Preparation of Mesoporous Metallosilicates via Post-synthetic Metal Implantation. *Chem. Commun.* 2225–6
- Sánchez, A. G. 2011, *Computational Study of Adsorption and Diffusion in Zeolites with Cations* (Universidad Pablo de Olavide)

- Sc Biswajit Santra, M., 2010, *Density-Functional Theory Exchange-Correlation Functionals for Hydrogen Bonds in Water* (The Technical University)
- Scott, B. J, Wirnsberger, G. and Stucky, G.D., 2001, Mesoporous and Mesostructured Materials for Optical Applications. *Chem. Mater.* **13**, 3140–50
- Scott, B. J. Wirnsberger, G. McGehee, M. D. Chmelka, B. F. and Stucky, G.D., 2001, Dyedoped Mesostructured Silica as a Distributed Feedback Laser Fabricated by Soft Lithography. *Adv. Mater.*, **13**, 1231–4
- Shaheen, S. M. Derbalah, A. S. and Moghanm, F. S., 2012, Removal of heavy metals from aqueous solution by zeolite in competitive sorption system. *Int. J. Environ. Sci. Dev.* **3**, 365–7
- Shevade, S. and Ford, R. G. 2004, Use of synthetic zeolites for arsenate removal from pollutant water. *Water Res.* **38**, 3197–204
- Sing, K.S.W. Everett, D. H. Haul, R. A.W. Moscou, L. Pierotti, R. A, Rouquerol, J. and Siemieniewska, T., 1985, *Pure and Applied Chemistry* **57**, 603–19
- Stumm, W. M. J., 1996, *Aquatic Chemistry – Chemical Equilibria and Rates in Natural Waters* (New York: John Wiley & Sons Inc.)
- TOP, A., 2001, *Cation Exchange (Ag<sup>+</sup>, Zn<sup>2+</sup>, Cu<sup>2+</sup>) Behaviour of Natural Zeolites*, (Izmir Institute of Technology, Izmir, Turkey)
- Treacy, M. M. J. and Foster, M. D., 2009, *Microporous Mesoporous Mater.* **118**
- Uzunova, E. L. and Mikosch, H., 2013, Cation site preference in zeolite clinoptilolite : A density functional study *Microporous Mesoporous Mater.* **117**, 113–9
- Uzunova, E. and Mikosch, H., 2013, Adsorption and Activation of Ethene in Transition Metal Exchanged Zeolite Clinoptilolite: a Density Functional Study *ACS Catal.* **3**, 2759–67
- Watanabe, Y, Yamada, H. Tanaka, J. Komatsu, Y. and Moriyoshi, Y., 2004, *Separation Science and Technology* **39**, 2091–104
- Wong, T.W., 2009, *Handbook of zeolites : structure, properties and applications* / ed T. W. Wong (New York : Nova Science Pub.,)
- Xiao, F. S. Han, Y. Yu, Y. Meng, X. Yang, M. and Wu S., 2002, Hydrothermally Stable Ordered Mesoporous Titanosilicates with Highly Active Catalytic Sites. *J. Am. Chem. Soc.*, **124**, 888–9
- Xu, R. Pang, W. Yu, J. Huo, Q. and Chen, J., 2009, *Chemistry of zeolites and related porous materials: synthesis and structure* (Singapore: John Wiley & Sons (Asia) Pte Ltd) 0
- Zarkovic, N. Zarkovic, K. Kralj, M. Borovic, S. Sabolovic, S. Blazi, M. P. Cipak, A. and Pavelic, K., 2003, *Anticancer Research* **23**, 1589–95

Zhang, Z. Han, Y.F. -S X, Qiu, S. Zhu, L. Wang, R. Yu, Y. Zou, B. Wang, Y. Sun, H. Zhao, D. and Wei, Y., 2001, Strongly Acidic and High-temperature Hydrothermally Stable Mesoporous Aluminosilicates with Ordered Hexagonal Structure. *Angew. Chem., Int. Ed.*, **40**, 1256–8

Zhang, Z. Han, Y. F. -S X, Qiu, S, Zhu, L. Wang, R. Yu, Y. Zou, B. Wang, Y. Sun, H. Zhao, D. and Wei, Y., 2001, Mesoporous Aluminosilicates with Ordered Hexagonal Structure, 18 Chemistry of Zeolites and Related Porous Materials Strong Acidity, and Extraordinary Hydrothermal Stability at High Temperatures. *J. Am. Chem. Soc.* **123**, 5014–21

Zhao, D. Feng, J. Huo, Q. Melosh, N. Fredrickson, G. H. Chmelka, B. F. and Stucky, G.D., 1998, Triblock Copolymer Syntheses of Mesoporous Silica with Periodic 50 to 300 Angstrom Pores. *Science (80-. )*. **279**, 548–52

Ziegler, T., 1991, Chem. Rev. *Chem. Rev.* **91**

